FINAL REPORT
ATTENUATION OF STRESS WAVES
IN
SINGLE AND MULTI-LAYERED STRUCTURES

by

Jackson C. S. Yang
Associate Professor

May 1972

Prepared for

Ames Research Center: N. A. S. A.
Structural Dynamics Branch
Moffett Field, California 94035

Under Contract NGR 21-002-292

Department of

MECHANICAL ENGINEERING

of

THE UNIVERSITY OF MARYLAND

FINAL REPORT

ATTENUATION OF STRESS WAVES
IN
SINGLE AND MULTI-LAYERED STRUCTURES

by

Jackson C. S. Yang
Associate Professor

and

C. Y. Tsui
Assistant Professor

Mechanical Engineering Department
University of Maryland

May 1972

Prepared for

Ames Research Center: N. A. S. A.
Structural Dynamics Branch
Moffett Field, California 94035

Under Contract NGR 21-002-292

CONTENTS

INTRODUCTION

In problems of impact such as those experienced by a vehicle landing on some planet, entering into some ocean or subjected to some high rate disturbances of the external pressure, the compressive stress wave emanating from the surface of contact could be quite severe. This may cause severe damage or failure to the vehicle or to the various components within the vehicle. Therefore, it becomes necessary to mitigate the loads felt by the payload so that the maximum allowable stress is not exceeded. The purpose of this effort is to study both analytically and experimentally the attenuation of the stress waves during passage through single and multilayer structures.

One method of attenuating the magnitude of the incident compressive stress is to incorporate into the system a material or multilayered material which may be permitted to deform plastically, thereby mitigating the load. The problem has been treated thus far with reasonable success by empirical means, but the intelligent design of such a shock mitigating system requires the understanding and the application of the theory of elastic and plastic wave propagation as well as extensive knowledge of the material properties of the mitigating device. With the support from the National Aeronautical and Space Administration to which this final report is submitted, several basic research studies, both analytically and experimentally, have been carried out with conclusive results.

The investigation included studies on elastic and plastic stress wave propagation in the composites and those on shock mitigating material characteristics such as dynamic stress-strain relations and energy absorption properties. Studies were performed on the behavior of composites under dynamic loading. A summary of the studies is presented in the following:

I. Stress wave propagation in composites:

  A. Propagation of elastic waves in composites.

  B. Propagation of elastic waves through areas of discontinuity.

  C. Propagation of radial elastic plastic waves in a circular disk.

  D. Elastic and Plastic wave cancellation.

II. Shock mitigating material characteristics:

  A. Energy absorption characteristics of several shock mitigating materials.

  B. Dynamic stress-strain relations of several shock mitigating materials.

III. Dynamic response of composites:

  A. The longitudinal vibration of axially symmetric composite bodies.

  B. Shock mitigation models.

I. STRESS WAVE PROPAGATION IN COMPOSITES

A. Propagation of Elastic Waves in Composites

The propagation of an initally sharp cylindrical pressure pulse through a linear elastic fiber reinforced composite medium is analysed, both experimentally and analytically. In the experiment, tests were performed on plates with single and multiple circular inclusions embedded in a matrix of lower characteristic impedance. Sharp compression pulses were generated at an edge of the plate by two methods: the detonation of a charge of lead azide and the impingement of a sharp knife-edged ram impacted at the opposite end by a short projectile. Strain gages were mounted on various positions of the plate to determine the attenuation of the transient stress in the fiber reinforced composite. The qualitative analytical treatment is based on the methods of propagating stress discontinuities. Computer programs were written to numerically determine the changes in the shape of the leading wave front and the stresses immediately behind it. Experimental results for the attenuation of stress wave on steel-aluminum and steel-brass fiber-matrix composites compared very well with the computed analytical results when the applied pressure is generated by small explosive charges. The results did not compare well when the applied pressure is generated by projectile impact.

Results of this portion of the investigation were presented and published at the AIAA/ASME/SAE 13th Structures, Structural Dynamics, and Materials Conference in San Antonio, Texas, April 1972. The paper is entitled, "Experimental and Theoretical Investigation of Stress Wave Attenuation in Fiber Reinforced Composites." A copy of the paper is included in the Appendix es.

B. Propagation of Elastic Waves Through Areas of Discontinuity

Elastic Stress Waves generated in structure consisting of cylindrical rods with grooves, holes, threads, and screws by the application of pressure pulses of various durations are investigated both experimentally and analytically. In the experiment, the stress pulse was introduced by using an air gun to impact aluminum projectiles on various configured aluminum rods. A schematic diagram of the experimental set-up is shown in Fig. 1. The 3/4 inch aluminum rods were machined to the configurations shown in Fig. 2 and 3. Strain gages were mounted on the rod in diametrically opposed pairs at locations shown in Figs. 2 and 3. Each pair of gages was connected to a full Wheatstone bridge using two dummy gages so that bending effects would be cancelled. The effect of grooves, holes, threads and screws on elastic waves in cylindrical rods were obtained from the various parameters from the experimental tests. A typical result is given in Fig. 4 for tests on a cylindrical rod with a 2 inch deep hole at the opposite end of impact. The maximum stress measured from the strain gage is obtained for various hole diameter. This is repeated for plain hole, hole with thread and hole with thread and screw. Another result is given in Fig. 5 for tests on a cylindrical rod with a 1 inch deep hole at the opposite end of impact. This and other results indicated that the threads and grooves had very little effect on elastic wave propagation. The results are very realistic and very predictable.

In the theoretical analysis, both a one-dimensional and a two-dimensional numerical method for the solution of elastic waves in various configured rods are utilized. For the one dimensional analysis the method of characteristics is employed to analyze the propagation of stress waves in the rods. A numerical integration of the characteristic equation in each section, in conjunction with appropriate procedures to ensure that the conditions on the external boundaries as well as the continuity conditions at the intersections are satisfied, yields the stress and the particle velocity of any arbitrary location. For the two-dimensional analysis, the exact equations of motion

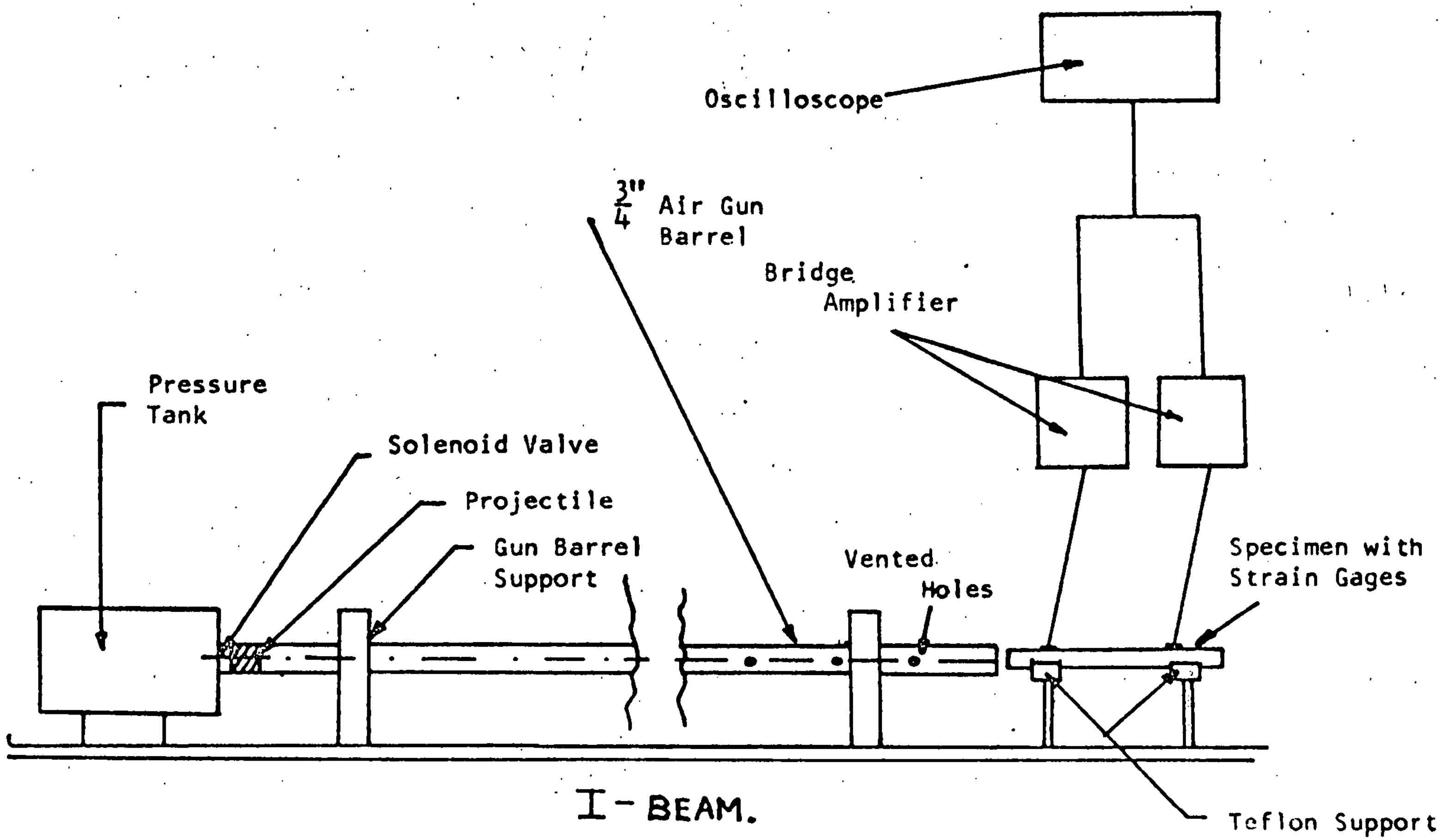

FIGURE I SCHEMATIC DIAGRAM OF INSTRUMENTAL SETTING

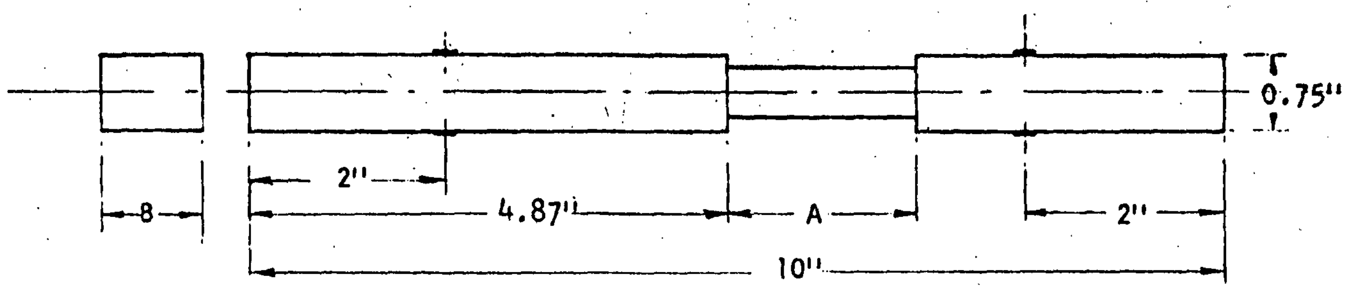

Experimental Parameters:
- a. Length A: 0.125" to 2.75"
- b. Length of projectile: 1" to 2".

FIGURE 2 GROOVED SPECIMEN

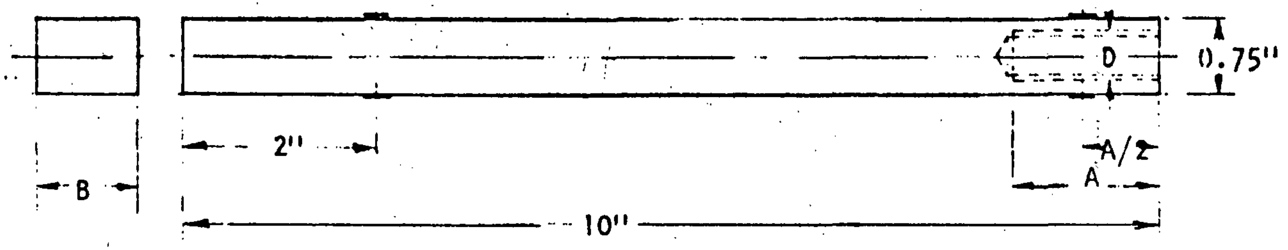

Experimental Parameters:

a. Length A: 1" to 2"
b. Outside diameter D: 0.25" to 0.625"
c. Thread configuration: NC threads or unthreaded
d. Screw configuration: With or without screw in threaded hole
e. Length of projectile: 1" to 2".

FIGURE 3 THREADED SPECIMEN

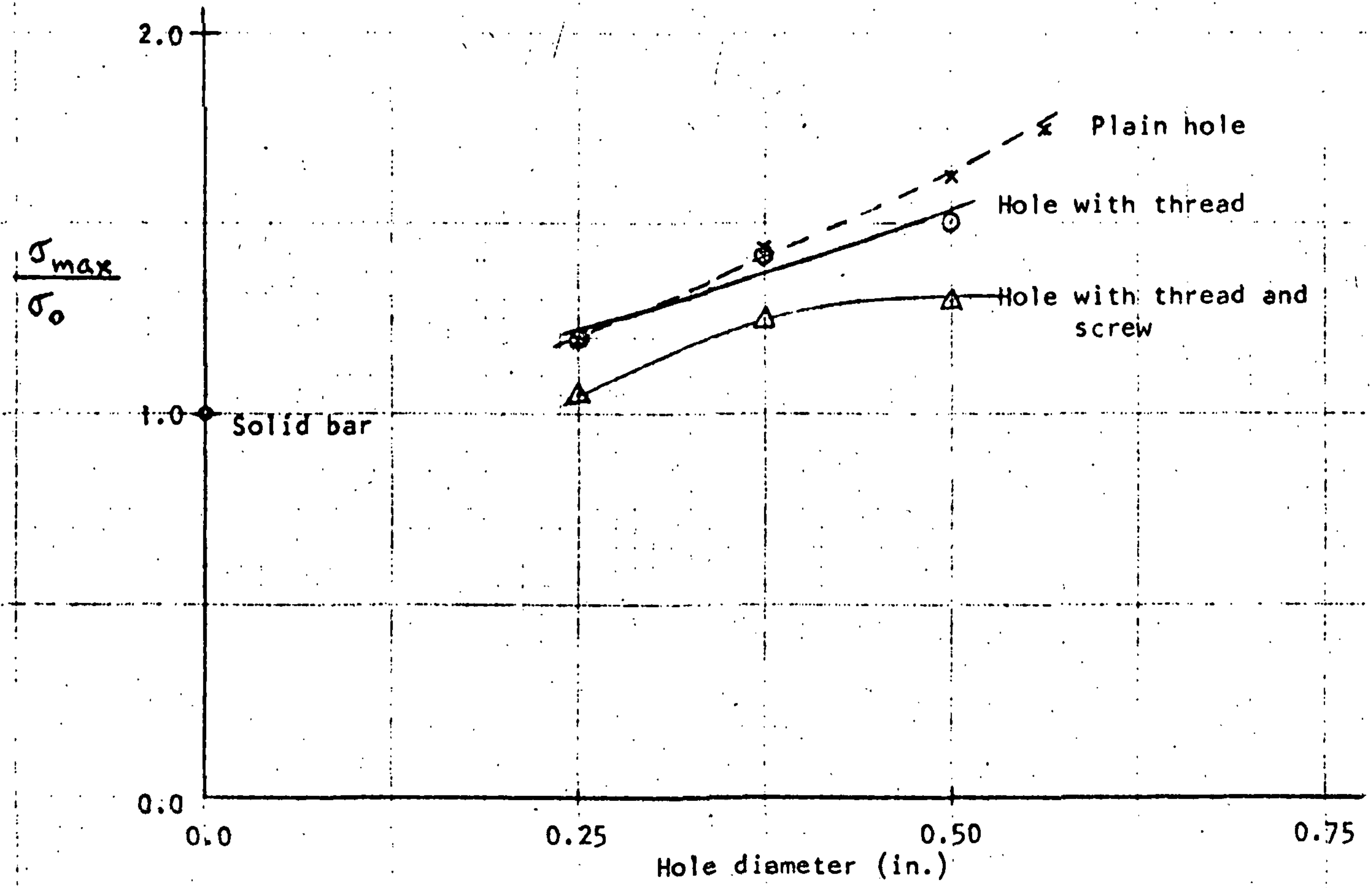

FIGURE 4 CYLINDRICAL ROD WITH 2" DEEP HOLE

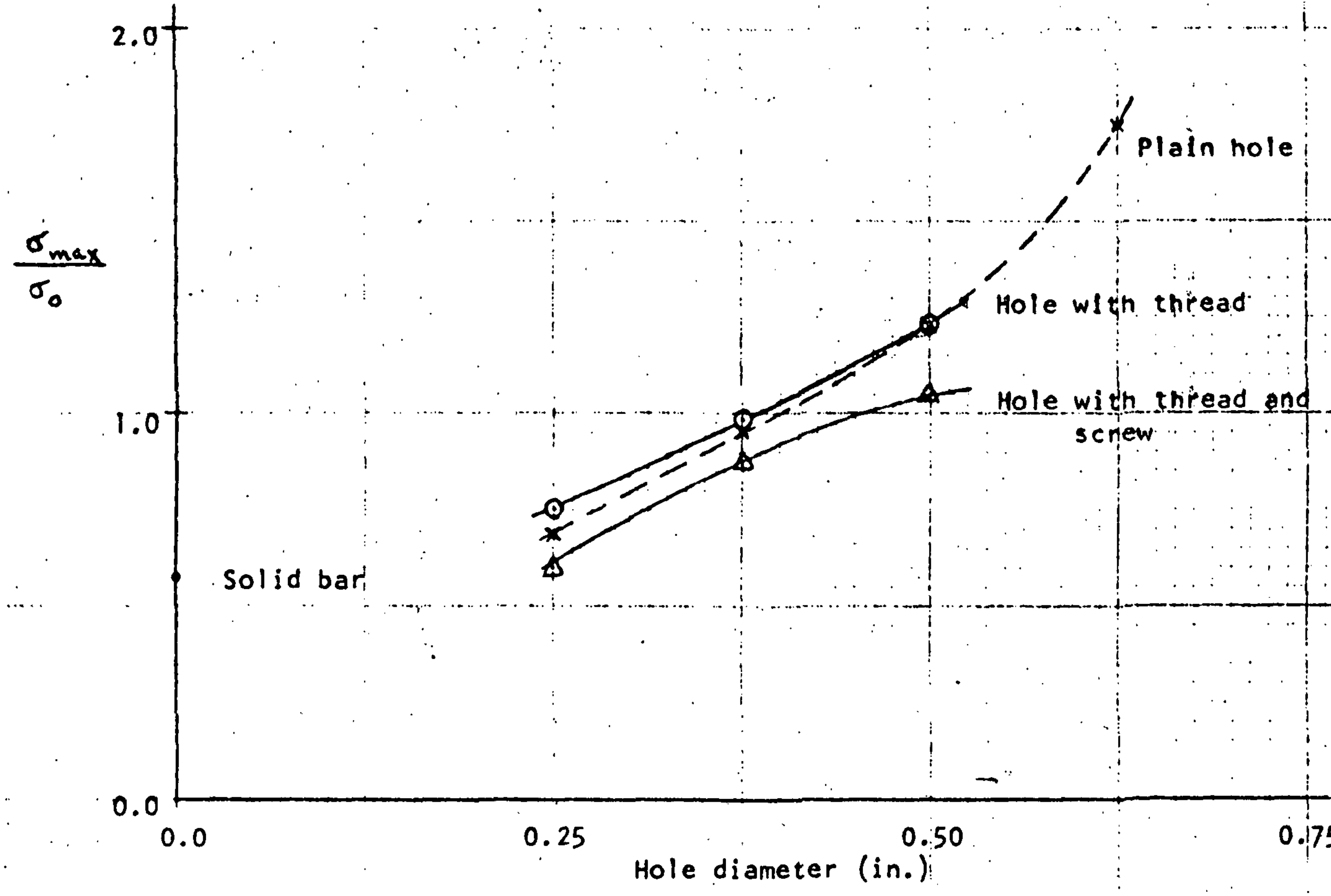

FIGURE 5 CYLINDRICAL ROD WITH 1'' DEEP HOLE

governing elastic, axisymmetric wave propagation in a cylindrical rod are approximated by a first-order finite-difference scheme. This difference scheme is based on a displacement rather than a velocity formulation, thereby making it unnecessary to explicitly introduce an artificial viscosity term into the finite-difference equations. Numerical results are obtained using the resulting difference equations in conjunction with the boundary and initial conditions. The numerical results compared very well with the experimental data. From a design standpoint, it is very desirable to be able to predict the magnitude of the transmitted and reflected protions of the waves.

Results of this protion of the investigation constituted the basic material for a Master's thesis and a paper submitted for presentation in the S.E.S.A. Winter Annual Meeting in Seattle, Washington, Oct. 1972. A copy of the thesis is included in the Appendixes.

C. Propagation of Radial Elastic-Plastic Waves in a Circular Disk.

The prupose of this work was to investigate the problem of radial elastic-plastic stress wave propagation in a thin, finite, work hardening disk using the method of characteristics and the method of successive elastic approximations. In this method the characteristic equations, derived for the elastic case, are applied to the plastic regime by allowing the modulus of elasticity E and the wave speed C appearing in the equations to assume values corresponding to the tangent modulus of the plastic stress-strain curve. The value of Poisson' Ratio, ν, is taken as 1/2 in the plastic range.

Three characteristic equations were derived from the governing conservation and elastic constituent equations as outlined in a paper by Chou and Koenig. They were used subsequently, along with the Prandtl-Reuss incremental plasticity theory and the method of successive elastic solutions, to calculate the problem variables at the nodes of the characteristic network which was generated in a step-by-step fashion as the solution progressed.

A modest experimental program consisting of two experimental techniques was conducted to check the accuracy of the proposed analytical method. A circular disk was used with a hole at the center to accommodate a pressure pulse applied either hydraulically or explosively to the inner surface. The hydraulic method produced poor results and was discarded in favor of the explosive technique.

The disk material was 1100-0 aluminum which exhibits a 0.2 percent offset yield strength of 5000 psi and a proportional limit of 2500 psi. Strain-rate effects were not included in the theory.

Two 350 ohm Micro-Measurement strain gages were used in addition to a TEKTRONIX Model 551 dual beam oscilloscope to obtain radial and circumfrential strain time histories at a radial distance of 0.75 inches on a 4 inch O.D. specimen.

A Piezotronics Model 109A ballistics pressure transducer was used with one channel of a second Model 551 TEKTRONIX dual beam oscilloscope to record the applied pressure pulse. A computer program incorporating the analytical procedures described previously was used to check the strain histories measured on the specimens. In addition, the theoretical solutions for a ramp followed by a steady state pressure were run as approximate checks against the known, closed form, static elastic and elastic-plastic solutions for a thick-walled cylinder.

Reasonable agreement between the theoretical and experimental results supports the hypothesis that this method can be used to solve problems of wave propagation in systems subjected to combined states of stress.

Results of this portion of the investigation constituted the basic material for a Ph.D. Thesis. A copy of the thesis is included in the Appendixes.

D. Elastic and Plastic Wave Cancellation

In order to understand this concept, it should be recalled that after a material has been loaded to a point where plastic deformation occurs, while the load is being released, the displacement will obey the Hooke's law instead of retracting its original path. Since stress waves will propagate at a speed directly proportional to the square root of the slope of the stress-strain curve, it may be seen that the transmission of stress waves during the unloading will take palce much faster than the transmission of the loading stresses above the yield point. Therefore, this method of mitigating the applied impulse is to make use of the overtaking and cancellation of high-intensity plastic stress waves by the faster-traveling elastic unloading stress waves.

A study was made to further develop the one-dimensional stress wave theory and confirm the method by which stress attenuation is attained. A one-dimensional elastic-plastic code was developed for the calculations of the stress deformation and particle velocity history. This code is applicable to problems of one-dimensional longitudinal wave propagation in rods and radial stress-wave propagation in circular disks. The method of characteristics was used and the characteristic equations were derived from the governing equilibrium and elastic constituent equations. These equations were used subsequently along with an incremental plasticity theory embodying the method of successive elastic approximations, to calculate the problem variables at the nodes of the characteristic network which was generated in a step-by-step fashion as the solution progresses.

A series of experimental tests were performed in order to verify the analytical results. One such experiment utilizes an air gun to accelerate a steel rod and impact it against an instrumented test rod protected by various mitigating materials or by various multilayered mitigating materials. A stress wave was developed in the test rod which was measured with strain gages. The reduced stress obtained was analyzed as a function of the applied force pulse, the material properties of the mitigators, the length of the mitigators, and the number and combination of the mitigators for optimum mitigation. The results, as shown in Figures 6 and 7 indicated that the polymer group, such as ethocel, teflon, lexan, and polyurethane, is very efficient for shock mitigation from both a weight and volume standpoint.

Then to verify the concept of wave cancellation, the theoretical determination of the stress and the strain distributions in a test where an air gun was used to accelerate a lexan rod and impact it against a second stationary lexan rod placed in front of an elastic measuring bar was performed. The stress and strain distributions obtained in such a dynamic compression test compared very satisfactorily with the stress and the strain distributions deduced from the theoretical analysis. Figures 8 through 10 give the comparison of the strain measurements from the strain gages to the theoretically calculated values for various lengths of mitigators with lexan projectiles of 1/2, 1, and 2 inches in length, respectively. Figure 11 gives the comparison of the strain measurements from the strain gages to the theoretically calculated values with a steel projectile 1 inch in length. From these results, it could be recommended that for design purposes, a mitigator length-to-projectile length ratio of 0.5 seems to offer the optimum shock mitigation for the materials tested.

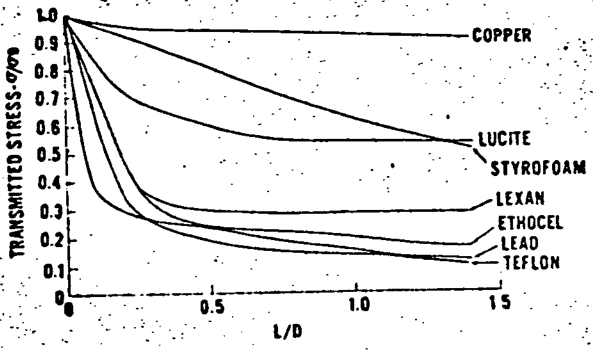

TRANSMITTED STRESS OF VARIOUS MITIGATORS (LENGTH)

Figure 6

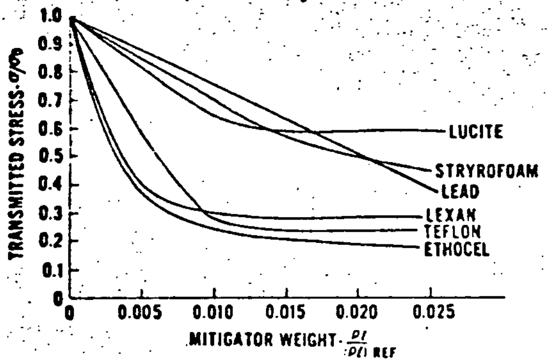

TRANSMITTED STRESS OF VARIOUS MITIGATORS (WEIGHT)

Figure 7

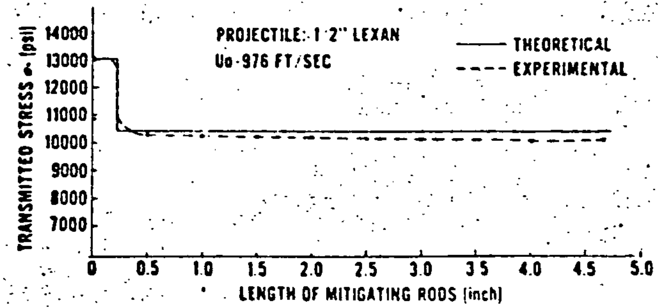

TRANSMITTED STRESS OF VARIOUS LEXAN LENGTHS

Figure 8

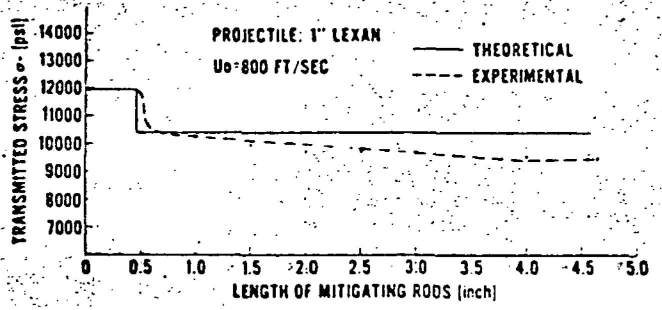

TRANSMITTED STRESS OF VARIOUS LEXAN LENGTHS

Figure 9

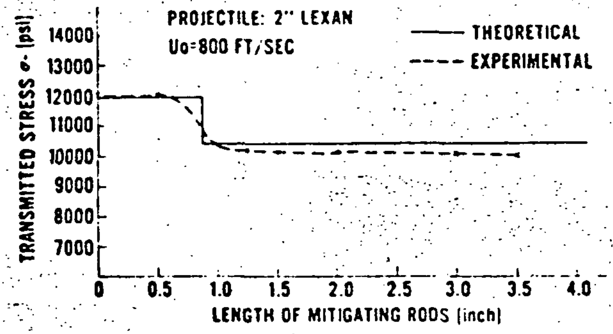

TRANSMITTED STRESS OF VARIOUS LEXAN LENGTHS

Figure 10

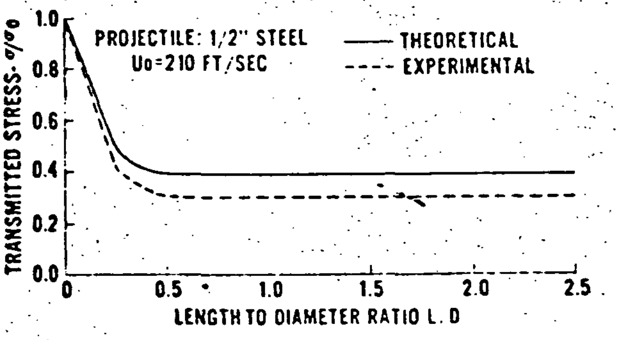

TRANSMISSION STRESS OF VARIOUS LEXAN LENGTHS

Figure 11

II. SHOCK MITIGATING MATERIAL CHARACTERISTICS

A. Energy Absorption Characteristics of Several Shock Mitigating Materials

The scope of this investigation is limited to the determination of the absorption characteristic with respect to the thickness of the shock mitigating materials under low impact velocity conditions. The materials tested included styrofoam, polyethylene, high and low density polyurethene and Balsa wood.

Specimens 3/4 inches in diameter were placed coaxially at the muzzle of the 3/4 inch gun with one end in contact with an instrumented rod, (Fig. 12). The impact was initiated by a low velocity bullet crushing against the specimen. The peak stress measured with strain gages in the instrumented rod was compared with that resulted in direct impact of the bullet to the instrumented rod. Similar experiments were also conducted by means of a 6 inch dia. drop weight tester, (Fig. 13). In this case, the specimens were crushed between a falling cylindrical weight and a stationary instrumented platform.

Experimental results indicated that for styrofoam, ployethylene and Balsa wood, the shock absorption capability generally increases with thickness. On the other hand, polyurethene was found to be a very poor shock absorbing material. The high density polyurethene retained virtually the same thickness under impact. The low density polyurethene was compressed easily but bounced back to its original thickness while offering little shock mitigating capability up to as thick as 4 inches.

Shock mitigating characteristics for styrofoam, polyethene and Balsa wood are presented in Figures 14 through 17.

B. Dynamic Stress-Strain Relations of Several Shock Mitigating Materials

Lightweight foam materials are used abundantly in contemporary design for shock isolation. It is well known that the dynamic properties of many materials differ from the static properties. Tests were performed to obtain dynamic stress-strain data for a representative foam material-rigid polyurethane foam.

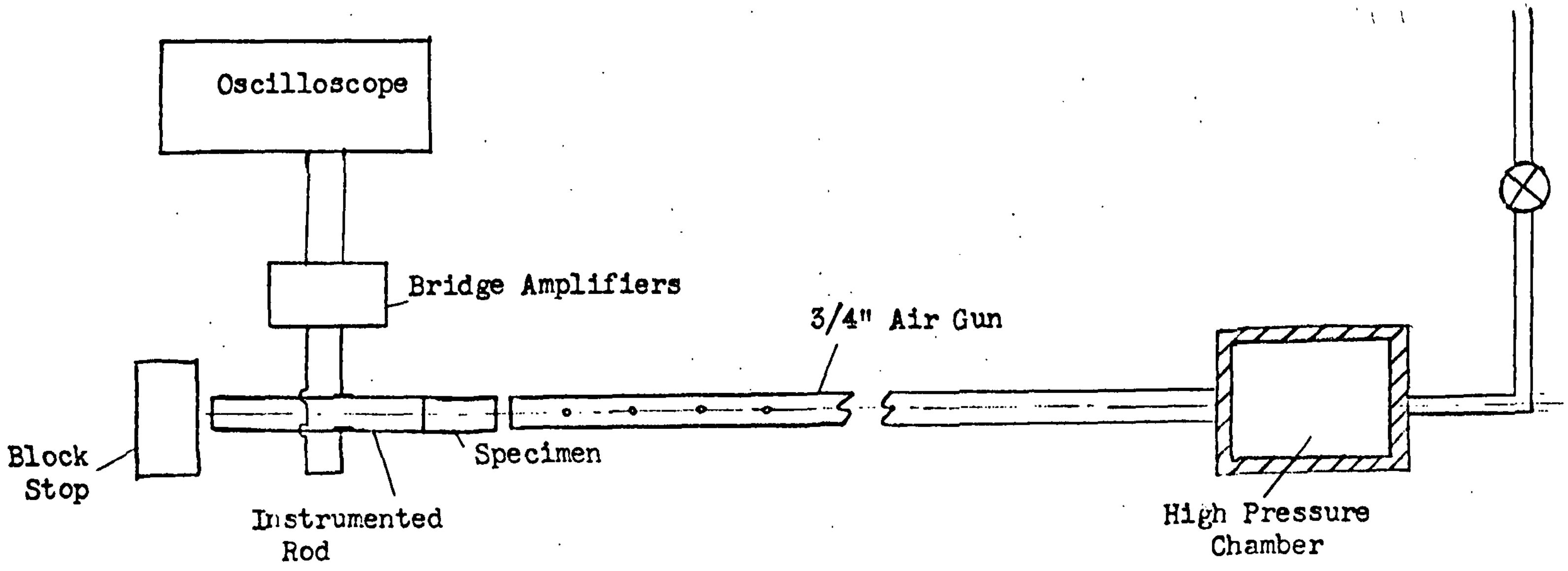

Figure 12 Air Gun Impact Test Apparatus.

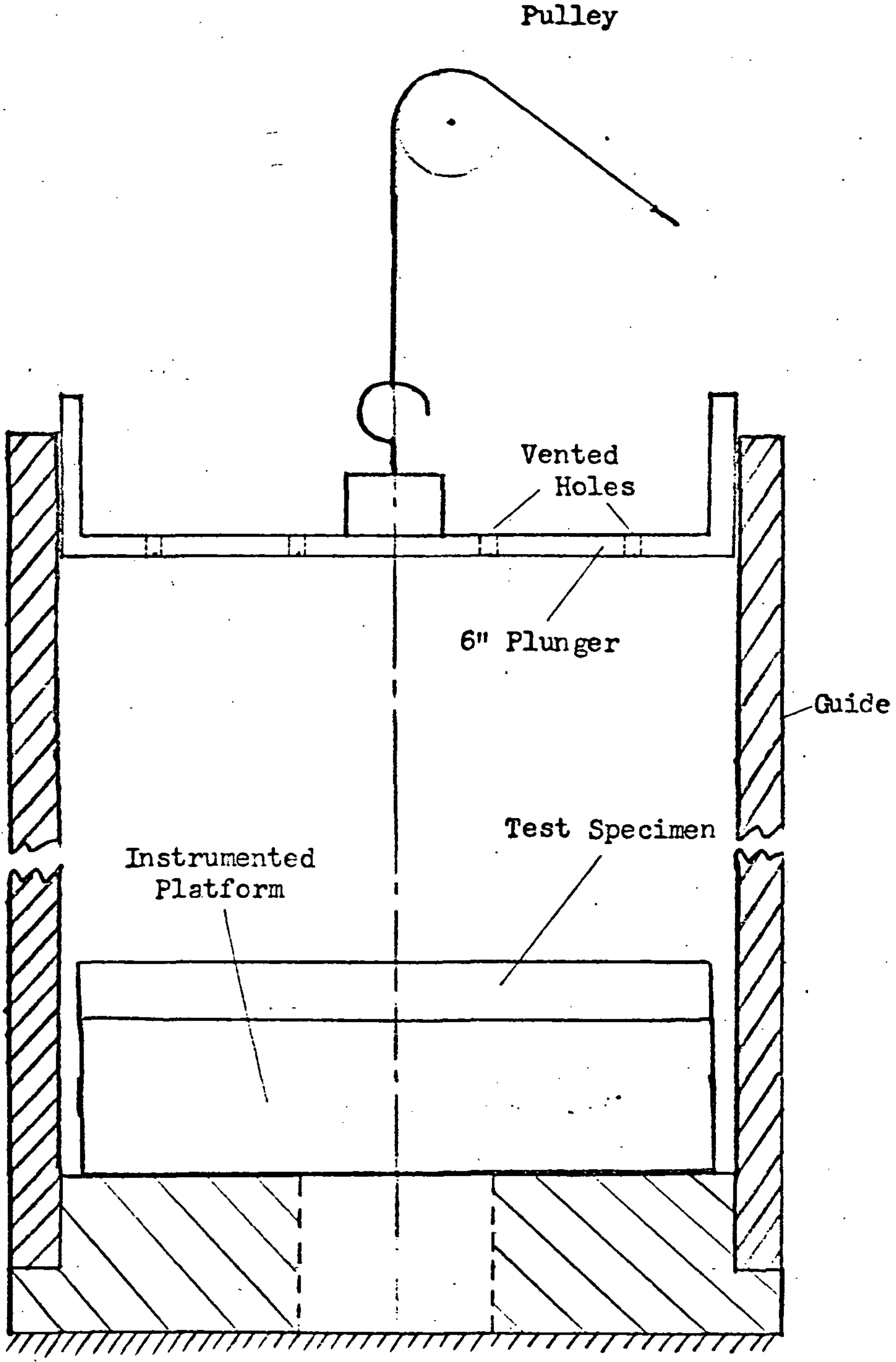

Figure 13 6" Drop Weight Tester.

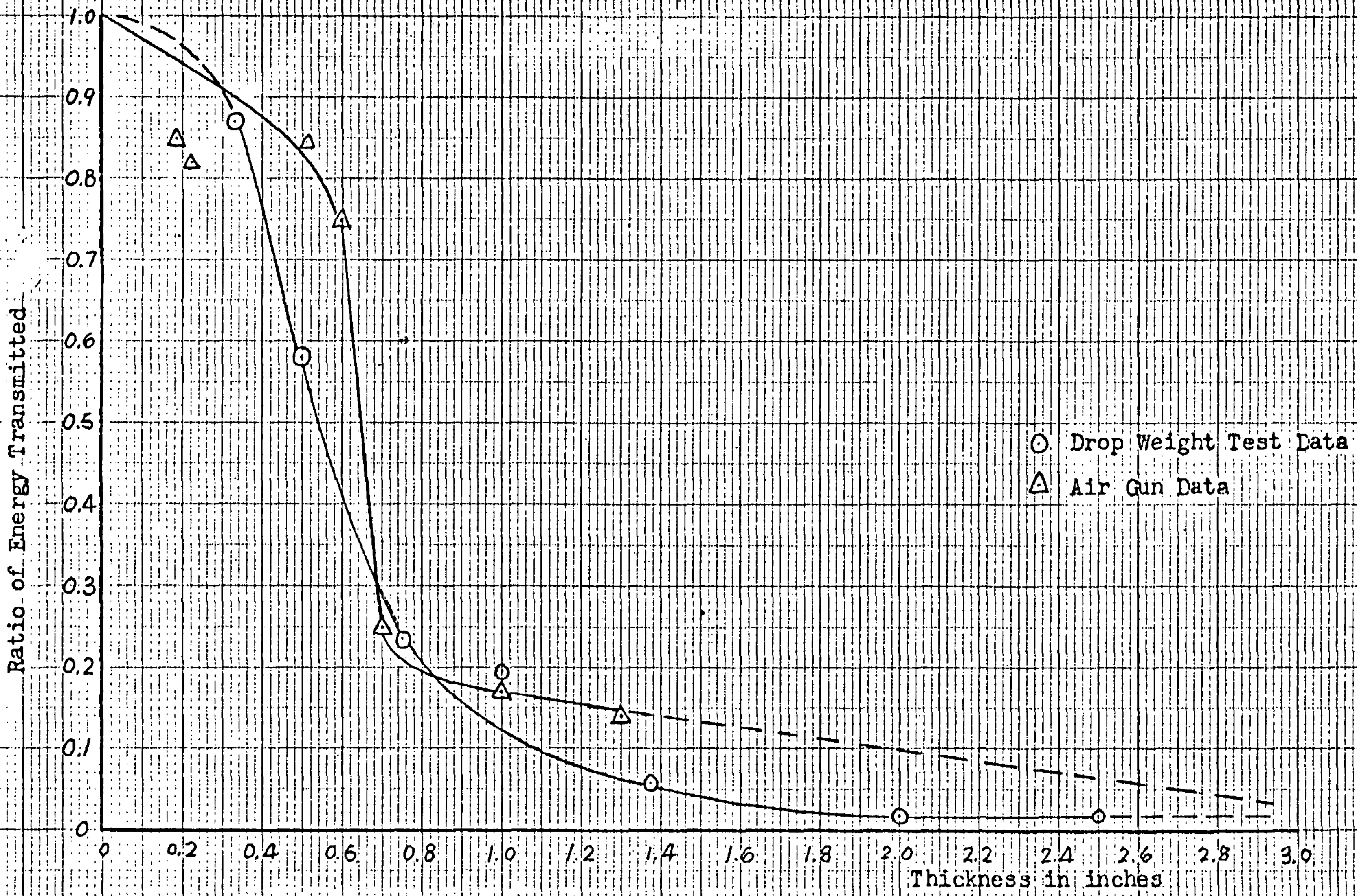

Figure 14 Energy Absorption Characteristics of Styrofoam.

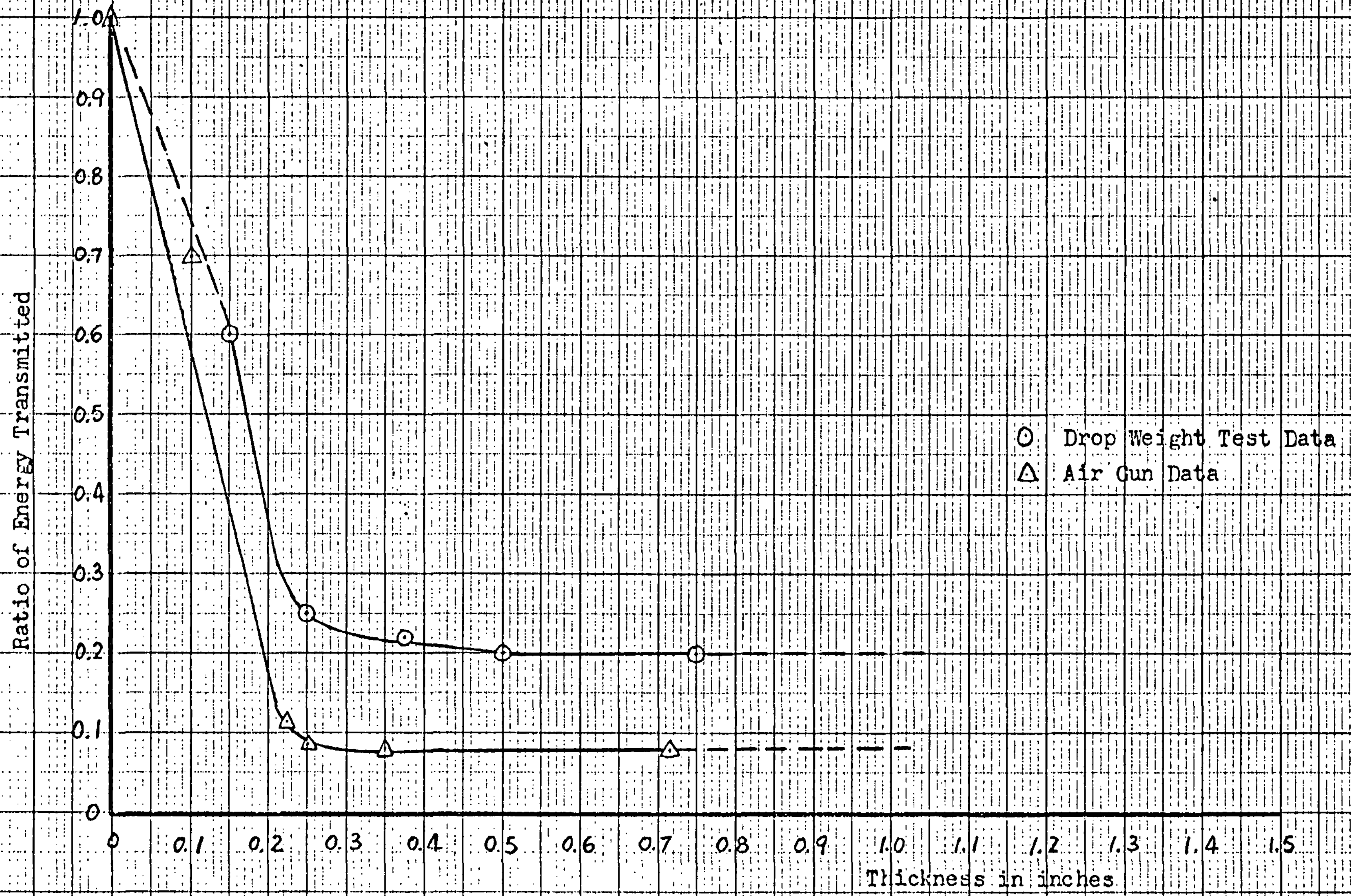

Figure 15 Energy Absorption Characteristics of Balsa Wood (along grain).

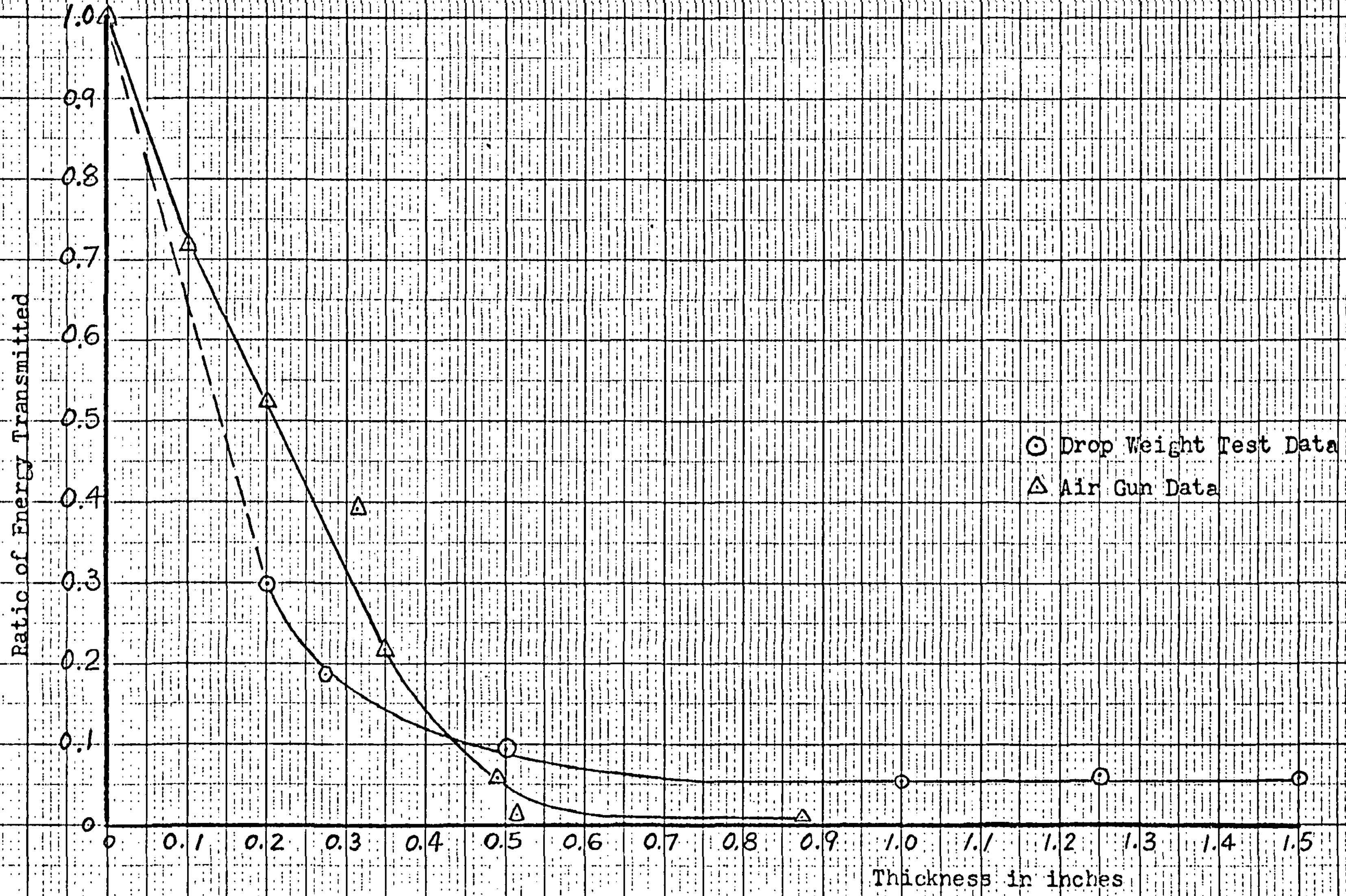

Figure 16 Energy Absorption Characteristics of Balsa Wood (Against grain).

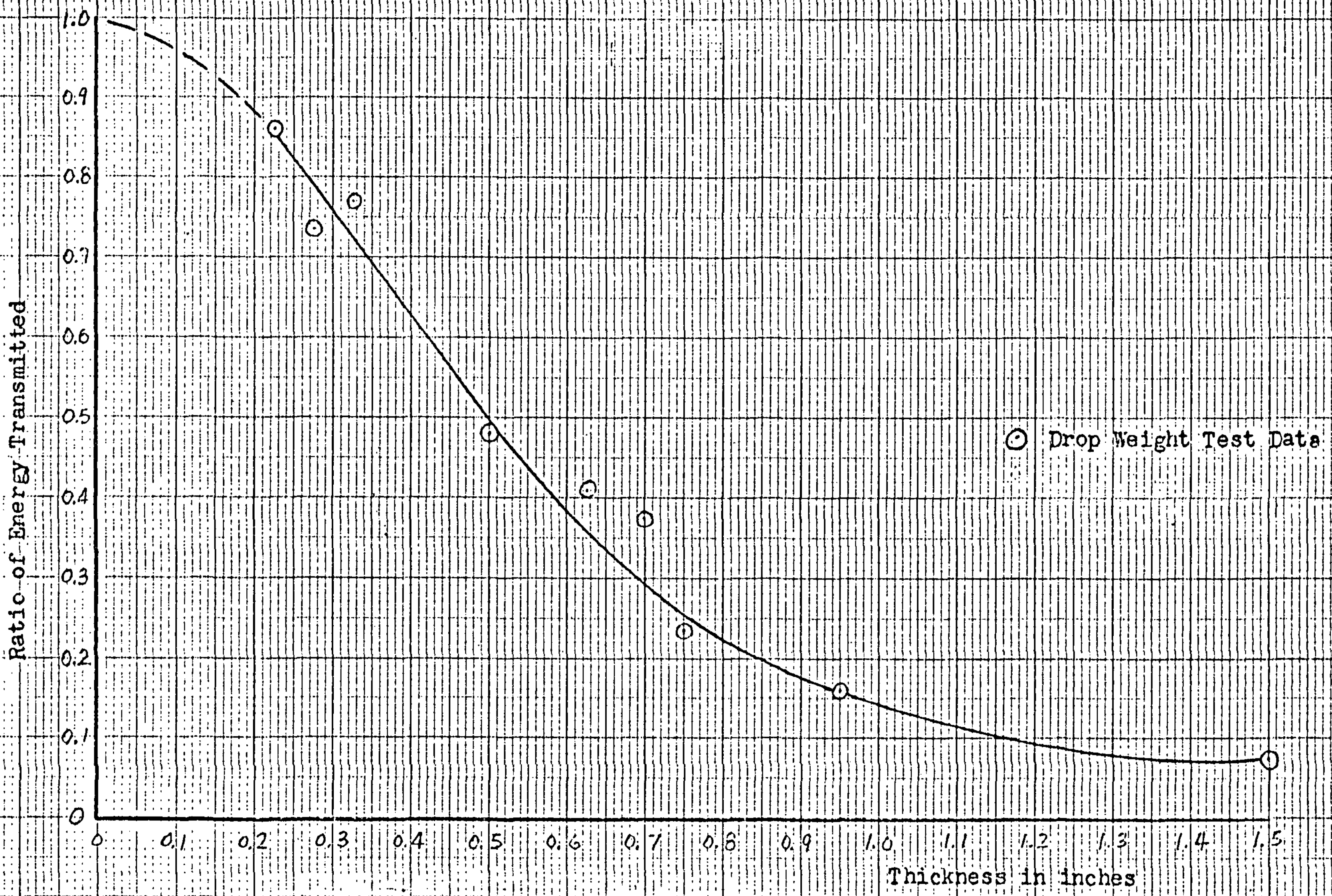

Figure 17 Energy Absorption Characteristics of Polyethylene.

Three densities of the foam (nominal 3.5, 7.0 and 14.5 lb/ft^3) were tested in compression and tension over a wide range of strain rates. The rates were varied between 10^{-2} and 10^4 in/in/sec for the compression tests and between 10^{-2} and 10 in/in/sec for the tension tests. The foam was tested parallel to the direction of rise and perpendicular to the direction of rise, to check for anisotropy.

Stress-strain relations were thus obtained as functions of strain rate for each of the densities and rise directions. Yield strengths and elastic moduli were then determined as functions of strain rate from the compressive stress-strain data. No definite yield points were observed in tension. Therefore, ultimate strengths and elastic moduli were obtained as functions of strain rage from the tensile stress-strain data.

Two test apparatus were required to obtain data over the wide range of strain rates. A Plastechon Model 581 Universal testing machine was used to produce the rates of strain between 10^{-2} and 10 in/in/sec. A split Hopkinson pressure bar was used to produce the rates of strain between 10^3 and 10^4 in/in/sec in compression.

One inch diameter cylindrical specimens having lengths of 0.5, 1 and 2 inches and axes parallel and perpendicular to the foam rise direction were tested in compression using the Model 581 machine. The 0.4 inch diameter cylindrical specimens having lengths of 0.2, 0.4, and 0.7 inches were tested in compression on the split Hopkinson bar. Specimens having 0.375 inches square cross-sections and 1.625 inch gauge lengths were tested in tension on the Model 581 machine.

Conclusions are drawn that nominal 3.5, 7.0 and 14.5 lb/ft^3 rigid polyurethane foams are strain rate sensitive in compression. The yield strength increases consistently over the range of strain rates between 10^{-2}

and 10 in/in/sec. The ultimate tensile strength and tensile elastic modulus are also not rate dependent between 10^{-2} and 10 in/in/sec. Any anisotropic behavior is small and obscurred by the scatter in the data. An increase in foam density results in an increase in both the yield strength, ultimate strength and elastic modulus.

III. DYNAMIC RESPONSE OF COMPOSITES

A. The Longitudinal Vibration of Axially Symmetric Composite Bodies.

The natural frequencies and corresponding mode shapes for composite, axisymmetric bodies of varying area undergoing longitudinal vibrations are determined both experimentally and theoretically. Composite rods, cones and conical shells of Lucite, Nylon, Polycarbonate and Polyethylene are investigated. Strain measurements are taken from strain gages mounted on the surface of the models which are excited at varying frequencies by a shaker table. Lumped parameter approximations of the continuous bodies are solved numerically on the digital computer for both fixed-free and free-free boundaries in order to determine the natural frequencies, mode shapes and relative strains. The method of characterisitcs is utilized in a wave propagation approach to obtain the response of a point in the model to a random input. The random input selected is white noise. The natural frequencies are obtained by performing a Fast Fourier Transform Analysis on the response.

Results of this portion of the investigation were published in the Shock and Vibration Bulletin, Bulletin 42, Part 5, pp. 227-234, January 1972. The paper is entitled "Longitudinal Vibration of Composite Bodies of Varying Area". A copy of the paper is included in the Appendixes.

B. Shock Mitigation Model

Many materials, e.g., rigid polyurethane foam, exhibit elastic, perfectly plastic stress-strain curves until compaction occurs at large strains. Stresses greater than the yield stress cannot be transmitted by such materials until compaction occurs. An investigation has been initiated using a lumped parameter spring mass analysis (for the constant area case) and a multiple spring mass analysis (for the changing area case), see Figure 18.

The mitigator is divided into a series of masses connected by springs and dashpots, figure 18. The force-deflection characterisitcs of the springs are related to the stress-strain relation of the mitigating material and the cross-sectional area of the corresponding mass. A rigid, perfectly plastic or linearly work-hardening, locking stress-strain curve is assumed for the material, Figure 19. No deflection recovery is allowed upon unloading. The dashpot is considered a locking device and can be used to incorporate strain rate effects.

The following experiments were performed to verify the theoretical analysis. The tests consist of impacting cylindrical and conical mitigators with cylindrical projectiles and measuring the transmitted force, Figure 20. The stress and strain distributions obtained in such dynamic compression tests will be compared with those calculated from the theoretical analysis. Two of the test results of the transmitted strain measurements are shown in Figures 21 and 22 for cylindrical and conical mitigators, respectively. It was observed that the transmitted strain did not remain at a constant level as expected for the constant area case. This drop in strain could be due to the strain-rate effect, since the rate of strain decreases as the mitigator is being crushed, thereby lowering the yield strength of the mitigator.

The projectile energy was varied by varying both the projectile mass and velocity. The energy absorbtion capability of the foam was varied by varying the length of the mitigator. In the future, the energy absorption capability will be varied by varying the foam density.

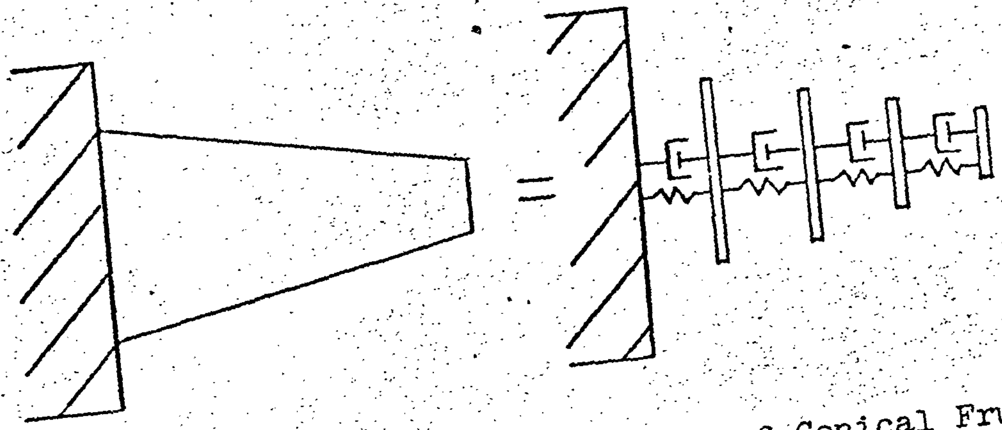

Figure 18 Multiple Spring Mass Model of Conical Frustrum

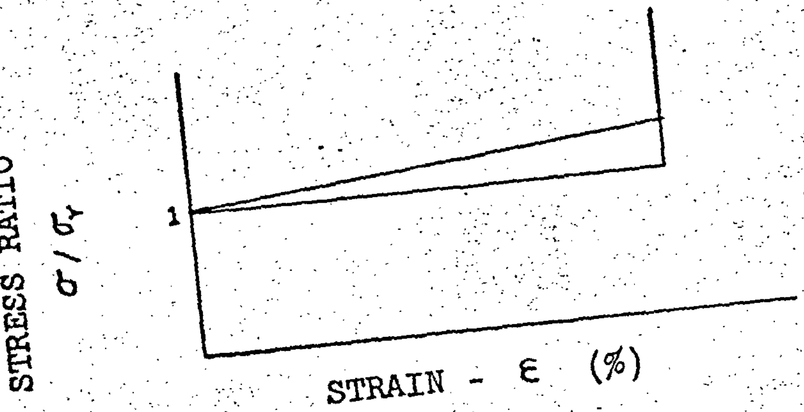

Figure 19 Stress-Strain Law for Foam Material

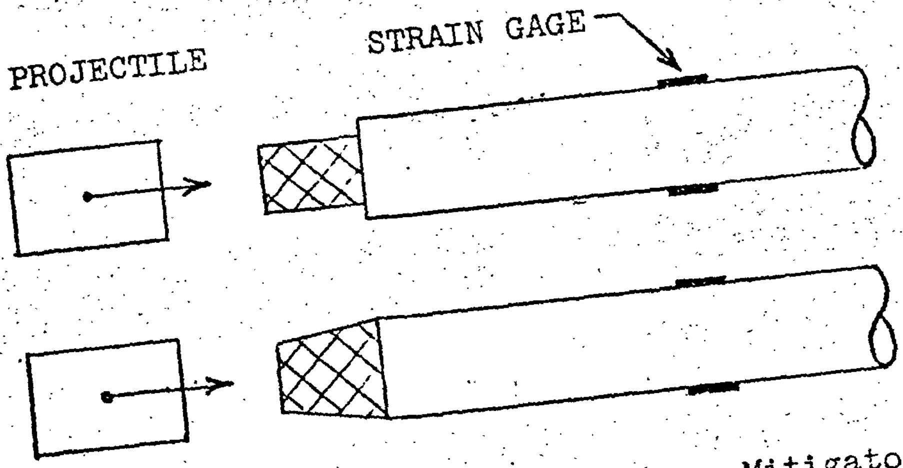

Figure 20 Experimental Test on Foam Mitigators

Figure 21 Typical Transmitted Strain with Cylindrical Mitigator

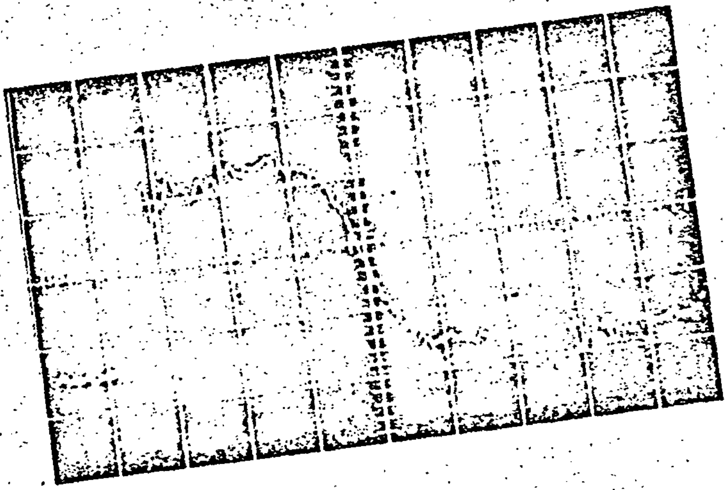

Figure 22 Typical Transmitted Strain with Conical Mitigator

APPENDIXES

APPENDIX A A72-25415	"Experimental and Theoretical Investigation of Stress Wave Attenuation in Fiber Reinforced Composites", by J.C.S. Yang and C.Y. Tsui, 8 pages.
APPENDIX B	'The Propagation of Elastic Stress Waves in Discontinuous Structures", M.S. Thesis by S. Limpisvasti, 53 pages.
APPENDIX C	"Radial Elastic-Plastic Stress Wave Propagation with an Unloading Shock in a Circular Disk by the Method of Characteristics and Successive Elastic Approximations" Ph. D. Thesis by D.W. Seaton, 93 pages.
APPENDIX D	"Longitudinal Vibration of Composite Bodies of Varying Area" by D.J. Guzy, J.C.S. Yang and W.H. Walston, Jr., 9 pages.

A72-25415

APPENDIX A

(8 pages)

Experimental and Theoretical Investigation of Stress Wave Attenuation in Fiber Reinforced Composites

APPENDIX B

(53 pages)

The Propagation of Elastic Stress Waves in Discontinuous Structures

The Propagation of Elastic Stress Waves in Discontinuous Structures

by

S. Limpisvasti, C. Y. Tsui and J. C. S. Yang

May 1972

Prepared for

NASA Ames Research Center

Structural Dynamic Branch

Moffett Field, California

Under Contract NGR 21-002-292

FOREWORD

This appendix is submitted in partial fulfillment of Contract NGR 21-002-292. It is also submitted by S. Limpisvasti to the Graduate School of the University of Maryland in partial fulfillment of the requirement for the Degree of Master of Science in Mechanical Engineering, 1972.

ABSTRACT

Title of Thesis: THE PROPAGATION OF ELASTIC STRESS WAVES IN DISCONTINUOUS STRUCTURES

Supachai Limpisvasti, Master of Science, 1972

Thesis directed by: Drs. C. Y. Tsui and J. C. S. Yang

The propagation of elastic stress waves of various pulse durations in cylindrical rods with grooves, holes, threaded holes and threaded holes with screws were investigated both experimentally and analytically.

In the experimental tests, the input stress pulse was generated in the configured aluminum rod by the impact of a projectile issuing from an air gun. Dynamic strain gages were used as the sensing device.

Analytical results were obtained by the method of characteristics for one dimensional wave propagation.

The effects of various sizes of grooves, holes, etc. on elastic stress wave propagation were examined and the decay of stress in regions close to the section of discontinuity was also studied.

ACKNOWLEDGEMENTS

I would like to thank foremost my thesis advisors Drs. Chung Y. Tsui and Jackson C. S. Yang for their suggestions of the thesis topic and for their guidance through out this research program. This thesis could not possibly have been accomplished without their very helpful advice. Their untiring attention and guidance to every detail during the conduct of the experiments and the writing of this thesis were very valuable. Appreciation is also given to Mr. Harry G. Appel for his suggestions in the making of the specimen. This research was supported under NASA Grant NGR 21-002-292.

TABLE OF CONTENTS

Chapter Page

LIST OF FIGURES

LIST OF SYMBOLS

A = area of bar

A_o = unstrained area of bar

a = Lagrangian coordinate

A_h = area of hole

C = velocity of propagation of a wave front with respect to the body

E = modulus of elasticity

g = shift rate of wave front

L = length of bar

M = mass

t = time

u = particle velocity

x = Eulerian co-ordinate

ε = strain

ρ = density

ρ_o = unstrained density

σ = stress

φ = impact function

m = mass flow rate

μ = micro

INTRODUCTION

Recently, increasing interest has developed in the transient response of structural elements involving the propagation of elastic stress waves. Among the different methods used in these investigations, a numerical method based on the integration of the characteristic equations along characteristic lines has proved to be simple and accurate. Chou with Mortimer (1) used this method to find the solution of the propagation of discontinuities in one dimensional plane elastic wave and then with Koeing (2) to find solutions of a step input stress for one dimensional cylindrical and spherical elastic waves. Also, Meng and McNiven (3) analyzed the transient excitation of an elastic rod by this method.

The method of characteristics is not restricted to single layer, homogeneous, constant area, elastic structures. Yang and Hasset (4) investigated stress waves in multilayered axisymmetrical bodies of varying area. Mao and Rader (5) investigated the longitudinal stress propagation in non-uniform elastic and viscoelastic bars.

The purpose of this thesis is to investigate both experimentally and analytically the propagation of elastic stress waves due to an impact loading in discontinuous structures such as rods with grooves, holes, threaded holes and threaded holes with screws.

For the analytical approach, the method of characteristics for one dimensional wave propagation is employed.

The distinguishing feature of impulsive loading arises from the fact that the action of a suddenly applied load is not simultaneously felt at all parts of the body. Parts of the body remote from the point of application of the load remain undisturbed until the stress wave in reaction to the load is propagated to those parts. The finite velocity of propagation of such waves depends upon inertial effects and upon mechanical properties of the material comprising the body.

The governing equation of the propagation of stress waves can be developed by means of either the Eulerian or the Lagrangian coordinate system. The Lagrangian coordinate system, however, exhibits one significant advantage over the Eulerian coordinate system in that the former provides a simpler expression for the law of conservation of mass. Therefore, in this thesis, the governing equation will be expressed in the Lagrangian coordinate system.

In the experimental investigations, strain gages were used as sensing devices to measure the strain caused by the propagation of the elastic stress wave in the specimen. Strain gages have been used by many investigators in such studies, giving very reliable results especially in the elastic range. Bickle (6) published the results of the use of strain gages for the measurement of propagating strain waves and applied them to many cases. Valather and Baker (7) used strain gages in investigating wave propagation and obtained good results. The input loading pulse is obtained by impacting various aluminum projectiles against the specimen with the aid of an air gun. The results will be analyzed and compared with analytical solutions.

CHAPTER I

THEORETICAL SOLUTION

In the theoretical analysis of stress wave propagation in the elastic region, three methods of solution are generally used, namely, the Laplace transformation method, the mode superposition method and the method of characteristics. In this thesis, the method of characteristics will be employed because the mathematics involved in the solution is simple and because the method can be applied very simply to any arbitrary input wave form.

The problem is easily described in the Lagrangian coordinate system with a single spatial variable, a, referred to the initial position of each layer of particles. In this system, the co-ordinate moves along with the particles which results in certain mathematical simplifications. In addition, since many strain measuring devices are attached to a set of particles and move along with these particles, the strain measurements are directly related to those predicted from this formulation.

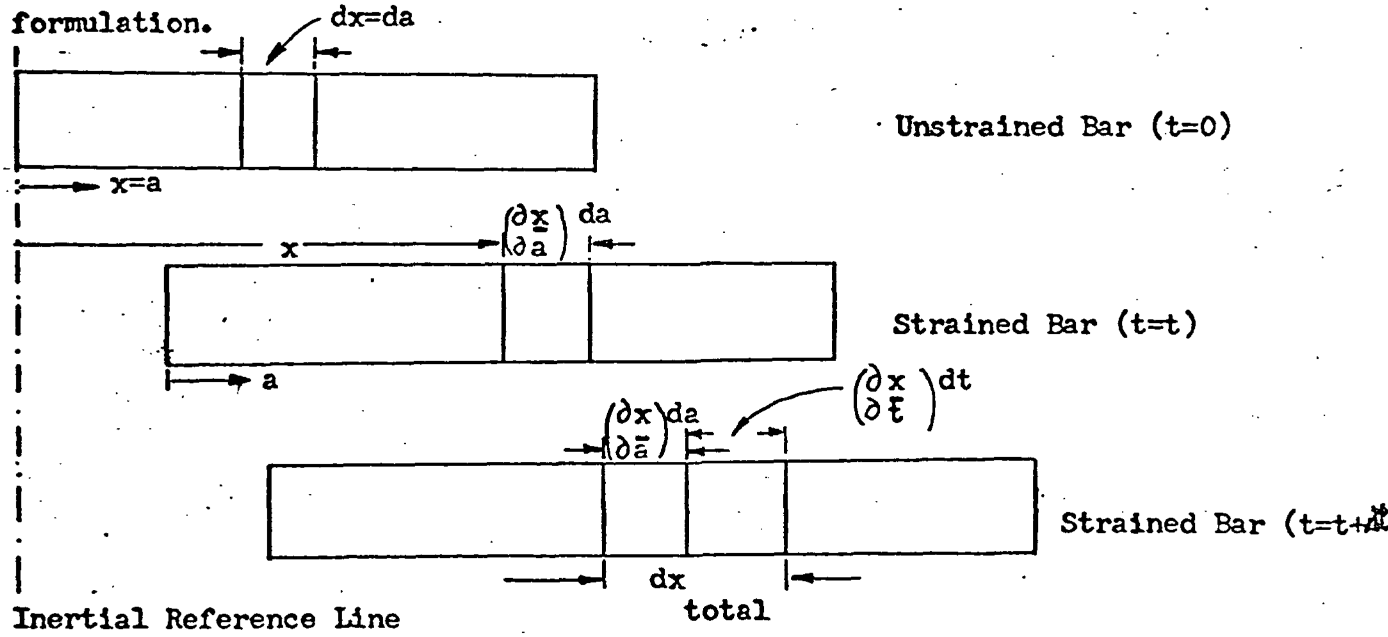

A. Method of Characteristics.

The particle velocity is defined as:

$$u = \left(\frac{\partial x}{\partial t}\right)_a$$

where x is the Eulerian coordinate, t is time and a is the Lagrangian coordinate. Since the engineering strain is caused by the change in x due to a change in a, it can be defined as:

$$\varepsilon = \frac{\left(\frac{\partial x}{\partial a}\right)_t da - da}{da}$$

or

$$\left(\frac{\partial x}{\partial a}\right)_t = 1 + \varepsilon \quad \text{.............................(1)}$$

For an infinitesimal alice of an object, the mass, M, will be the same for the strained and the unstrained conditions:

$$M = \rho_0 A_0 \, da = \rho A \left(\frac{\partial x}{\partial a}\right)_t da$$

$$\left(\frac{\partial x}{\partial a}\right)_t = \frac{\rho_0 A_0}{\rho A}$$

or

$$\frac{\rho_0 A_0}{\rho A} = 1 + \varepsilon \quad \text{..........................(2)}$$

Also, the rate of mass, m, entering the wave front will be equal to that leaving the wave front:

$$m = C \rho A = (C - du)(\rho A + d(\rho A))$$

where C is the velocity of proapgation of the wave front with respect to the object.

Therefore $$du = \frac{C\, d(\rho A)}{\rho A} \quad \text{.........................(3)}$$

According to momentum equation, the net force across the wave front is equal to the change in momentum across the wave front

$$-\sigma A_o - d(\sigma A_o) + \sigma A_o = -(C - du)\, m + Cm$$

$$m du = -d(\sigma A_o)$$

or, $$du = -\frac{A_o\, d\sigma}{C \rho A} \quad \text{.......................(4)}$$

Equating du yields, $$C^2 = -\frac{A_o\, d\sigma}{d(\rho A)}$$

From (2) $$d(\rho A) = -\frac{\rho_o A_o d\varepsilon}{(1 + \varepsilon)^2}$$

$$C^2 = \frac{(1 + \varepsilon)^2}{\rho_o} \frac{d\sigma}{d\varepsilon}$$

In the elastic region, the slope of the stress-strain curve is equal to the modulus of elasticity, giving

$$C^2 = (1 + \varepsilon)^2 \frac{E}{\rho_o}$$

which implies that the velocity of disturbance is depenent on strain. In Eulerian co-ordinate, the distance covered by the disturbance in time dt is,

$$dx = (u \pm C)\, dt$$

From the definition of total change in x

$$dx = \left(\frac{\partial x}{\partial t}\right)_a dt + \left(\frac{\partial x}{\partial a}\right)_t da$$

Equating the two equations yields:

$$\pm C = \left(\frac{\partial x}{\partial a}\right)_t da$$

Therefore, the wave speed in terms of the Lagrangian co-ordinate system is:

$$\frac{da}{dt} = \pm \frac{C}{\left(\frac{\partial x}{\partial a}\right)_t} = \pm \frac{C}{1+\varepsilon}$$

This wave speed is sometimes called the shift rate, g, in the solutions by the method of characteristics.

Therefore,

$$g^2 = \left(\frac{da}{dt}\right)^2 = \frac{C^2}{(1+\varepsilon)^2}$$

$$= \frac{E}{\rho_o} \quad \text{in the elastic region,}$$

or

$$g = \pm\sqrt{\frac{E}{\rho_o}}$$

Define the impact function φ as:

$$\partial\varphi = g\,\partial\varepsilon$$

or

$$\partial\varphi = \frac{1}{\rho_o}\frac{\partial\sigma}{g}$$

From Newton's law, the momentum equation of an infinitesimal slice of an object at constant time can be derived as;

$$\sigma A_o + A_o\frac{\partial\sigma}{\partial a}\,da - \sigma A_o = (\rho_o A_o\,da)\frac{\partial u}{\partial t}$$

or

$$\frac{\partial u}{\partial t} - \frac{1}{\rho_o}\frac{\partial\sigma}{\partial a} = 0$$

therefore

$$\frac{\partial u}{\partial t} - g\frac{\partial\varphi}{\partial a} = 0 \quad \text{......................} (5)$$

Differentiating (1) with respect to t yields,

$$\frac{\partial}{\partial t}\left(\frac{\partial x}{\partial a}\right) = \frac{\partial u}{\partial a} = \frac{\partial\varepsilon}{\partial t} = \frac{1}{g}\frac{\partial\varphi}{\partial t}$$

therefore

$$g\frac{\partial u}{\partial a} - \frac{\partial\varphi}{\partial t} = 0 \quad \text{......................} (6)$$

Combining (5) and (6) yields,

$$\frac{\partial}{\partial t}(u - \varphi) + g\frac{\partial}{\partial a}(u + \varphi) = 0$$

and

$$\frac{\partial}{\partial t}(u + \varphi) - g\frac{\partial}{\partial a}(u + \varphi) = 0 .$$

Therefore $\frac{\partial}{\partial t}(u \pm \varphi) \mp g\frac{\partial}{\partial a}(u \pm \varphi) = 0$

But $d(u \mp \varphi) = \frac{\partial}{\partial t}(u \mp \varphi)\,dt + \frac{\partial}{\partial a}(u \mp \varphi)\,da$

$$\frac{d}{dt}(u \mp \varphi) = \frac{\partial}{\partial t}(u \mp \varphi) + \frac{\partial}{\partial a}(u \mp \varphi)\frac{da}{dt}$$

also $\pm g = \frac{da}{dt}$

Therefore $\frac{d}{dt}(u \mp \varphi) = \frac{\partial}{\partial t}(u \mp \varphi) \pm g\frac{\partial}{\partial a}(u \mp \varphi) = 0$

which is the Characteristic equation.

The equation establishes that, along the lines of slope $\mp g$

$(u \pm \varphi)$ equals to a constant.

B. Boundary and Initial Conditions.

At the interface of any two materials, the forces and the particle velocities are equal:

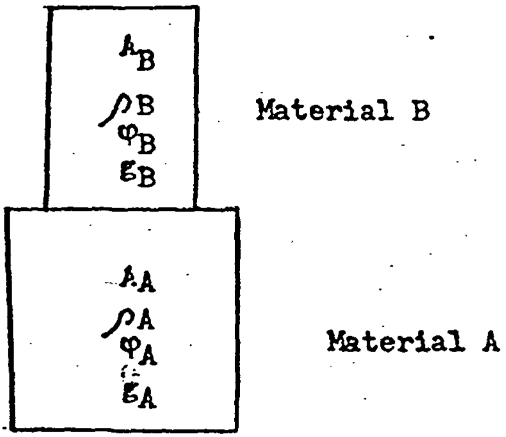

$$u_A = u_B \quad \text{.....(7)}$$

and

$$F_A = F_B \quad \text{......(8)}$$

In the elastic region:

$$F = \sigma A = \varphi \rho g A$$

Therefore

$$\varphi_A \rho_A g_A A_A = \varphi_B \rho_B g_B A_B$$

or

$$\varphi_A = \varphi_B \cdot \frac{\rho_B g_B A_B}{\rho_A g_A A_A}$$

If the structuresare of the same material the relationship above reduces to

$$\varphi_A = \varphi_B \cdot \frac{A_B}{A_A}$$

In this thesis the body of the specimen is initially at rest and undisturbed, and thus the field variables vanish identically ahead of the first wave front.

If, at time $t = 0$, a continuous particle velocity (or stress) is applied at the boundary, discontinuity in φ and u will propagated along with the wave front. The characteristic equation can be conveniently used to compute the magnitudes of the propagating discontinuities.

CHAPTER II

EXPERIMENTAL INVESTIGATIONS

A. Experimental Arrangements

Specimens are impacted by a projectile issuing from a 0.75 inch inside diameter air gun. The air gun consists of two main parts; a high pressure chamber and a barrel, 120 inches in length. It is mounted on a steel I- Beam and maintained at a horizontal level. Along the air gun barrel, vented holes are drilled to let out the air pressure behind the projectile to provide a constant impact velocity. The pressure chamber is pressurized by air from the air main.

In the experiments, the compressed air can be released by opening a solenoid valve operated by a 12 Volts D.C. battery. The projectiles made from machined aluminum rods of various lengths are loaded through the open end of the gun barrel. Two adjustable teflon supports are mounted on the I- Beam close to the open end of the air gun. Teflon was used to reduce the friction between the support and the specimen after it was hit by the projectile so that free impact could be achieved. (Fig. 1)

The specimens were machined from 10 inches long, 0.75 inch diameter aluminum rods to the proper configurations (Figs. 2 and 3). Four 0.25 inch long dynamic strain gages were mounted on each specimen as sensing devices. The gages were mounted in diametrically opposite pairs to cancel any stress due to bending effects.

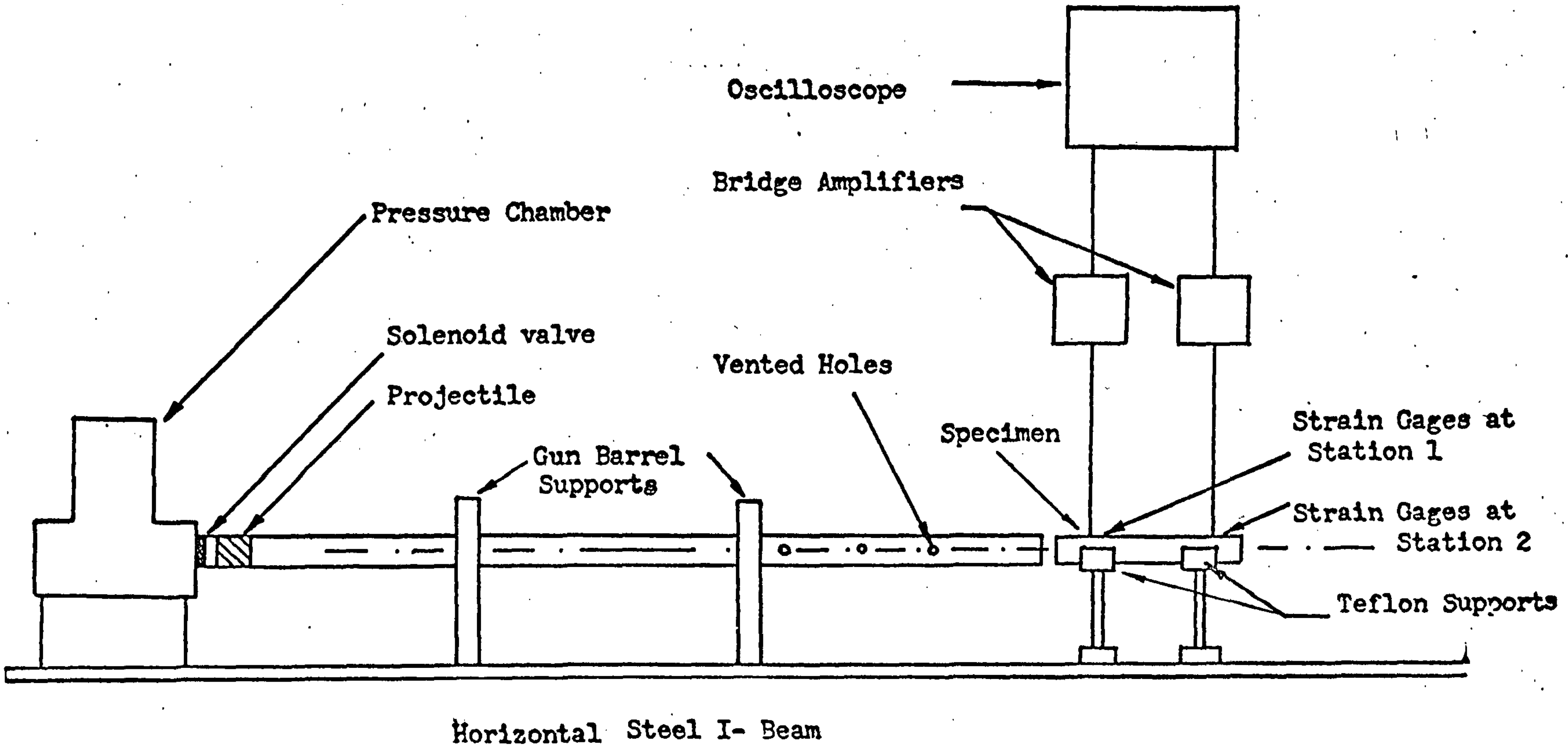

Fig. 1 Schematic Diagram of Experimental Set-up

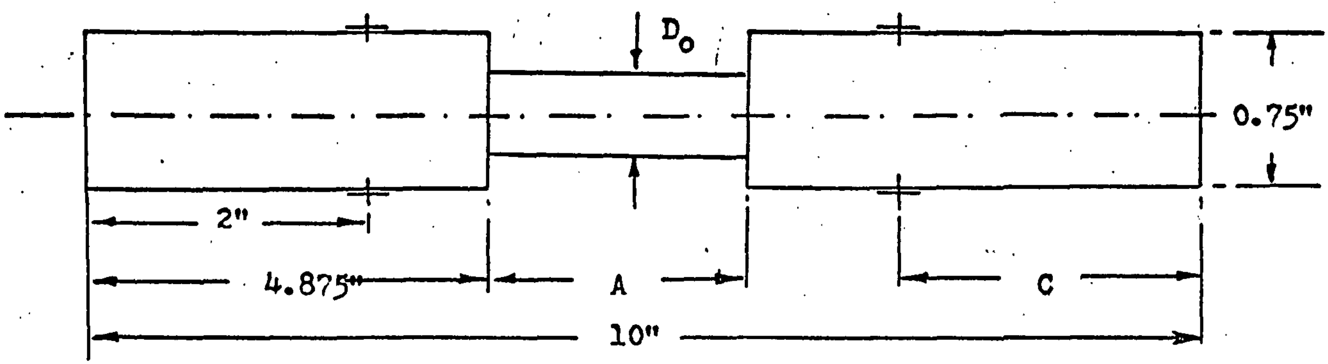

Experimental Parameters:

a. Length A : 0.125" to 2.937"

b. Length C : 2.00" and 3.00"

c. Diameter of Groove D_o : 0.70" to 0.40"

d. Length of projectile : 1.00" to 2.00"

Fig. 2 Grooved Specimen and the Experimental Parameters.

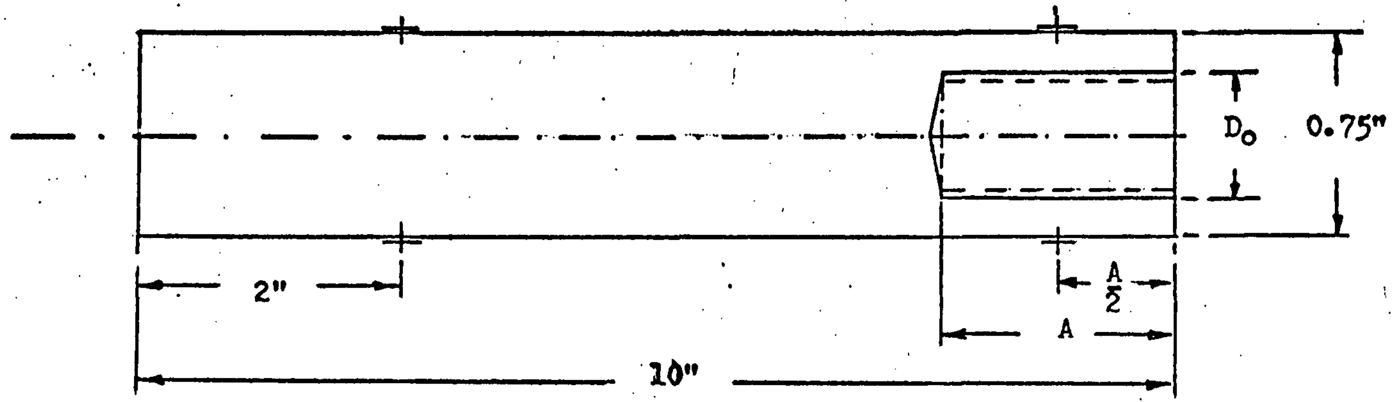

Experimental Parameters:

a. Depth of Hole A: 1.00" and 2.00"

b. Diameter of Hole D_o: 0.25" to 0.625"

(Plain Hole, Threaded Hole and Threaded Hole with Screw)

c. Length of Projectile: 1.00" to 2.00"

Fig. 3 Hole specimen and the Experimental Parameters

B. Experimental Procedure

Each pair of strain gages was connected to the opposite arms of the Wheatstone circuit of a bridge amplifier together with resistors as dummy gages. For discussion purposes, the location of the first pair of strain gages from the impact end of the specimen is called station 1, that of the downstream pair is called station 2, respectively. The bridge amplifiers were calibrated at the same gain for the consistancy of results. Every specimen was grounded to eliminate noise which might be introduced through the gages.

The output signals from the bridge amplifiers were connected to a dual beam oscilloscope. The signals from station 1 and 2 were given by the upper beam and the lower beam, respectively. The oscilloscope was set at internal trigger and single sweep mode using the signal from station 1 as the triggering signal.

Soon after the projectile hit the specimen, the first stress pulse which passes through gages at station 1 is transmitted through the bridge amplifier to the oscilloscope. The rising part of this pulse triggers the single sweep setting and gives the shape of the pulse. At the same time the lower beam which represents the signal from station 2 traces along the reference line until the gages "feel" the first stress pulse passing through.

The traces were recorded by a Polaroid scope-camera. An example of the recorded signals is given in Fig 4.

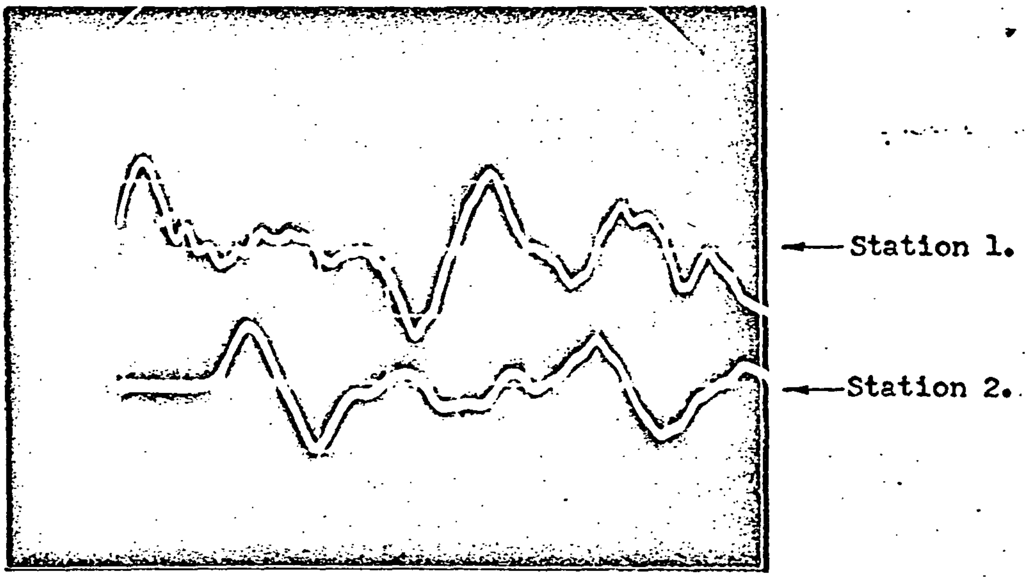

Sweep Rate	20 μsec/cm
Sensitivity	2 V/cm

Fig. 4 Example of the Recorded-Signals.

A complete list of major instrumentations and test facilities is given in Appendix II.

C. Experimental Programs.

To study the configuration effects in stress wave propagation, specimens were made with strain gages mounted at various positions as shown in Figs. 2 and 3. The tolerance of machining of the specimens was ± 0.005". In the grooved specimen (Fig.2), the length of the groove in one set of experiments was changed from 0.125" to 2.937" with the diameter of the groove held at 0.531". In another set of experiments, the diameter of the groove was changed from 0.40" to 0.70" with the length of the groove held at 2.00".

To study the effects of threads in stress wave propagation, experiments were conducted using specimens with plain holes, threaded holes and threaded holes with screws. The parameters were the depth and the diameter. The threads were American Standard and the sizes corresponding to the sizes of the holes being used in the investigations.

In all above experiments, three different lengths of projectile were also used.

To study the stress decay in regions close to a section of discontinuity, specimens similar to those in Fig. 2 were made. Three sets of experiments were conducted, in the first two sets the diameters of the grooves were held at 0.531" and 0.45" respectively while the length of the groove was varied from 0.125" to 2.50". In the third set of experiment, the distance from station 2 to the downstream edge of the groove was held at 0.10" while the diameter was changed from 0.40" to 0.70".

Experimental programs with the grooved specimen and the hole specimen are summarized in Tables 1 and 2.

TABLE 1

Experimental Program with Grooved Specimen

Length of Groove, A (in.)	Diameter of Groove, D_o (in.)	Projectile length (in.
0.125	0.700	1.00
0.250	0.600	1.50
0.500	0.575	2.00
1.000	0.550	
1.500	0.531	
2.000	0.525	
2.500	0.500	
2.750	0.475	
2.875	0.450	
2.937	0.400	
D_o = 0.531", C = 2.000"	A = 2.00", C = 2.00"	
D_o = 0.450", C = 3.000"	A = 2.00", C = 3.00"	

TABLE 2

Experimental Program with Hole Specimen

Depth of Hole = 1.00"		Depth of Hole = 2.00"	
Plain Hole D_o(inch)	Threaded Hole, Threaded Hole with Screw, D_o(inch)	Plain Hole D_o(inch)	Threaded Hole, Threadedhole with Screw, D_o(inch)
0.25	0.25	0.25	0.25
0.375	0.375	0.375	0.375
0.50	0.50	0.50	0.50
0.625		0.625	

* For all specimens, the length of projectile was varied as Table 1.

CHAPTER III

RESULTS, DISCUSSIONS AND CONCLUSIONS

A. Comparison of Experimental Results to Numerical Solutions

A computer written by Yang (Ref. 4, Appendix I) was used to obtain results to numerically check against those of the experiments. The 10" long specimen was divided into 100 imaginary layers of 0.1" in thickness. Because the computer program is based on the calculation along grid networks, the smaller the characteristic grid, the more accurate the results will be. For an input pulse of duration 20μsec and a wave speed of 0.2 inch/μsec in aluminum , the input pulse will be sampled into 20 sample periods of 1μsec. each. This sample period yields acceptable results.

At a boundary of discontinuity,(Fig.5), the stress magnitudes of the reflected and the transmitted waves are related to the magnitude of the incident wave by the formulas.

$$\sigma_r = \frac{\sigma_o (A_t - A_o)}{A_t}$$

$$\sigma_t = \frac{\sigma_o A_o}{A_t}$$

Where

σ_r = Reflected Stress

σ_t = Transmitted Stress

σ_o = Incident Stress

A_o = Original Area

A_t = Transmitted Area

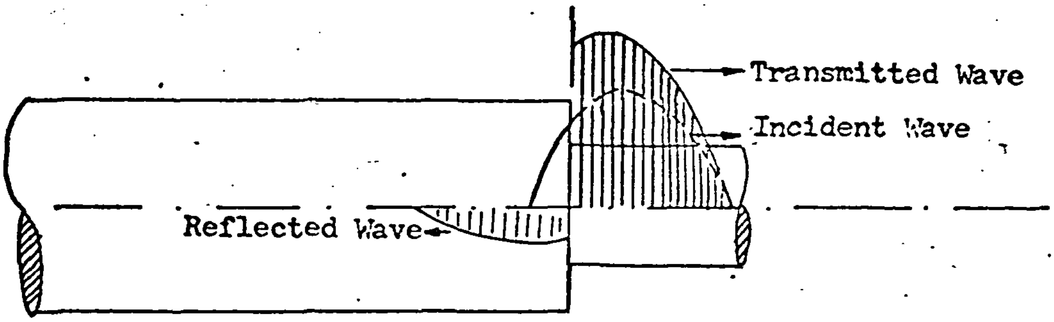

Fig. 5 Stress Wave at a Section of Discontinuity

The stress and particle velocity at the free end must satisfy the end conditions. In this case, the free surface can not be subjected to any longitudinal stress, therefore the stresses of the incident and reflected waves must add up algebraically to zero. The sense of the stress in the reflected wave is the opposite of the incident wave and the magnitudes are the same. The particle velocities for the reflected waves add up to double the particle velocity in the incident wave. (Fig 6)

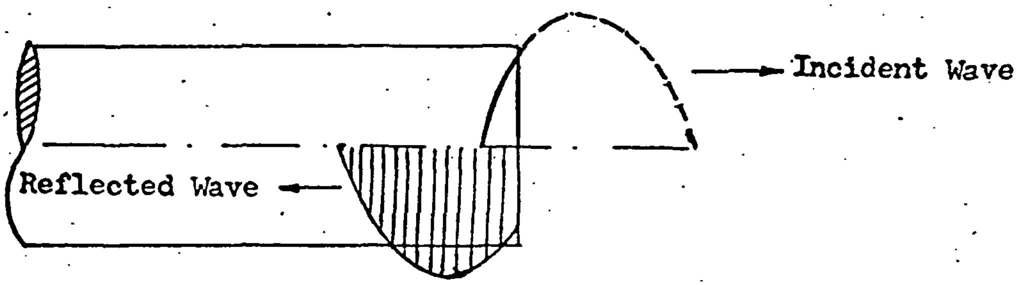

Fig. 6 Stress Wave at a Free End

Numerical computations were done for stress wave propagation in a grooved specimen and in a hole specimen. In the computations, the input stress pulse given by the gages at station 1 was approximated by a sine wave. The comparison of the numerical computations to the experimental results is very good as can be seen from Figs. 7 and 8.

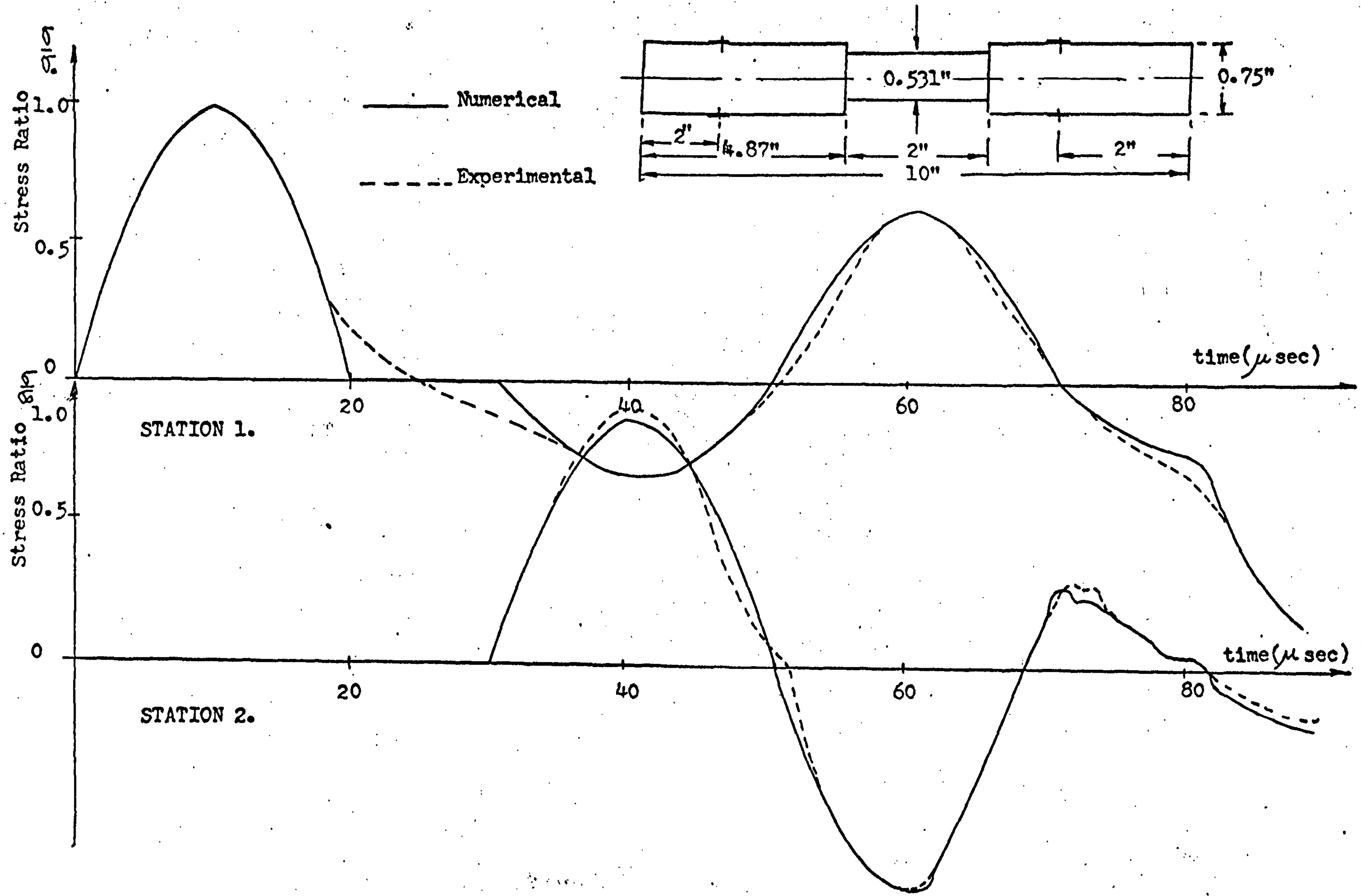

Fig. 7 Comparison of Experimental and Numerical Results in Grooved Specimen.

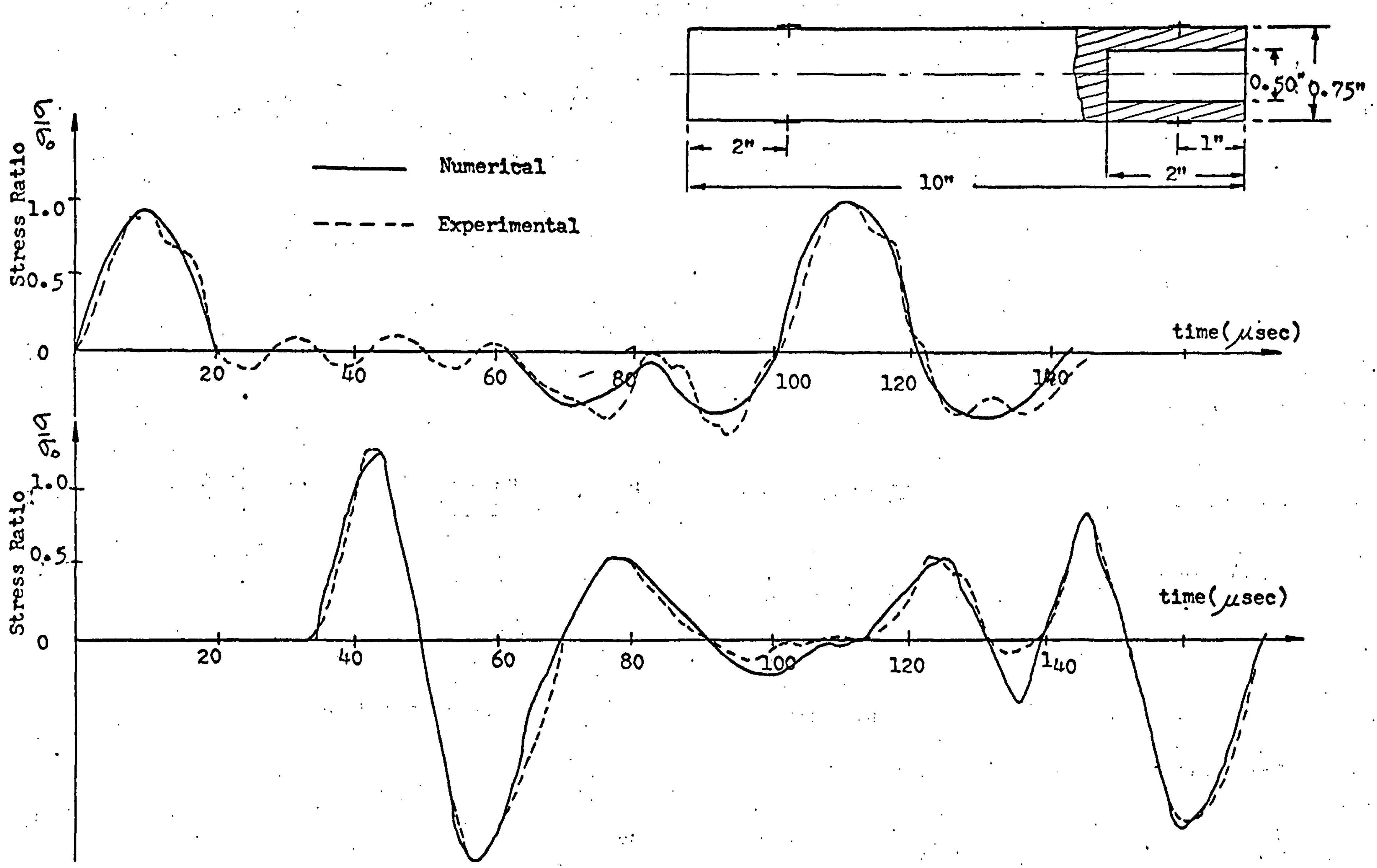

Fig. 8 Comparison of Experimental and Numerical Results in Hole Specimen

B. Configuration Effects.

1. Effects of Grooves, Holes, Threads, Threaded Holes and Threaded Holes with Screws.

As the stress wave propagates through the discontinuity, part of the wave is reflected and part transmitted; their magnitudes are dependent upon the area ratio at the boundary. This phenomenon repeats itself at the next discontinuity but with a time difference. The stress at any point in the specimen at any time is the algebraic sum of the magnitudes of the waves arriving at that point at that time.

A hole in a specimen constitutes a reduction in area in that section of the specimen. For one dimensional analysis and calculation of stress waves propagation, the hole section can be treated as a solid rod with a cross- sectional area A_r, smaller than that of the specimen.

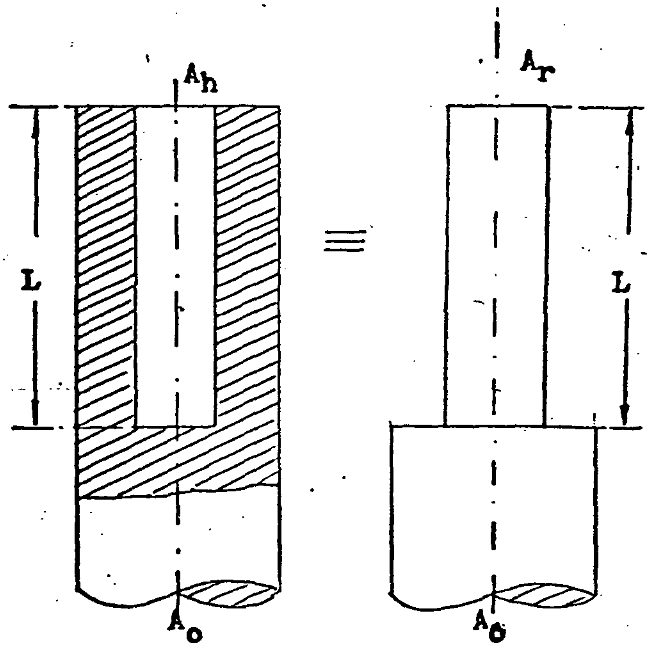

A_o = Cross-sectional Area of Specimen

A_h = Cross-sectional Area of Hole

A_r = Cross-sectional Area of Solid Rod

L = Depth of Hole

Fig. 9 Modification of Hole Parameters in Calculation.

For the threaded holes, American Standard taps of diameters equal to those of the plain holes were used.

In this case, the cross-sectional area is smaller than that of the plain hole due to the threads. Since the depth of the threads is small compared to the diameter (see Table 3), the overall effects to stress wave propagation are expected to be small. In calculations, an effective area of ($A_o - A_h + \frac{1}{2}A_t$) where A_t is the annular area of the thread can conveniently be used.

TABLE 3

American Standard Threads

Thread/inch	Outside Diameter (inch)	Thread Depth (inch)
20	0.25	0.019
16	0.375	0.037
13	0.50	0.040

When a screw is tighten in the threaded hole, the specimen theoretically will act as a solid rod. However, due to machining errors there are gaps between the threads and the screw which can be considered as a small hole in the rod.The magnitude of the stress is expected to be higher than that of the solid rod.

Experimental results of stress wave propagation in rods with hole threaded hole and threaded hole with screw are presented in Fig.10.

The comparison of the maximum stresses σ_{max} at station 2 to the input stress pulse σ_o , for the cases of plain hole, threaded hole and threaded hole with screw are plotted in Figs. 11 and 12.

From the plots, it can be seen that as the diameter of the hole becomes larger, giving smaller annular area for stress waves propagation, the stress peaks gradually increase. For the case of threaded hole with screw, the peak values approach a certain constant value slightly larger than that of the solid rod.

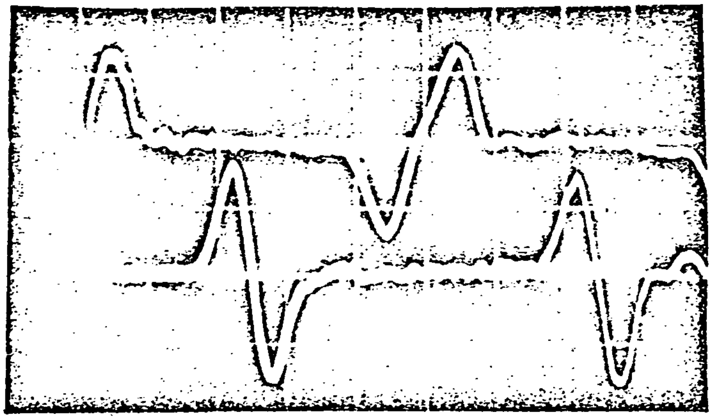

a) Plain Hole

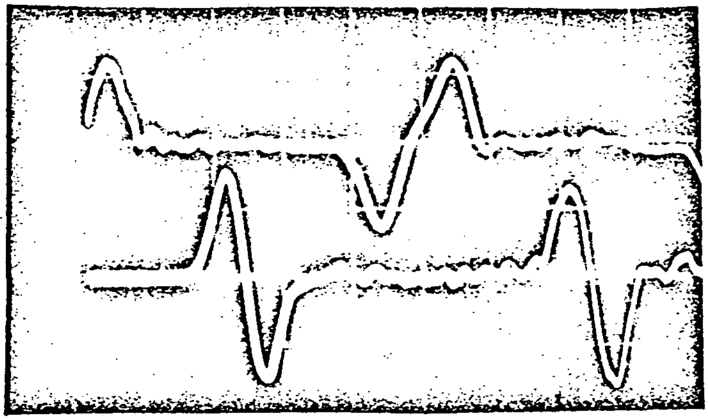

b) Threaded Hole

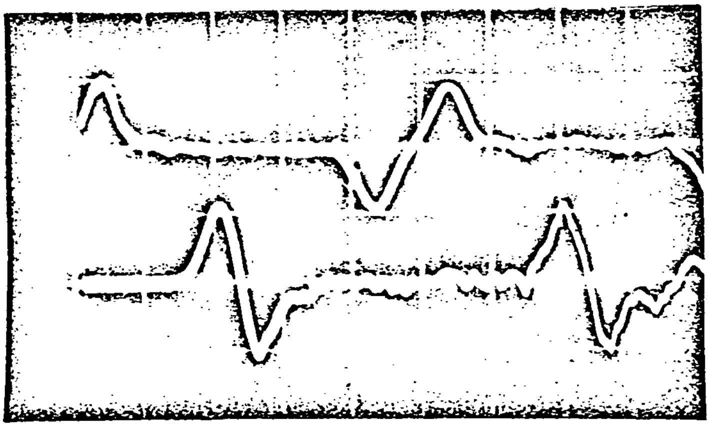

c) Threaded Hole with Screw

Fig. 10 Sample Results of Plain Hole, Threaded Hole and Threaded Hole with Screw in Stress Wave Propagation.

($A = 2.00''$, $D_0 = 0.25''$)

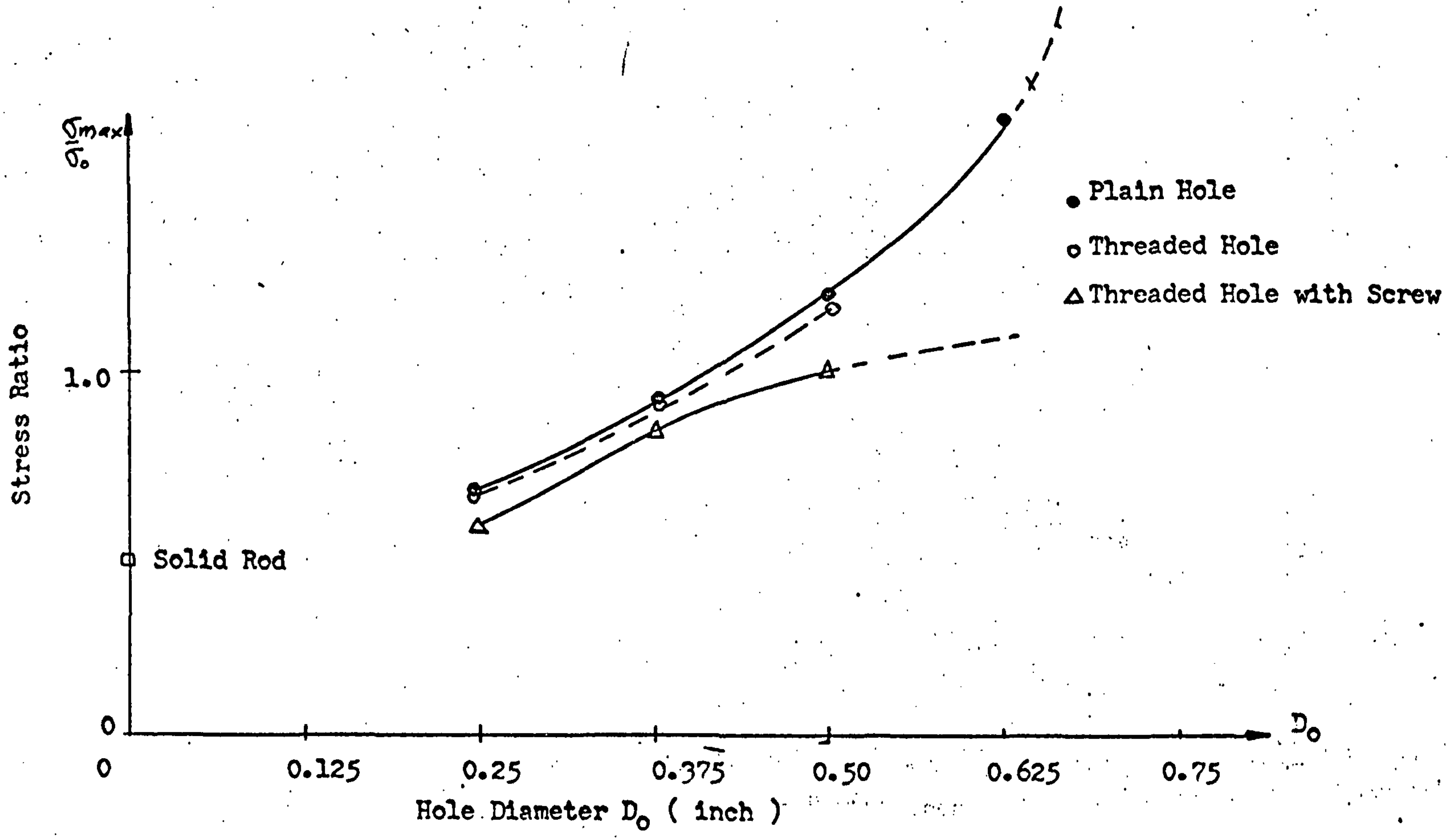

Fig. 11 Comparison of Maximum Stress in Plain Hole, Threaded Hole and Threaded Hole with Screw

(1" Deep Hole in 0.75" Diameter Rod)

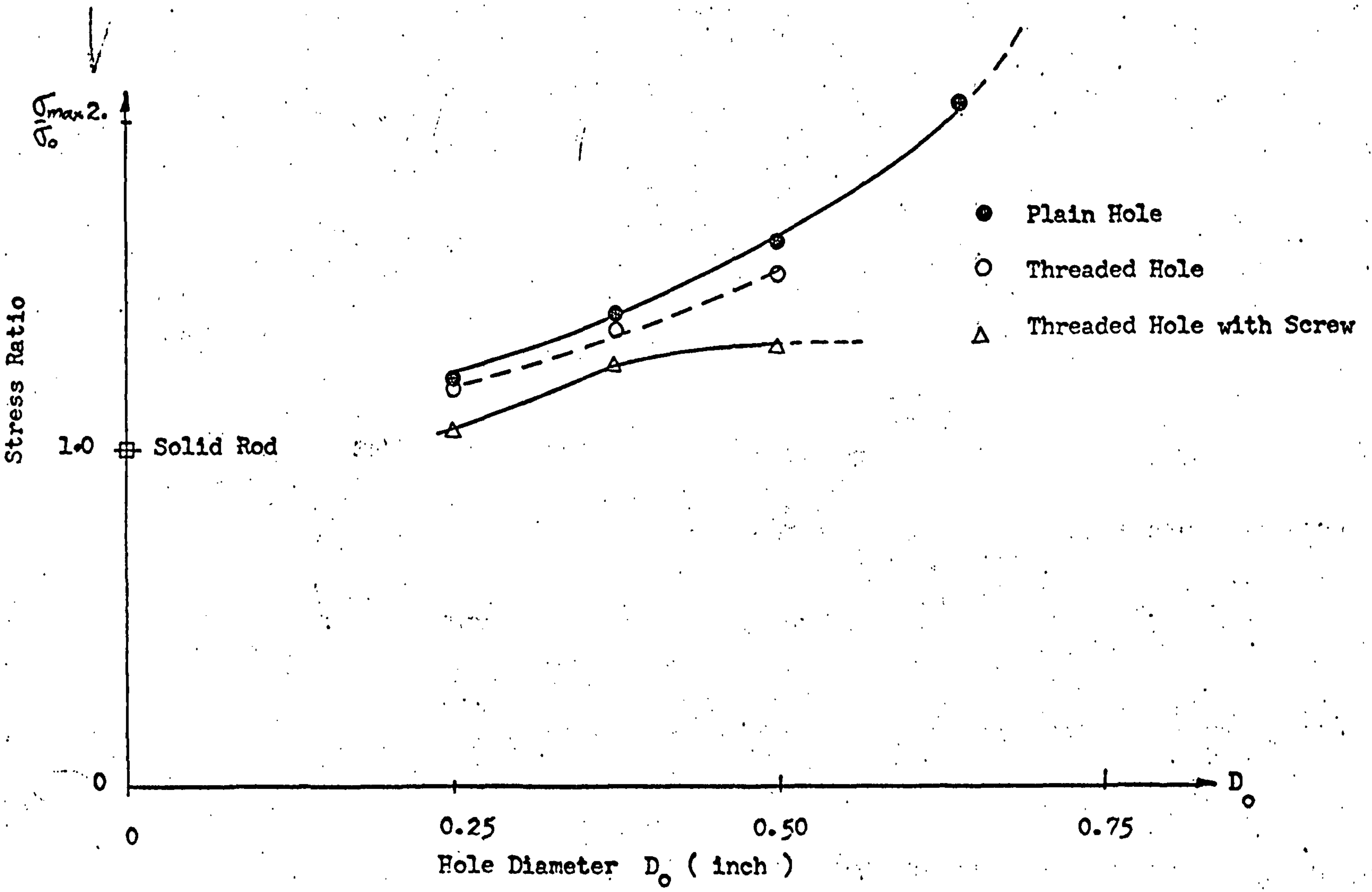

Fig. 12 Comparison of Maximum Stress in Plain Hole, Threaded Hole and Threaded Hole with Screw

(2" Deep Hole in 0.75" Diameter Rod)

2. Effects of the Length of Projectile

The stress wave is generated by collision of the projectile to the specimen. By the method of characteristics, it can be easily shown that the duration of the pulse is equal to twice the time elapsed T in stress propagating through the projectile's length. The field variables u and φ for the projectile and the specimen in Fig 13 show that contact will be maintained for a duration of 2T when $u_1 = u_1' = \frac{V}{2}$. After this duration, there will be no contact since $u_2' > u_3$.

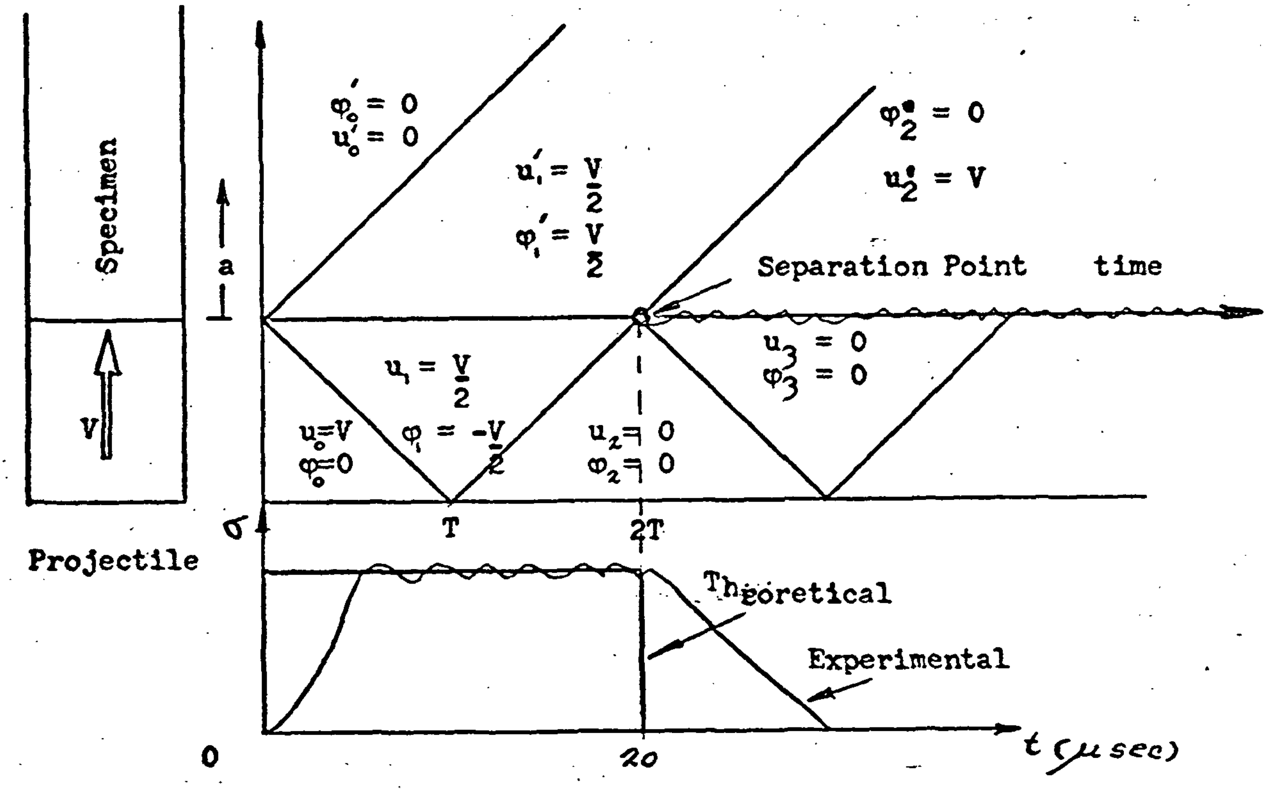

Fig. 13 Pulse Duration of a 2" long Aluminum Projectile

From the experiments, the duration of the applied pulse is slightly longer than theoretical result because the alignment in colliding is not perfect.

The experimental results of the pulse durations for the projectiles of length 1", 1.5" and 2" are shown in Fig 14.

a) 1" projectile pulse duration

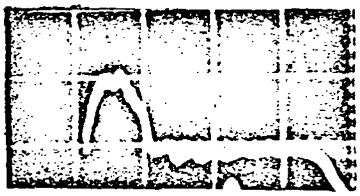

b) 1.5" projectile pulse duration

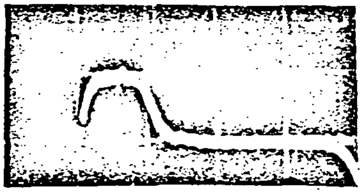

c) 2" projectile pulse duration

Fig. 14 Experimental Results Showing Change of Pulse Duration Due to Various Projectile Length

C. The Stress Decay in Regions Close to a Section of Discontinuity

The behavior of stress wave propagation in discontinuous structures resembles the flow of a fluid through pipes of unequal diameters (Fig. 15). It will be some distance downstreams from the discontinuous boundary before the stress resumes its predicted proper magnitude.

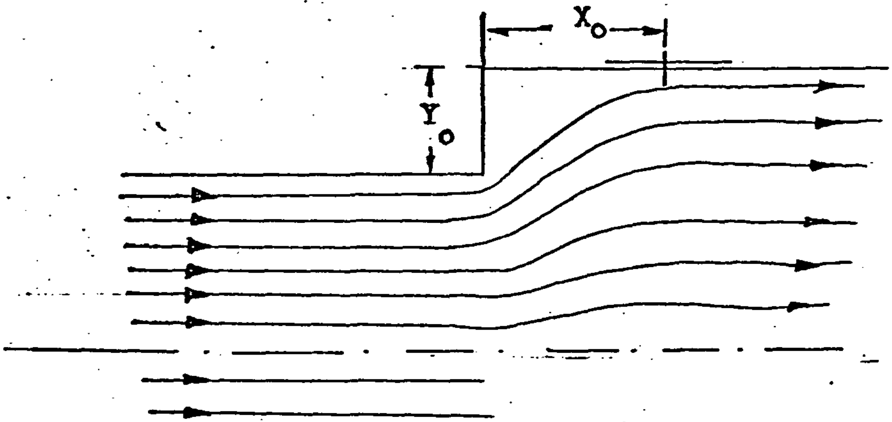

Fig. 15 Stress Flow Analogy at a Section of Discontinuity

To investigate the phenomenon of stress decay in the vicinity of an area of discontinuity, grooved specimens with step Y_o (Fig.15) were made with strain gages mounted at a distance, X_o, downstream from the section of discontinuity. The stress decay can be detected by comparing the first peak stress at station 2 to that obtained from the theoretical calculations. This first peak stress is the stress felt by the strain gages at station 2 as the input stress wave first swept by. For a sufficiently large value of X_o , the experimental and the theoretical peak stresses should be equal.

The program of investigation has been outlined in the section of Experimental Programs. Briefly, with Y_o =0.109", X_o was varied from 0.15" to 1.00". The result of the comparison of the peak stress, σ_{max} to the input stress σ_o, was plotted in Fig. 16. It can be seen that a distance $X_o = 3.4\ Y_o$ from the section of discontinuity is required for the stress to completely resume its predicted magnitude.

Additional experiments were conducted with X_o = 0.10" while Y_o was varied from 0.40" to 0.70". The ratio of σ_{max} to σ_o was plotted in Fig. 17. The result indicates that the gages at station 2 detect very little stress for value of $\frac{Y_o}{X_o} \geq 1.5$

A sample result of the experiment (X_o = 0.125, Y_o= 0.109", $\frac{Y_o}{X_o} \doteq 0.87$) as compared to the numerical solution is presented in Fig. 18.

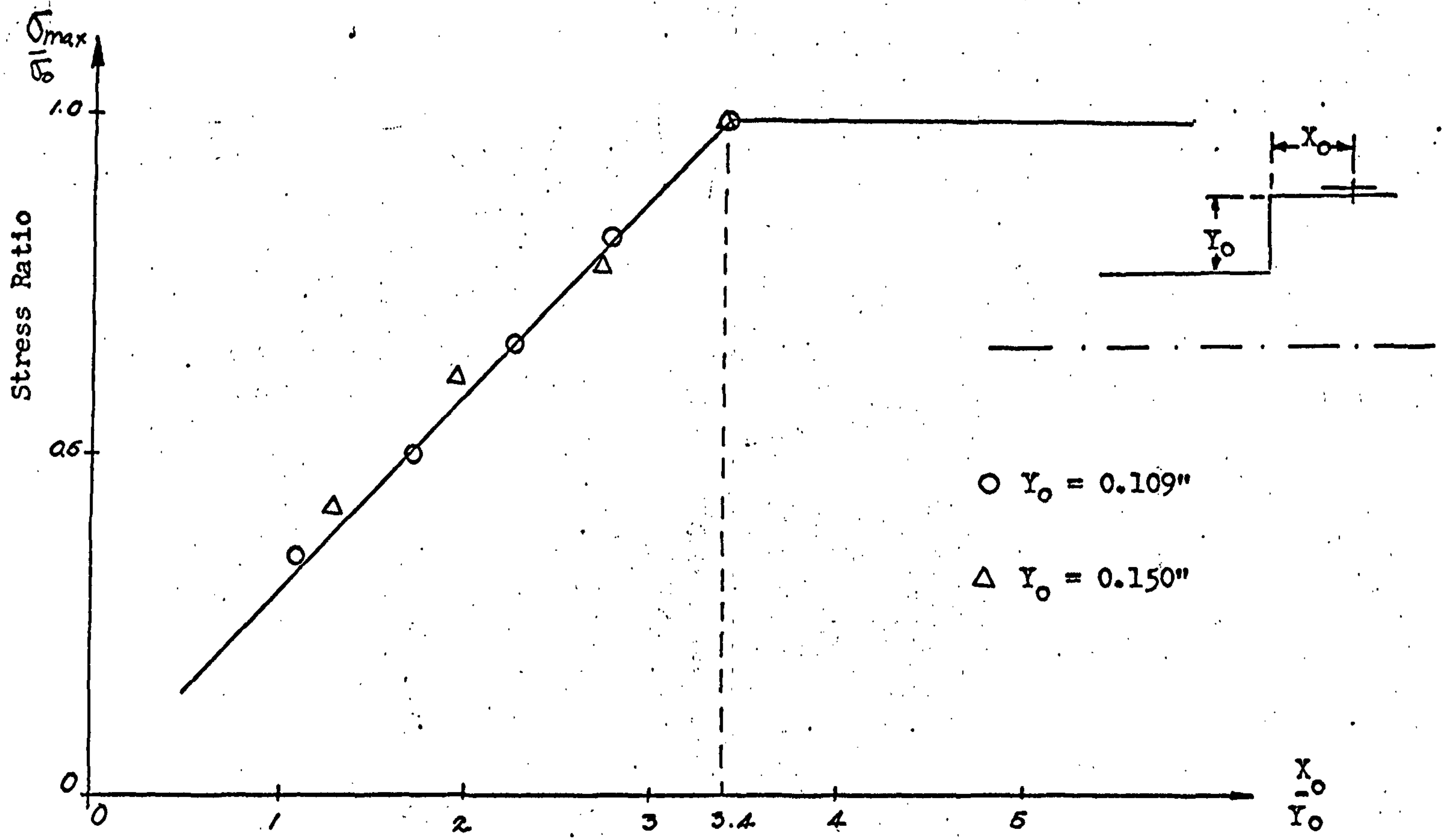

Fig. 16 Stress Decay in Regions Close to Section of Discontinuity

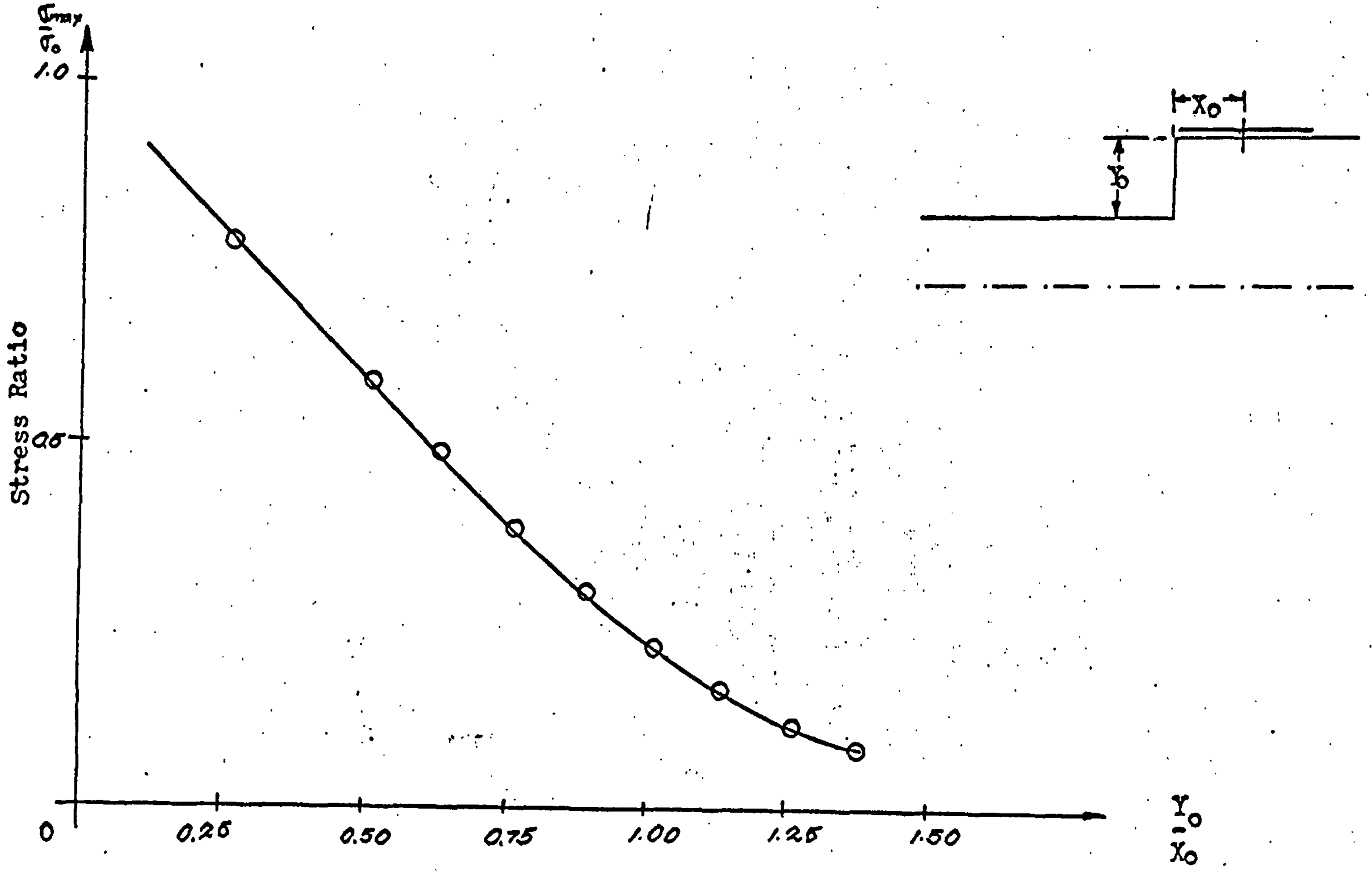

Fig. 17 Stress Decay in Regions Close to Section of Discontinuity (X_o = 0.100")

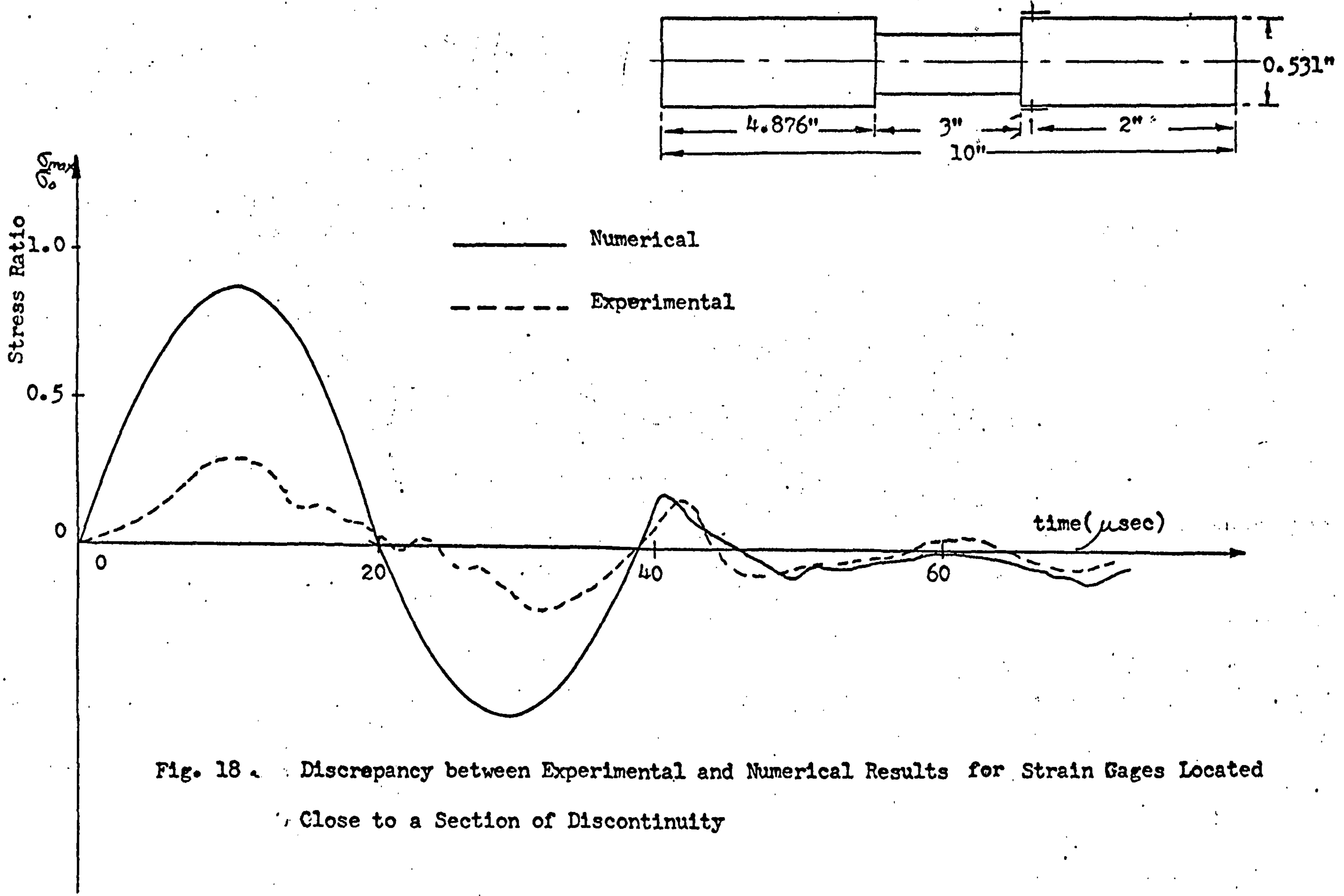

Fig. 18. Discrepancy between Experimental and Numerical Results for Strain Gages Located Close to a Section of Discontinuity

D. Conclusions and Recommendations

From the analysis of the experimental results, it is concluded that:

1) It is possible to apply one dimensional wave theory to obtain stress information for discontinuous structures. (A computer program has been written for the purpose of obtaining such information.)

2) Small discontinuity in structures such as threaded hole, threaded hole with screw has little effect in stress wave propagation. In the analysis plain holes using an average area can conveniently be used in place of the threaded holes. For design purposes, structures consisting of threaded holes and threaded holes with screws can be conservatively approximated using dimensions of the plain holes.

3) As in the cases of fluid flow through the pipe sections, streamlining will not be reached until some distance downstream. Stress wave propagation shows the same behavior. Experimental results indicate that to obtain the proper stress magnitude, strain gages should be placed at a distance from the section of discontinuity at least equal to 3.4 times the length of the step.

APPENDIX I

NUMERICAL PROCEDURE AND COMPUTER PROGRAM (Ref. 4)

Consider the grid system of the characteristic lines in the a-t plane as shown in Fig 19. The ordinate $a = a_1$ represents the boundary of the specimen, where the inputs(external disturbances) are applied. The numerical procedure involving stepwise integration along the characteristics of $u \pm \varphi$ = constant along the line of slope $\mp g$ is employed to compute the response for various inputs. The stresses and the particle velocity are calculated at all grid points.

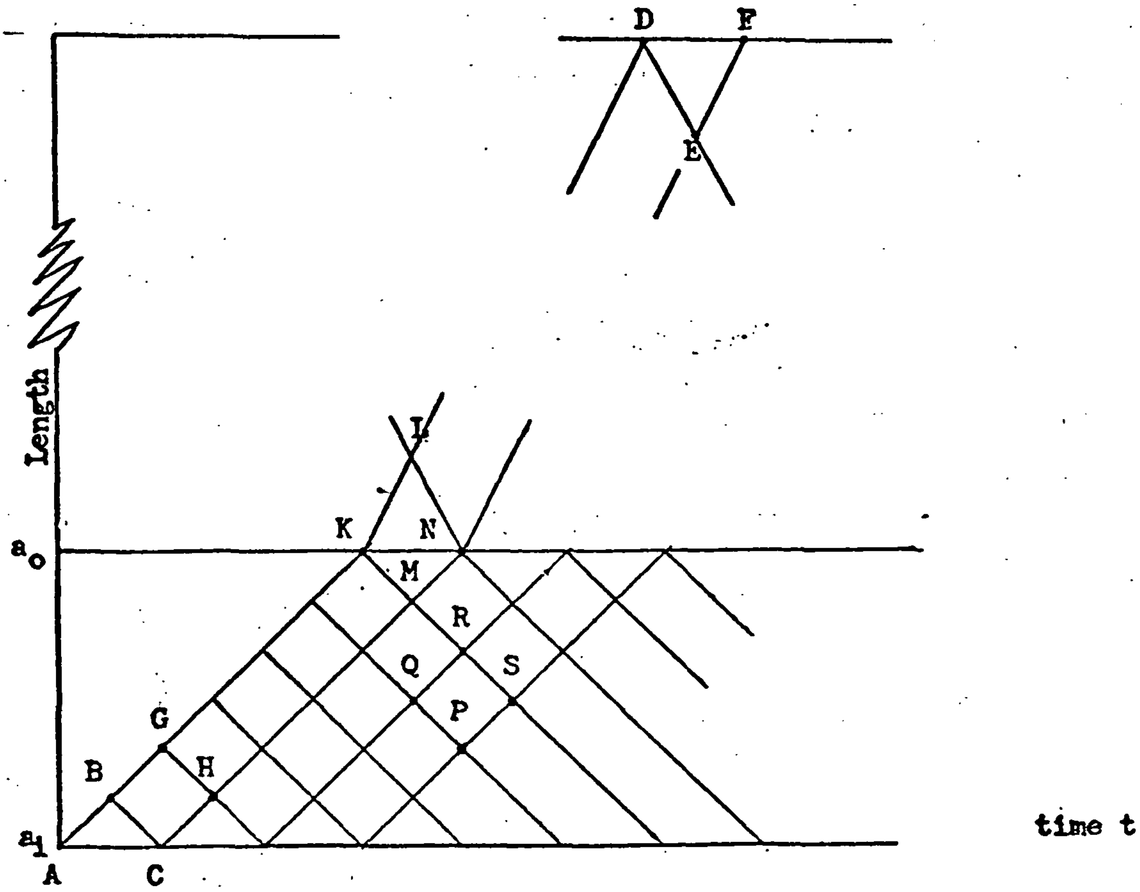

Fig 19 Characteristic Network

Since the external input has a finite rise time, φ and u are identically zero along the wave front A B G the grid points are devided into 3 groups

- interior points
- boundary points
- interface points

Boundary Points

Along the boundaries at $a = a_i$ and $a = a_o$ one of the two variables φ and u is perscribed as a function of time. The remaining variable may be determined by representing the characteristic equation in finite difference form along the characteristic curve referring to Fig 19, since the field variables vanished at A and B for the interior boundary $a = a_i$, only the equation along g - (C to B is used). For the exterior boundary $a = a_o$, only the equation along g + (E to F) is employed.

Interior Points

The field variables vanish at B and G, and they have been computed at the boundary point C, the value of φ and u at the grid point H can then be computed by employing the characteristic equations in finite difference form along CH (g+) and GH (g-)

The computation at other interior points proceeds step by step procedure. Thus, to compute the field variables at S , we employ the values at P and R, which have previously been computed, and we use the characteristic finite difference equations along g- and g +, respectively.

Interface Points

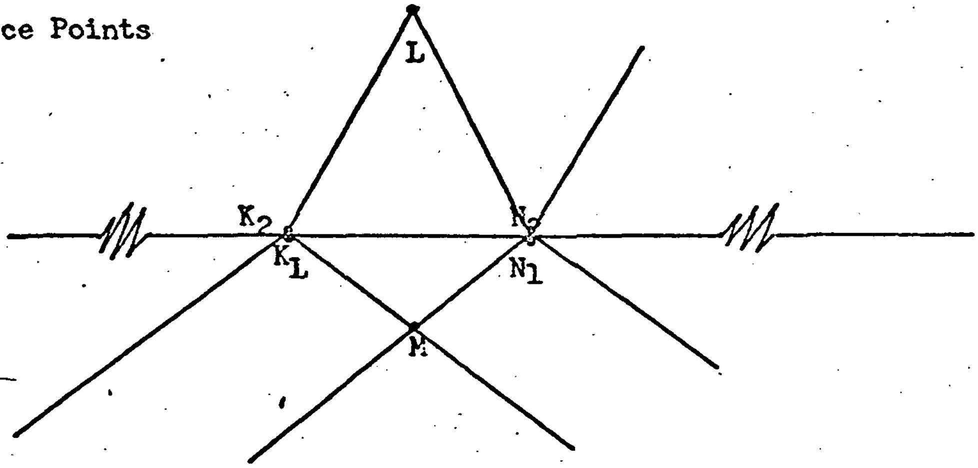

Fig 20 Detail of Grid at Interface

To compute the field variables near an interface, we consider the points N_1 and N_2 , which are located on different sides of an interface, but very close to the interface, as shown in Fig 20. There are altogether four unknown field variables at the points N_1 and N_2 . Above the interface, the characteristic equation along N_1 can be utilized. Underneath the interface, we can use the characteristic equation along LN_2. Two additional equations, adding to a total of four equations, are obtained from the interface conditions (7) and (8), which relate the field variables at N_1 and N_2.

The four field variables at the interface can thus be computed by solving four algebraic equations simultaneously.

The computations described above were carried out on a digital computer. It is apparent that the smaller the characteristic grid, the more accurate the numerical results will be.

Care must be exercised to ensure that the $g+$ characteristic lines reaching an interface meet up with the $g-$ characteristics of the next layer which carry the reflected waves from the next interface. This can be accomplished by relating the increments Δa in the ith and (i+1)th layer by the relation

$$g_i \Delta a_i = g_{i+1} \Delta a_{i+1}$$

where g_i and g_{i+1} are the dilatational wave speed in the ith and (i+1)th layers.

```
@RUN TODBAR,306-01-122,YANG
@FOR,IS MAIN
C               C(N)= C(I)/C(I+1)  RATIO OF WAVE VELOCITY
C               E(N)= E(I)/SO      RATIO OF MODULING TO INPUT STRESS
C               K IS THE NO OF LAYERS
C              KK(N) IS THE LAST GRID PT. OF EACH LAYER
C               V(N) IS THE POISSON RATIO
C               S(2,I) IS THE RADIAL STRESS
C               U(2,I) IS THE PARTICLE VELOCITY
C                  JT.JE IDENTIFIES THE TRIANGULAR INPUT
C               L IS THE TIME THAT PROGRAM ENDS
      DIMENSION U(2,1000),S(2,1000)
      DIMENSION KK(3),H(2)
      REAL J1,JT
      READ 1,L,K,JT
    1 FORMAT (2X,2I4,F5.1)
      READ 2, H(1),H(2)
    2 FORMAT (2X,2F5.3)
      READ 3,KK(1),KK(2),KK(3)
    3 FORMAT (2X,3I4)
      K1=KK(K)
      DO 60 I=1,K1
      S(1,I)=0.
      U(1,I)=0.
   60 CONTINUE
      DO 500 J=2,L
      J1=J-1
      IF (J1-JT) 75,75,78
   75 R=J1/JT
      S(2,1)=SIN(3.1417*R)
      GO TO 90
   78 S(2,1)=0.
   90 U(2,1)=U(1,2)+S(1,2)-S(2,1)
      DO 400 N=1,K
      M=KK(N)-1
      IF (N-1) 124,124,125
  124 NI=2
      GO TO 126
  125 NI=2+KK(N-1)
  126 DO 130 I=NI,M
      S(2,I)=(U(1,I+1)+S(1,I+1)-U(2,I-1)+S(2,I-1))/2.
      U(2,I)=(U(1,I+1)+S(1,I+1)+U(2,I-1)-S(2,I-1))/2.
  130 CONTINUE
      IF (N-K) 140,420,420
  140 KMMM=KK(N)
```

```
      MM=KMMM+1
      MMM=KK(N)+2
      S(2,KMMM)=(U(1,MMM)+S(1,MMM)-U(2,M)+S(2,M))
      S(2,KMMM)=S(2,KMMM)/(1.+H(N))
      U(2,KMMM)=(U(1,MMM)+S(1,MMM)+H(N)*(U(2,M)-S(2,M)))/(1.+H(N))
      S(2,MM)=H(N)*S(2,KMMM)
      U(2,MM)=U(2,KMMM)
  400 CONTINUE
  420 KMMN=KK(K)
      S(2,KMMN)=0.
      U(2,KMMN)=U(2,M)-S(2,M)
  250 PRINT 255,J,S(2,1),S(2,21),S(2,82),S(2,83)
  255 FORMAT (2X,I4,4F10.6)
      DO 490 I=1,KMMN
      S(1,I)=S(2,I)
      U(1,I)=U(2,I)
  490 CONTINUE
  500 CONTINUE
      STOP
      END
```

APPENDIX II

LIST OF INSTRUMENTATIONS

ITEM	SPECIFICATION
Strain Gage	Micro-Measurement, Type ED-DY-125AD-350 Resistance 350.0 ± 0.3 % ohms. Gage Factor 3.2 ± 2.0% at 75° F Gage Length 0.25 inch
Bridge Amplifier	Ellis-Vishey Bridge Amplifier Model BAM-1B, Cutoff frequency 130,000 C/S
Oscilloscope	Textronix Type 551 Dual Beam Oscilloscope with 1A5 and CA Plug-in units
Wire	Alpha 4 Shielded Wire

BIBLIOGRAPHY

1) Chou, P.C. and Mortimer, R.W.; "Solution of One Dimensional Elastic Wave Problem by the Method of Characteristics" Journal of Applied Mechanics, Sept., 1967

2) Chou, P.C. and Koeing, H.A.: "A Unified Approach to Cylindrical and Spherical Elastic Waves by Method of Characteristics" Journal of Applied Mechanics, March, 1966

3) Meng, Y. and McNiven, H.D.; "Analysis of Transient Exitation of An Elastic Rod by Method of Characteristics" Int. Journal Solids Structures, Vol.6 pp.871 to 892, 1970

4) Yang, J.C.S. and Hasset, W.H.; "Stress Wave Propagation in Multilayered Axisymmetric Bodies of Varying Area" NOL. Tech. Report NOLTR 70-253, Dec.,1970

5) Mao, M. and Rader, D.;"Longitudinal Stress Pulse Propagation in Non-Uniform Elastic and Viscoelastic Bars" Int. Journal Solids Structures Vol.6 pp.519 to 538, 1970

6) Bickle, L.W.;"The Use of Strain Gages for the measurement of Propagating Strain Waves" Sandia Corp. Tech. Report SC-DC-70-5193, 1970

7) Valather, M. and Baker, W.E.;"Wave Propagation Resulting from Very High Impact Velocities" Journal of Applied Mechnanics, pp.555 to 557, June, 1971

APPENDIX C

(93 pages)

Radial Elastic-Plastic Stress Wave Propagation With an Unloading Shock in a Circular Disk by the Method of Characteristics and Successive Elastic Approximations

RADIAL ELASTIC-PLASTIC STRESS WAVE PROPAGATION WITH AN UNLOADING SHOCK IN A CIRCULAR DISK BY THE METHOD OF CHARACTERISTICS AND SUCCESSIVE ELASTIC APPROXIMATIONS

by
D. W. Seaton, J.C.S. Yang and A. E. Seigel

May 1972

Prepared for
NASA Ames Research Center
Structural Dynamics Branch
Moffett Field, California
Under Contract NGR 21-002-292

FOREWORD

This appendix is submitted in partial fulfillment of Contract NGR 21-002-292. It is also submitted by Donald W. Seaton to the Graduate College of University of Maryland in partial fulfillment of the requirements for the degree of Doctor of Philosophy in Mechanical Engineering 1972.

ABSTRACT

Title of Thesis: Radial Elastic-Plastic Stress Wave Propagation
with an Unloading Shock in a Circular Disk by
the Method of Characteristics and Successive
Elastic Approximations

Donald W. Seaton, Doctor of Philosophy, 1972

Thesis directed by: Dr. Jackson C. S. Yang
Dr. Arnold E. Seigel

The purpose of this work was to investigate the problem of radial elastic-plastic stress wave propagation in a thin, finite, work hardening disk using the method of characteristics and the method of successive elastic approximations. In this method the characteristic equations, derived for the elastic case, are applied to the plastic regime by allowing the modulus of elasticity E and the wave speed C appearing in the equations to assume values corresponding to the tangent modulus of the plastic stress-strain curve. The value of Poisson's Ratio, ν, is taken as 1/2 in the plastic range.

Three characteristic equations were derived from the governing conservation and elastic constituent equations as outlined in a paper by Chou and Koenig. They were used subsequently, along with the Prandtl-Reuss incremental plasticity theory and the method of successive elastic solutions, to calculate the problem variables at the nodes of the characteristic network which was generated in a step-by-step fashion as the solution progressed.

A modest experimental program consisting of two experimental techniques was conducted to check the accuracy of the proposed analytical method. A circular disk was used with a hole at the center to accommodate a pressure pulse applied either hydraulically or explosively to the inner surface. The hydraulic method produced poor results and was discarded in favor of the explosive technique.

The disk material was 1100-0 aluminum which exhibits a 0.2 percent offset yield strength of 5000 psi and a proportional limit of 2500 psi. Strain-rate effects were not included in the theory.

Two 350 ohm Micro-Measurement strain gages were used in addition to a TEKTRONIX Model 551 dual beam oscilloscope to obtain radial and circumferential strain time histories at a radial distance of 0.75 inches on a 4 inch O.D. specimen.

A Piezotronics Model 109A ballistics pressure transducer was used with one channel of a second Model 551 TEKTRONIX dual beam oscilloscope to record the applied pressure pulse. A computer program incorporating the analytical procedures described previously was used to check the strain histories measured on the specimens. In addition, the theoretical solutions for a ramp followed by a steady state pressure were run as approximate checks against the known, closed form, static elastic and elastic-plastic solutions for a thick-walled cylinder.

Reasonable agreement between the theoretical and experimental results supports the hypothesis that this method can be used to solve problems of wave propagation in systems subjected to combined states of stress.

ACKNOWLEDGMENT

I would like to express my sincere appreciation to Dr. Jackson C. S. Yang and Dr. Arnold E. Seigel for their guidance and many helpful suggestions during the preparation of this thesis. A special word of thanks is also due Messrs. Richard E. Calkins and Edward A. Wallish for their extremely capable and conscientious effort in programming the material for computer solution. Also my sincerest thanks to Mrs. Elizabeth Boles for her very experienced and meticulous typing of the manuscript. Finally, I am indebted to my employer, Vitro Laboratories, for the liberal use of their IBM 360-65 computer facility and to a number of staff members of the United States Naval Ordnance Laboratory, White Oak, Maryland and the University of Maryland, notably Mr. Philip Aronson and Dr. C. Y. Tsui, for their advice and assistance in the experimental aspects of the project.

This project was partially financed by funds from the NASA Ames Research Center under contract NGR 21-002-292 with the University of Maryland.

TABLE OF CONTENTS

Section Page

LIST OF FIGURES

SECTION I

INTRODUCTION

The theoretical study of plastic stress wave propagation in solids first received serious attention in 1941 with the pioneering work of Von Karman and Duwez, later published in 1950 [1], and the concurrent work by G. I. Taylor in England [2] and Rakhmatulin in the Soviet Union [3].

Out of this work came a strain rate independent theory for the propagation of one-dimensional, plastic waves. However, as mentioned in [1], strain rate effects were observed in experimental results for which the rate of straining was reasonably above that encountered in static or quasi-static loading. Accordingly, later investigators such as Malvern [4] modified the basic governing equations to include the effects of strain rate which resulted in improved agreement between theoretical predictions and experimental results. Active research has continued in an effort to develop more accurate experimental techniques to test the validity of various theoretical formulations as evidenced, for example, by the work of Bell [5].

Considerable work is also being done on the propagation of combined states of stress in one or more spatial dimensions such as that presented by Clifton [6], Ziv [7], Chou and Koenig [8], Fyfe and Swift [9], and Lawrence [10].

It is the purpose of the present work to develop a method of solving the problem of radial elastic-plastic stress wave propagation with an unloading shock in a thin, finite, work hardening circular disk by combining the method of characteristics and successive elastic approximations utilizing the Prandtl-Reuss incremental plasticity theory. A computer program utilizing this method and included as Appendix D, calculates the time history of the problem variables. By using final values of the appropriate variables as initial values for a second run, the program can also simulate the case of repetitive loadings on a single specimen.

The results of a modest experimental program confirming the theoretical solution is also presented.

SECTION II

PROBLEM DESCRIPTION

As mentioned in Section I, the present work deals with the theoretical and experimental analysis of the propagation of elastic-plastic stress waves in a finite, circular disk with a central hole in which is initiated a symmetric, radial pressure pulse. The outer boundary of the disk is considered free.

The characteristic equations governing the propagation of elastic stresses and strains are derived in detail in Section III along with the relationships describing the method of successive elastic approximations. A thorough discussion of the computational procedures is given in Section IV. It is sufficient to say here that as the material is loaded into the plastic range, the elastic characteristic equations are applied in an incremental fashion to each of the characteristic network nodes which are generated one-by-one as the solution progresses. During this process the modulus of elasticity E, Poisson's Ratio, ν, and wave speed C, appearing in the elastic equations are adjusted to values corresponding to the local tangent modulus of the plastic stress-strain curve. The value of Poisson's Ratio, ν, is taken as 1/2 in the plastic range.

In addition to the propagation of elastic-plastic characteristics, the problem of an unloading shock wave is also treated. This occurs whenever the equivalent plastic stress at any radial coordinate decreases with time. The equations describing the unloading wave phenomena are also derived in Section III. It is assumed during unloading that reverse yielding does not occur.

During experimental testing two methods have been used to initiate the pressure pulse. The first consists of applying the pressure hydraulically by dropping a weight on a piston which compresses a quantity of water constrained in the central specimen hole. This procedure, however, yields unsatisfactory results. The second method uses a fuse ignited explosive charge and has been found to yield more realistic data.

For the sake of completeness the experimental fixture used in the hydraulic method and typical test measurements are included although computer solutions attempting to simulate these measurements are not presented, but instead are restricted to the results simulating the explosive tests.

As a result of the applied pulse, a stress wave propagates radially outward to the free surface where it reflects and propagates inward to repeat the cycle. The amplitude of the pulse has been chosesn so that the material behind the wave fronts is eventually stressed into the plastic range throughout a central, annular region of the disk. The state of stress is one of plane stress wherein only the radial and circumferential components are significant. There are, however, radial, circumferential, and axial components of strain.

The strain history is measured at one radial location with two 350 ohm Micro-Measurement strain gages mounted 90° from one another on the flat surface of the disk. The sensitive axis of one gage is oriented along the radial direction while the axis of the remaining one is positioned along the tangential or circumferential direction. (See Figure 1b.) The gage outputs are recorded on a Type 551 TEKTRONIX dual beam oscilloscope and polaroid film.

The input pressure pulse signature is measured with a Piezotronics quartz transducer, Model 109A, mounted in the support plate with the input surface centered immediately below the central hold in the specimen. (See Figure 1a.) The output of the transducer is also recorded on one channel of a Type 551 TEKTRONIX dual beam oscilloscope and on polaroid film.

A more complete description of the experimental procedure and a detailed sketch of the apparatus can be found in Section V and Figures 1a - 1e respectively.

SECTION III

DEVELOPMENT OF GOVERNING EQUATIONS

If we consider an infinitesimal element removed from a sector of a disk and subjected to a circumferentially symmetrical state of plane stress as shown in Figure (2), we may easily show that the equilibrium equation in the radial direction is

$$\frac{\partial \sigma_r}{\partial r} + \frac{\sigma_r - \sigma_\theta}{r} = \rho \frac{\partial v}{\partial t} \qquad 3\text{-}1$$

Here, and in what follows, we are referring to polar, Lagrangian type coordinates where the origin of the coordinate system is fixed at the center of the disk. There is no equilibrium equation in the θ-direction since we are assuming circumferential symmetry. Furthermore, since plane stress is being considered there are no stress components in the Z- direction. Two other equations which are at our disposal include the elastic constituitive equations; i.e., the stress equations in the r, θ, and z directions. It will be seen, however, that only two of these are required to provide three equations in three unknowns; σ_r, σ_θ, and the particle velocity v.

The constituitive equations are

$$\epsilon_r = \frac{\partial u}{\partial r} = \frac{1}{E_o}\left[\sigma_r - \nu\sigma_\theta\right] \qquad 3\text{-}2$$

$$\epsilon_\theta = \frac{u}{r} = \frac{1}{E_o}\left[\sigma_\theta - \nu\sigma_r\right] \qquad 3\text{-}3$$

$$\epsilon_z = \frac{\partial w}{\partial z} = \frac{1}{E_o}\left[-\nu(\sigma_r + \sigma_0)\right] \qquad 3\text{-}4$$

Differentiating the first two of these with respect to time and noting that the particle velocity $v = \frac{\partial u}{\partial t}$ gives,

$$\frac{\partial v}{\partial r} = \frac{1}{E}\left[\frac{\partial \sigma_r}{\partial t} - \nu \frac{\partial \sigma_\theta}{\partial t}\right] \qquad 3\text{-}5$$

$$\frac{v}{r} = \frac{1}{E}\left[\frac{\partial \sigma_\theta}{\partial t} - \nu \frac{\partial \sigma_r}{\partial t}\right] \qquad 3\text{-}6$$

Characteristic Equations

Equations 3-1, 3-5, and 3-6 are sufficient to derive the characteristic relationships which consist of a set of differential equations relating the dependent variables σ_r, σ_θ, and v to the independent variables r and t along the characteristic lines in the r-t plane. These are lines along which weak disturbances propagate and across which the dependent variables are continuous but the derivatives of the variables may be discontinuous.

There is more than one way to derive these equations, (see [6] for instance) but in view of the above definition, it is perhaps easiest to solve 3-1, 3-5, and 3-6 directly for the derivatives by Cramer's rule and then to impose conditions which will cause the derivatives to become undefined.

Accordingly, we rearrange the equations in the following form and also include the general relationships for the differential changes of σ_r, σ_θ, and v as a function of infinitesimal changes in r and t.

$$\begin{aligned}
\frac{\partial\sigma_r}{\partial r} \qquad\qquad\qquad\qquad\qquad - \rho\frac{\partial v}{\partial t} &= \frac{\sigma_\theta - \sigma_r}{r} \\
\frac{1}{E}\frac{\partial\sigma_r}{\partial t} - \frac{\nu}{E}\frac{\partial\sigma_\theta}{\partial t} - \frac{\partial v}{\partial r} &= 0 \\
-\frac{\nu}{E}\frac{\partial\sigma_r}{\partial t} + \frac{1}{E}\frac{\partial\sigma_\theta}{\partial t} &= \frac{v}{r} \\
\frac{\partial\sigma_r}{\partial r}\,dr + \frac{\partial\sigma_r}{\partial t}\,dt &= d\sigma_r \\
\frac{\partial\sigma_\theta}{\partial r}\,dr + \frac{\partial\sigma_\theta}{\partial t}\,dt &= d\sigma_\theta \\
\frac{\partial v}{\partial r}\,dr + \frac{\partial v}{\partial t}\,dt &= dv
\end{aligned} \qquad 3\text{-}7$$

We may solve the above system for $\frac{\partial\sigma_r}{\partial r}$, for example, by Cramer's rule. The result is a fraction consisting of a determinant in both numerator and denominator. If the denominator is set equal to zero and expanded, we get a relationship describing the slopes, or directions, of the characteristics in the r-t plane. Similarly, if we set the determinant in the numerator equal to zero we obtain the differential equations relating the unknown variables along the characteristics. (See Appendix B.) The same relationship would be obtained if we chose to solve for any of the other derivatives.

The results of these computations show that the characteristic directions are given by the following three equations

$$\frac{dr}{dt} = + c \qquad 3\text{-}8$$

$$\frac{dr}{dt} = - c \qquad 3\text{-}9$$

$$dr = 0 \qquad 3\text{-}10$$

Along the first of these directions,

$$d\sigma_r - \rho c\, dv = \left[- (\sigma_r - \sigma_\theta) + \rho \nu c v \right] \frac{dr}{r} \qquad 3\text{-}11$$

Along the second,

$$d\sigma_r + \rho c\, dv = \left[- (\sigma_r - \sigma_\theta) - \rho \nu c v \right] \frac{dr}{r} \qquad 3\text{-}12$$

and finally, along the third,

$$d\sigma_r = \frac{1}{\nu} \left[d\sigma_\theta - E \frac{v}{r}\, dt \right] \qquad 3\text{-}13$$

In these equations E, c, and ν are to be regarded as variable quantities the values of which depend upon whether the state of stress in the material is in the elastic or plastic regime.

Plasticity Relations

Equations 3-1 to 3-13 are sufficient to define the state of stress and strain in a perfectly elastic, homogeneous, isotropic, strain rate independent material at constant temperature. However, when the stresses become sufficiently high a yield point is reached and the material behaves plastically thereafter or until unloading occurs. In the latter case unloading proceeds along a curve parallel to the original elastic curve resulting in a permanent set when the stresses reach zero. Upon reloading, the material remains elastic until the stresses again become equal to the maximum value previously attained. (See Figure 3.) It is also assumed in what follows that the stress-strain curve in compression is identical to that in tension.

A detailed development and discussion of the various plasticity theories in common use is given in [11] as well as in a number of other excellent references. Therefore, only a brief outline will be given of the theory which is used here.

In the case of uniaxial loading, a material specimen will behave elastically only until the applied stress reaches the yield point σ_0. Beyond this value plastic deformation occurs and the relationship between the stress and strain is no longer linear; i.e., yielding is said to occur when σ applied $\geq \sigma_0$. When a multi-axial stress state prevails one of several possible yield criteria is used to define the onset of yielding. In this work the Von Mises or Distortion Energy criterion for biaxial stress is used in which yielding is assumed to occur when

$$\left[\sigma_r{}^2 + \sigma_\theta{}^2 - \sigma_r \sigma_\theta\right]^{\frac{1}{2}} \geq \sigma_0 \qquad 3\text{-}14$$

This function, however, is also the definition of the equivalent stress, σ_{eq}, which represents the "effective stress" on the material. Thus, yielding occurs when

$$\sigma_{eq} = \sigma_0$$

When σ_{eq} becomes greater than σ_0, the functional relationship between the stresses and strains is non-linear. The extension of 3-2, 3-3, and 3-4 to include the plastic strains can be written

$$\epsilon_r = \frac{1}{E}\left[\sigma_r - \nu\sigma_\theta\right] + \epsilon_r{}^P + d\epsilon_r{}^P \qquad 3\text{-}15$$

$$\epsilon_\theta = \frac{1}{E}\left[\sigma_\theta - \nu\sigma_r\right] + \epsilon_\theta{}^P + d\epsilon_\theta{}^P \qquad 3\text{-}16$$

$$\epsilon_z = \frac{1}{E}\left[-\nu(\sigma_r + \sigma_\theta)\right] + \epsilon_z^P + d\epsilon_z^P \qquad 3\text{-}17$$

These equations suggest that the strains are computed from the applied loads in an incremental fashion. This is done with the aid of the Prandtl-Reuss equations which are given in general differential form as

$$d\epsilon_{ij}^P = S_{ij}\, d\lambda \qquad 3\text{-}18$$

where S_{ij} is the deviatoric stress tensor and represents the stress components which are in excess of the mean hydrostatic stress which produces no yielding. For the case at hand, this can be written

$$S_{ij} = \begin{bmatrix} \sigma_r - \sigma_m & 0 & 0 \\ 0 & \sigma_\theta - \sigma_m & 0 \\ 0 & 0 & \sigma_z - \sigma_m \end{bmatrix}$$

Since the mean stress is defined as

$$\sigma_m = \frac{1}{3}\left[\sigma_r + \sigma_\theta + \sigma_z\right],$$

the deviatoric stress tensor finally becomes

$$S_{ij} = \begin{bmatrix} \frac{2\sigma_r - \sigma_\theta - \sigma_z}{3} & 0 & 0 \\ 0 & \frac{2\sigma_\theta - \sigma_z - \sigma_r}{3} & 0 \\ 0 & 0 & \frac{2\sigma_z - \sigma_r - \sigma_\theta}{3} \end{bmatrix} \qquad 3\text{-}19$$

By invoking the yield criterion it is shown in [11] that the constant

$$d\lambda = 3/2 \frac{d\epsilon_P}{\sigma_{eq}}$$

where $d\epsilon_P$ is the equivalent plastic strain increment and is given by

$$d\epsilon_P = \frac{\sqrt{2}}{3}\left[(d\epsilon_r^P - d\epsilon_\theta^P)^2 + (d\epsilon_\theta^P - d\epsilon_z^P)^2 + (d\epsilon_z^P - d\epsilon_r^P)^2\right]^{\frac{1}{2}} \qquad 3\text{-}20$$

Substituting this relationship and 3-19 into 3-18 gives the following expressions for the plastic strain increments in finite difference form with $\sigma_z \equiv 0$.

$$\Delta\epsilon_r^P = \frac{\Delta\epsilon_P}{2\sigma_{eq}}\left[2\sigma_r - \sigma_\theta\right] \qquad 3\text{-}21$$

$$\Delta\epsilon_\theta^P = \frac{\Delta\epsilon_P}{2\sigma_{eq}}\left[2\sigma_\theta - \sigma_r\right] \qquad 3\text{-}22$$

$$\Delta\epsilon_z^P = -\Delta\epsilon_r^P - \Delta\epsilon_\theta^P \qquad 3\text{-}23$$

Equation 3-23 follows from the fact that the first order approximation for the relative change in volume of a strained element is,

$$\frac{\Delta V}{V_o} = \epsilon_r + \epsilon_\theta + \epsilon_z$$

which in the plastic range is neglected in comparison with the deformations. Furthermore, it may also be shown that the relative volume change is given by

$$\frac{\Delta V}{V} = \frac{1 - 2\nu}{E}\left[\sigma_r + \sigma_\theta\right]$$

which implies that $\nu = 1/2$ when the change in volume can be neglected, i.e., in the plastic regime.

Equations 3-21, 3-22, and 3-23 are the so-called Prandtl-Reuss flow rules for the incremental plasticity theory.

Only one additional set of equations is required to define the stress-strain time histories. These are the unloading shock relationships to be discussed next.

Unloading Shock

If at any radial distance r the material is stressed beyond the yield point so that $\sigma_{eq} \geq$ SIGMAX, the maximum equivalent stress previously attained, and subsequently decreases with time, then unloading is said to occur as depicted in Figure (3). Since unloading proceeds along an elastic curve, such a "disturbance" propagates with the elastic wave speed c_o. It therefore overtakes the slower plastic waves and may prevent them from reaching the outer boundary or may itself be prevented from reaching the boundary. The method of determining this behavior will be discussed later in this section.

As previously stated, the characteristic equations given by 3-8 to 3-13 are applicable to problems in which the variables are continuous but the derivatives of the variables may be discontinuous. In the case of an unloading shock the variables themselves are discontinuous across the shock and are therefore not governed by equations 3-8 to 3-13. The shock equations, or equations describing the propagation of a discontinuity may be derived however, by employing equations 3-11, 3-12, and 3-13 in a limiting process. The following closely parallels the derivation given in [8], originally credited to Leonard and Budiansky and Jahsman.

Consider an infinitesimally thin shock wave, or discontinuity, propagating along a + c_o direction in the r-t plane as shown in Figure (4).

If we also consider, as shown in Figure (4), a - c_o characteristic intersecting the shock discontinuity, we can write equation 3-12 between two points A and B on either side of the shock with the result that

$$(\sigma_{rB} - \sigma_{rA}) + \rho c_o(v_B - v_A) = \int_A^B \left[- (\sigma_r - \sigma_\theta) - \rho\nu c v \right] \frac{dr}{r} \qquad 3\text{-}24$$

As B is allowed to approach A, or as dr → 0, the integrand contains bounded values of σ_r, σ_θ, and v so that the right-hand side vanishes. Also, $\sigma_{rB} - \sigma_{rA}$ is finite but different from zero and represents the jump in σ_r at point A across the shock propagating along c_o. If we define

$$\delta\sigma_r = \sigma_{rB} - \sigma_{rA} ,$$

with analogous expressions for the other variables, equation 3-23 can be written finally

$$\delta\sigma_r + \rho c_o \delta v = 0 \qquad 3\text{-}25$$

In a similar fashion, if we had considered the shock to be propagating along a - c_o line and instead of using equation 3-12 we had written equation 3-11 along a + c_o characteristic intersecting the shock, equation 3-25 would be replaced by

$$\delta\sigma_r - \rho c_o \delta v = 0 \qquad 3\text{-}26$$

Finally, if equation 3-13 is applied between points A and D in Figure (4), we get

$$\sigma_{rD} - \sigma_{rA} = \frac{1}{\nu}\left[\sigma_{\theta D} - \sigma_{\theta A} - \int_A^D E \frac{v}{r}\, dt\right]$$

As dt → 0, the integral approaches 0 and we are left with

$$\sigma_{rD} - \sigma_{rA} = \frac{1}{\nu}\left[\sigma_{\theta D} - \sigma_{\theta A}\right]$$

and since in the limit $\sigma_{rD} \rightarrow \sigma_{rB} \rightarrow \sigma_{rA}$ we have finally the static relation at a given value of r.

$$\delta\sigma_r = \frac{1}{\nu}\,\delta\sigma_\theta \qquad 3\text{-}27$$

Equations 3-25, 3-26, and 3-27 relate the jumps in the variables σ_r, σ_θ, and v at a point along a discontinuity in the r-t plane. However, we would also like to know how the amplitudes of these jumps vary as they propagate outward or inward along $+\,c_o$ or $-\,c_o$ respectively. This is done for propagation along the $+\,c_o$ direction, for example, by writing equation 3-11 along the right hand (upstream) edge of the shock while applying equations 3-25 and 3-27 across the shock. This provides three equations in the three unknowns σ_r, σ_θ, and v at a desired point along the upstream edge of the shock. The finite difference representation of these equations will be presented in Section IV.

Boundary Conditions

There are two boundary conditions in this problem corresponding to conditions on the inner and outer surfaces, or edges, of the disk.

The inner surface experiences an applied pressure as a function of time which, of course, is equivalent to radial stress σ_r as a function of time. The outer surface is stress free and hence $\sigma_r \equiv 0$.

SECTION IV

NUMERICAL ANALYSIS PROCEDURES

Equations 3-11, 3-12, and 3-13 are the differential equations which will be used to compute the quantities σ_r, σ_θ, and v in a stepwise fashion along the characteristics in the continuous field region.

Consider a typical r-t plane as depicted in Figure (5) with a plot of the input pressure (σ_r) shown directly below. We divide this plane into a number of lines of constant r which shall be designated by the index I running from I = 1 to I = NA. (In this analysis A stands for segment A. In the future, if one should desire to consider several concentric disks or rings these may be conveniently labeled B, C, D, etc.) The + c characteristics beginning at the I = 1 line and propagating (either elastically or plastically) to the I = NA line are denoted by the index J and cover the range from 1 to problem termination or the limit JLIM.

By using equations 3-8 and 3-9 in addition to the three differential equations, we may construct the characteristic network of Figure (5) point-by-point in an incremental fashion. A more detailed description of this procedure will be given presently.

Finite Difference Equations

Before proceeding further, equations 3-11, 3-12, and 3-13 will be written in finite difference form then rearranged in their final form as three linear, algebraic equations in the three unknowns σ_r, σ_θ, and v. During this process E and C are treated as variables which are functions of the location of σ_{eq} on the stress-strain curve. In the elastic regime, E and C are constants while in the plastic regime E is taken as the tangent modulus with C assuming the plastic wave speed based upon the current value of E.

If we consider any two points 1 and 2 along a + c characteristic and apply equation 3-11 between them we get

$$\sigma_{r2} - \sigma_{r1} - \rho\bar{c}\,(v_2 - v_1)$$

$$= \frac{1}{2}\left\{\left[-\,(\sigma_r - \sigma_\theta) + \rho\nu cv\right]_1 + \left[-\,(\sigma_r - \sigma_\theta) + \rho\nu cv\right]_2\right\}\frac{2\Delta r}{r_1 + r_2}$$

where the right side of the equation has been averaged between points 1 and 2 and the quantity $\bar{c}$ also denotes an average value between the same points.

If we suppose now that the variables are known at point 1 while those at point 2 represent unknowns, we may transpose all variables with subscript 1 to the right side of the equation while retaining all subscript 2 variables on the left side with the result that,

$$\sigma_{r2} - \rho\bar{c}v_2 - \left[(\sigma_\theta - \sigma_r)\,\frac{\Delta r}{r_1 + r_2} + \rho\nu cv\,\frac{\Delta r}{r_1 + r_2}\right]_2$$

$$= \left[(\sigma_\theta - \sigma_r)\,\frac{\Delta r}{r_1 + r_2} + \rho\nu cv\,\frac{\Delta r}{r_1 + r_2}\right]_1 + \sigma_{r1} - \rho\bar{c}v_1$$

If we clear parentheses on the left side of this equation, collect terms in σ_r, σ_θ and v, and denote by a subscript 2 those variables which are to be evaluated at point 2, we obtain

$$\left[1 + \frac{\Delta r}{r_1 + r_2}\right] \sigma_{r2} - \frac{\Delta r}{r_1 + r_2} \sigma_{\theta 2} - \left[\rho\bar{c} + \rho\nu c_2 \frac{\Delta r}{r_1 + r_2}\right] v_2$$

$$= \left[(\sigma_\theta - \sigma_r) + \rho\nu c\ v\right]_1 \frac{\Delta r}{r_1 + r_2} + \sigma_{r1} - \rho\bar{c}v_1 \qquad 4\text{-}1$$

Since the equation along a-c characteristic differs from (4-1) only in two algebraic signs, an identical development of equation 3-12 along a-c line leads to

$$\left[1 - \frac{\Delta r}{r_1 + r_2}\right] \sigma_{r2} + \frac{\Delta r}{r_1 + r_2} \sigma_{\theta 2} + \left[\rho\bar{c} - \rho\nu c_2 \frac{\Delta r}{r_1 + r_2}\right] v_2$$

$$= - \left[(\sigma_\theta - \sigma_r) - \rho\nu c v\right]_1 \frac{\Delta r}{r_1 + r_2} + \sigma_{r1} + \rho\bar{c}v_1 \qquad 4\text{-}2$$

In analogous fashion equation 3-13 along a dr = 0 line may be written as

$$\sigma_{r2} - \sigma_{r1} = \frac{1}{\nu}\left[\sigma_{\theta 2} - \sigma_{\theta 1} - \frac{\bar{E}\ \Delta t}{r}\ \frac{(v_1 + v_2)}{2}\right]$$

where $\bar{E}$ denotes the average value between two adjacent points.

By expanding the above equation as before, collecting terms in σ_r, σ_θ, and v, and placing subscript 1 and subscript 2 variables on opposite sides of the equation we have,

$$\sigma_{r2} - \frac{1}{\nu}\sigma_{\theta 2} + \frac{\bar{E}\ \Delta t}{2r\ \nu} v_2 = \sigma_{r1} - \frac{1}{\nu}\sigma_{\theta 2} - \frac{\bar{E}\ \Delta t}{2r\ \nu} v_1 \qquad 4\text{-}3$$

Referring again to Figure (5), let (i,j) be a general point at which the variables σ_r, σ_θ, and v are to be solved. Then the adjacent point along a + c characteristic at which the variables are known ~~is~~ labeled (i-1,j). Similarly, the adjacent point along a - c characteristic has indices (i+1,j-1), and finally along the dr = 0 line the adjacent point is denoted by (i,j-1).

With this notation equations 4-1, 4-2, and 4-3 can be written in their final form, with subscripts for σ_r, σ_θ, and v enclosed in parentheses.

$$\left[1 + \frac{\Delta r}{r_{i-1} + r_i}\right] \sigma_r(i,j) - \frac{\Delta r}{r_{i-1} + r_i} \sigma_\theta(i,j) - \rho\left[\frac{c_{i-1,j} + c_{i,j}}{2} + \nu c_{i,j} \frac{\Delta r}{r_{i-1} + r_i}\right] v(i,j)$$

$$= \left[\sigma_\theta(i-1,j) - \sigma_r(i-1,j) + \rho\nu c_{i-1,j}.v(i-1,j)\right] \frac{\Delta r}{r_{i-1} + r_i} + \sigma_r(i-1,j) - \rho \frac{c_{i-1,j} + c_{i,j}}{2} v(i-1,j) \quad \text{(along + c)}$$

4-4

$$\left[1 - \frac{\Delta r}{r_i + r_{i+1}}\right] \sigma_r(i,j) + \frac{\Delta r}{r_i + r_{i+1}} \sigma_\theta(i,j) + \rho\left[\frac{c_{i,j} + c_{i+1,j-1}}{2} - \nu c_{i,j} \frac{\Delta r}{r_i + r_{i+1}}\right] v(i,j)$$

$$= -\left[\sigma_\theta(i+1,j-1) - \sigma_r(i+1,j-1) - \rho\nu c_{i+1,j-1}\, v(i+1,j-1)\right] \frac{\Delta r}{r_i + r_{i+1}} + \sigma_r(i+1,j-1) + \rho \frac{c_{i,j} + c_{i+1,j-1}}{2} v(i+1,j-1)$$

(along - c)

4-5

$$\sigma_r(i,j) - \frac{1}{\nu}\sigma_\theta(i,j) + \frac{E_{i,j} + E_{i,j-1}}{4\ r_i\ \nu}\,\Delta t\ v(i,j)$$

$$= \sigma_r(i,j-1) - \frac{}{}\,\sigma_\theta(i,j-1) - \frac{E_{i,j} + E_{i,j-1}}{4\ r_i\ \nu}\,\Delta t\ v(i,j-1)\ \text{(along } dr = 0\text{)} \tag{4-6}$$

The foregoing relations constitute 3 equations in 3 unknowns and are of the form AX = B where [X] is the column matrix of unknowns, [A] is the coefficient matrix, and [B] is the column vector corresponding to the right side of the equations. The system as given by 4-4 through 4-6 is valid for an interior point of the characteristic grid; however, along the $i = 1$ line σ_r is given as the applied pressure vs. time. In this case only two equations along the - c and $dr = 0$ lines are used. Thus, σ_r is transposed to the right side of the equations as a known quantity and equations 4-5 and 4-6 are solved as 2 equations in the two unknowns σ_θ and v.

Similarly, when i = NA at the outer edge of the disk, only the equations along the + c and $dr = 0$ directions are used with $\sigma_r \equiv 0$. Again we have 2 equations (4-4 and 4-6) in 2 unknowns σ_θ and v.

The equations used to compute the variation in shock amplitude as a function of radial distance r for the general case have already been briefly discussed. The finite difference form of the equations follows.

Referring to Figure 5, we may develop equation 3-11 between points (i,j) and (i-1,j) along the upstream edge of the shock in a manner analogous to that leading to 4-1 except that the values of c assume only the elastic value c_o.

$$\left[1 + \frac{\Delta r}{r_{i-1} + r_i}\right] \sigma_r(i,j) - \frac{\Delta r}{r_{i-1} + r_i} \sigma_\theta(i,j)$$

$$- \rho c_o\left[1 + \nu \frac{\Delta r}{r_{i-1} + r_i}\right] v(i,j)$$

$$= \left[\sigma_\theta(i-1,j) - \sigma_r(i-1,j) + \rho\nu c_o\ v(i-1,j)\right] \frac{\Delta r}{r_{i-1} + r_i}$$

$$+ \sigma_r(i-1,j) - \rho c_o\ v(i-1,j) \qquad 4\text{-}7$$

Similarly, equation 3-25 may be written

$$\sigma_r(i,j) + \rho c_o\ v(i,j) = \sigma_r(i,j-1) + \rho c_o\ v(i,j-1) \qquad 4\text{-}8$$

Finally, equation 3-27 can be written

$$\sigma_r(i,j) - \frac{1}{\nu} \sigma_\theta(i,j) = \sigma_r(i,j-1) - \frac{1}{\nu} \sigma_\theta(i,j-1) \qquad 4\text{-}9$$

Equations 4-7, 4-8, and 4-9 thus comprise the unloading shock equations.

Computational Procedures

An outline of the computational procedures will be given next as an aid to understanding the program computer listings given in Appendix D.

In this problem either a smoothly increasing and decreasing pressure pulse as a function of time is considered or a ramp input followed by a constant plateau.

Referring again to Figure 5 and Appendix D, after the initial data is read into the computer the following computations are performed: (line numbers refer to the computer listing in Appendix D)

1) A differentiation subroutine is called to compute the value of E (tangent modulus) at selected points along the specimen stress-strain curve (line 0046).

2) The variable plastic wave velocity C(I) and the constant elastic wave velocity CO are computed at points corresponding to the previously determined values of E (lines 0048 and 0061).

3) Lines of constant R are determined using the input increment ΔR (line 0064).

4) The intercept time of an elastic wave with each of the constant r lines is determined (line 0067).

5) All variables along this line except C and E are set = 0. These are set equal to their elastic values (line 0069).

6) From point $i = 2$, $j = 1$, the time of intercept of an elastic wave with the $I = 1$ line is computed (line 0092). This is point $I = 1$, $J = 2$.

7) The Aitken-Lagrangian interpolation routine (ATSM and ALI) is called to interpolate the value of input pressure, σ_r, at this point (line 0094).

8) Equations 4-5 and 4-6 are called with GAUSS to solve for σ_θ and v at this point (line 0104).

9) The equivalent stress is computed and a check is made to see if yielding or unloading has begun (line 0106).

10) New values of C and E are interpolated, for recomputing the average values specified in the equation coefficients (line 0115). Equations 4-5 and 4-6 are solved a second time for "improved" values of σ_θ and v.

11) Using the final values of σ_r, σ_θ and v, the elastic strains are computed (line 0139).

12) Beginning with line 0159 the iterative calculations for the plastic strain increments are carried out prior to adding them to the elastic strains (line 0182). See Step 15 for a more thorough discussion.

13) From point i = 1, j = 2 the intercept of a + c characteristic with the i = 2 line is computed. This point is the initial estimate of TA(2,2) (line 0198). Similarly from point i = 3, j = 1, the intercept of a - c characteristic with the i = 2 line is computed. This is denoted by TANN (line 0202). In general TAPP and TANN will not coincide in the plastic regime in which case the earlier arrival is designated as the actual time intercept for that particular i, j point. In this example i = 2, j = 2. If TAPP > TANN an interpolation subroutine (TRANSL) is called in which the values of the variables at point i = 1, j = 2 are reduced linearly by the ratio (TAPP-TANN)/[TAPP-TA(2,1)]. In this way a new value of TAPP originating from a new point corresponding to the values of the interpolated variables more closely coincides with the value of TANN. If the stress field were entirely elastic in this region the foregoing procedure would be equivalent to translating the characteristic line segment defining the TAPP intercept parallel to itself until TAPP coincided with TANN. Of course, if the field is completely elastic then TAPP and TANN automatically coincide.

If TANN > TAPP a similar procedure is carried out with the interpolation being performed now on the variables along the i = 3 line. Of course, in this particular case when j = 2 an interpolation cannot be carried out since it would involve variables on the j = 1 line and also a j = 0 line which is non-existent. At all other points, however, for which j > 2 the interpolation is performed (line 0218).

14) The process described in Step 13 is continued for each i line through i = NA. The procedure then returns to the i = 1 line with j incremented by one and is repeated until all of the input values of pressure vs. time have been used or until the unloading shock occurs (line 0112).

15) Whenever the value of σ_{eq} at a given point becomes > SIGMAX, which is the largest plastic value of σ_{eq} attained thus far along a particular i line, the material is continuing to yield. An initial estimate is made of the equivalent plastic strain increment $\Delta\epsilon_p$ by taking the difference between the current and preceding interpolated values of plastic strain after the latter has been increased by the elastic strain increments (line 0164). This value is then used in equations 3-21 to 3-23 to compute estimates of the individual plastic strain increments (lines 0168 - 0170). These are used in equation 3-20 to compute an improved estimate of $\Delta\epsilon_p$. The iteration is repeated until two successive estimates of the strain increments differ by no more than TESTEP, an assigned test value.

16) Several checks are made at each point after the final

computation of equivalent stress. If $\sigma_{eq} > \sigma_o$, i.e., the material is in the plastic range at a given value of i, and if σ_{eq} at a point (i, j) becomes less than the value at point (i, j-1) then unloading has occurred and an elastic unloading shock propagates radially outward from this point (lines 0108 - 0112 typically). Unloading is assumed to occur first along the I = 1 line [SIGEQ < SIGMAX(1)]. If it occurs along some other I line an error message is printed and the program terminated. If ISWITCH = 1 transfer to the unloading shock computations is bypassed.

17) The time intercepts of this shock with each i line are computed (line 0353).

18) At each intercept point a search is made for bounding values of time, TA (line 0354).

19) The problem variables are interpolated between these values of time and are stored as the downstream (earlier time) values along the shock. If the shock line does not cross any of the j-lines and therefore there are no bounding values, then the last previous values are stored along the downstream edge of the shock (line 0379).

20) Equations 4-7, 4-8, and 4-9 are called to compute the values of the variables upstream of the shock. The process is continued to the i = NA-1 line (line 0405).

21) At each i line a comparison is made between the values of σ_{eq} downstream and upstream of the shock. If the downstream value is less than the upstream value, the shock

computations continue, otherwise the shock computations are terminated (line 0453).

22) At the i = NA line $\sigma_r \equiv 0$. The jump in the value of v across the reflected shock is computed from equation 3-26 (line 0461) along with the accompanying values of σ_θ and the strains. The shock computations are then terminated.

23) All previously computed variables for values of time greater than the shock intercept times are set equal to zero (line 0368).

24) If the shock does not propagate to the NA line but is terminated as discussed in Step 21, the time intercepts of the extended shock line are computed (line 0473).

25) At each of these points a search is made for the bounding values of time and the problem variables are interpolated (line 0477) as in Steps 18 and 19 and are stored. All later values previously computed, if any, are set equal to 0.

26) The calculations then return to the I = 1 line and the usual characteristic computations continue in the elastic mode until the values of input pressure are exhausted. The final stresses and strains thus computed are the residual stresses and permanent set strains.

SECTION V

EXPERIMENTAL EQUIPMENT

As mentioned previously, a modest experimental program consisting of two methods for initiating a pressure pulse was conducted to verify the theoretically predicted solutions for the distribution of strain history in the specimens.

A schematic diagram of the experimental fixture used in the hydraulic technique is shown in Figure 1 while Figure 6 presents a photograph of the fixture and instrumentation. The explosive method utilizes only the support plate and a tripod supported steel rod covering the specimen central hole to retain and better distribute the explosive gases.

A pressure pulse is initiated on the inside surface of the specimen by igniting a quantity of explosive with a fuse or by dropping a weight onto a plunger in the case of the hydraulic method. Since it has been stated that the hydraulic method produced poor results, the following equipment specifications and configurations are those used with the explosive method.

Two 350 ohm strain gages are mounted on the surface of the disk at a radial distance of 0.75 inches from the center. One gage is oriented with its sensitive axis along the radial direction while the second is mounted with its sensitive axis oriented perpendicular to the first in order to measure circumferential strain. The gages are connected to a bridge circuit and amplifier which in turn transfers the signals to a 2-channel oscilloscope where they are permanently recorded on polaroid film.

The pressure pulse is sensed by a Piezo-electric pressure transducer and integral amplifier unit before proceeding to a single channel of a dual channel oscilloscope where it is also recorded on film.

Listed below are the manufacturers, model or type numbers, and major performance parameters of the various instruments used with the explosives technique.

Item	Manufacturer	Model/Type	Performance Parameters
Strain Gages	Micro-Measurements Company	Type: ED-DY-125AD-350	350 ohm gage factor = 3.20
Pressure Transducer	Piezotronics	Model: 109A	pressure 0-80000 psi; frequency range 0-500000 hertz; rise time 1 micro-sec.
Bridge	Leeds & Northrop Company	---	frequency range 0-120,000 hertz
Bridge Amplifier	Vishay Instrument Company	---	frequency range 0-120,000 hertz
Oscilloscopes	TEKTRONIX	Model: 551 dual beam	---
Plug-in Unit		Type: 53/54C	pre-amp rise time 0.01 micro-sec.

SECTION VI

RESULTS

The hydraulic tests were the first ones conducted and resulted in typical pressure histories and strain histories as shown in Figures 7 and 8. As can be seen in Figure 8, the circumferential strain initially is compressive before becoming tensile which is contrary to expectations. Furthermore, the time at which the first positive pulse of the radial strain peaks is much too long relative to the peak of the pressure pulse. As a result there was some doubt as to whether the recorded strain signatures were due solely to the pressure pulse. It was anticipated that plate bending modes may also have been excited, especially in view of the bending moment applied by the O-ring seals during clamping.

As a result of these considerations it was decided to conduct the explosive test program to obtain more reliable data. The strain histories from the explosive tests presented in Figures 11 and 12 show much better behavior than those of the hydraulic method. Accordingly, the results obtained from the hydraulic method will not be discussed further while those of the explosive program and two other test cases, as well as the multiple runs option on a prestressed specimen will be considered subsequently.

Three test cases have been evaluated as a means of verifying the validity of the theoretical solution. In addition, a fourth case has been run to illustrate the use of the multiple runs option in which a set of final permanent stress and strain distributions and equivalent yield stresses for each I-line are used as initial values for a succeeding run.

The cases considered include:

a) Steady state elastic solution with specimen 1 of Figure 1b

b) Steady state elastic-plastic solution with specimen 1 of Figure 1b

c) Transient solution using the pressure pulse of Figures 10 and 12 with specimen 2 of Figure 1b

d) Transient solution using a previously stressed specimen (specimen 1 from Figure 1b) with the pressure pulse shown in Figure 25.

Each of these cases will be discussed individually. In each instance a positive stress denotes compression while a negative stress denotes tension.

Case a) The steady elastic solution has been obtained by applying a pressure input consisting of a ramp to 5000 psi in 8 μsec followed by a constant plateau of 5000 psi to 225 μsec and program termination. A fictitious yield stress = 20000 psi has been used to insure an elastic stress field. The final stresses at four selected radial locations have been obtained from Figures 13, 14, 15, and 16 and are tabulated below in addition to the values calculated from the standard thick walled cylinder equations from reference 12.[1] It is noteworthy that during the first 25 to 35 μ seconds, depending upon the particular I-line,

---

[1] The thick walled cylinder equations referenced in cases (a) and (b) assume a state of plane strain rather than plane stress. These equations nevertheless serve as a useful approximate check.

these curves behave in the same manner as those given in reference 8. Thereafter the disturbing effects of the reflected waves from the free boundary are evident in the form of oscillations about the estimated, best-fit steady state solution. These appear to continue indefinitely in the absence of damping effects.

		I = 1 R = 0.75	I = 3 R = 1.00	I = 7 R = 1.50	I = 19 R = 3.00
Computer solution	σ_r :	5000	2800*	1200*	200*
	σ_θ :	-5000*	-2800*	-1400*	-500*
Thick Walled Cylinder	σ_r :	5000	2750	1140	178
	σ_θ :	-5260	-3020	-1425	-464

*Estimated best fit steady state solution.

The agreement between the computer solutions and the known solutions is quite good, on the order of 5 to 10 percent.

Case b) The steady state elastic-plastic solution has been obtained in a manner identical to that of the previous case except that the actual yield stress of 2500 psi has been used.

In this case the circumferential stress does not attain as large a negative (tension) value as in the elastic case. Furthermore, because of the slower plastic wave speed the effects of the reflected waves do not arrive at the I = 1 line until a later time.

The final stresses at the same radial locations as case (a) have been obtained from Figures 17, 18, 19, and 20. They are tabulated below in addition to the values calculated from the elastic-linear strain hardening, thick walled cylinder equations given in reference 11 using an equivalent yield stress of 4000 psi. Again agreement between the computer solutions and the closed form solutions is reasonably good with an error on the order of 5 to 10 percent except for the circumferential stress at the I = 3 line. Also note that it is somewhat difficult to accurately estimate the best-fit steady state response in the oscillating region of the curves.[2]

		I = 1	I = 3	I = 7	I = 19
		R = 0.75	R = 1.00	R = 1.50	R - 3.00
Computer solution	σ_r :	5000	3600*	1800*	300*
	σ_θ :	-500*	-800*	-2000*	-800*
Thick Walled Cylinder	σ_r :	5000	3740	2060	280
	σ_θ :	-415	-515	-1960	-800

*Estimated best fit steady state solution.

Case c) Figures 21 and 22 present the stress-time computer solutions along the I = 1 and I = 24 lines using the typical pressure pulse of Figures 10 and 12 while Figures 23 and 24 present the strain-time solutions for the same data at the same radial locations. The I = 24 line (R = 0.75 in.) corresponds to the location of the strain gages on the experimental specimen. These provide the only means of correlating the experimental and theoretical results for this test data. Figure 11 presents typical tracings of the experimental strains while Figure 12 shows a plot of the same data. The plotted data has also been superimposed on the computed solutions of Figure 24 for ease of comparison.

The information required to convert the experimental pressure and strain tracings to actual pressure and strain values is given below. The calibration factors were taken from the appropriate instrument

---

[2] See Footnote (1) page

manufacturer's instruction manual.

Oscilloscope Settings During Explosive Tests

	Vertical Sensitivity (mv/cm)	Sweep Rate (μsec/cm)
Pressure transducer	200	2
Radial stress gage	50	2
Circumferential strain gage	50	2

The slope of the pressure input/voltage output calibration curve of the pressure transducer is 18.3 psi/mv.

A known test signal from the strain gage bridge instrument was used in conjunction with the manufacturer's calibration factor to convert the strain gage data to actual strain values. This conversion factor is 1.95 μ in/in per mv.

Comparison of the experimental data in Figure 24 with the computed solutions indicates that the magnitude of the first positive peak of the measured radial strain is 56 μ in/in while the computed value is 42 μ in/in. The corresponding values for the second positive peak are 51 μ in/in versus 15 μ in/in respectively. It can be seen that the times at which the measured and theoretical peaks occur agree exactly. Similarly, the first negative peak of the experimental results agrees precisely with the computed value, whereas the second negative experimental peak is -55 μ in/in compared to the smaller theoretical result of -15 μ in/in and occurs approximately 1 μsec later.

The behavior of the circumferential strain is predicted with reasonable accuracy; the major difference being in the magnitude. Experimentally, -28 μ in/in was obtained versus -18 μ in/in for the predicted value. The times at which these peaks occur are again seen to be identical.

Although there are some discrepancies between the experimental and theoretical results as discussed above, the shape and phasing of the curves is excellent. In view of the somewhat unsophisticated experimental technique used it is also considered that the magnitude of the curves are in reasonable agreement. In particular, the discharge of a quantity of powder in the central specimen hole creates a pressure pulse that is not entirely uniform over the depth of the hole. As a result, a purely radial pressure pulse is not realized, but instead a complicated system of oblique waves resulting in reflections from the specimen free surfaces, the generation of shear waves, and complicated wave interaction effects.

In view of these considerations it is concluded that the experimental data presented is in agreement with the theoretical calculations to within the expected accuracy of the experimental technique.

Case d) This run has been conducted to illustrate the analysis of a previously stressed specimen wherein each I-line begins with permanent set values of the stresses, strains, and yield stress obtained from a previous run. These are read in either as initial values along the J = 1 line or merely as values associated with each particular I-line. To illustrate, the following arbitrary but typical values of the variables were input as initial data for specimen 1 which was subdivided into 32 I-lines.

Variable	I-line Range	Value
EPSEQ1(I)	1 - 7	.0021265
	8 - 32	.0002500
SIGMAO(I)	1 - 7	4823.8
	8 - 32	2500.0
STNRA(I,1)	All	.0001
STNCA(I,1)	All	- .0001
STNZA(I,1)	All	- .0001
SRADA(I,1)	All	500
SCIRCA(I,1)	All	- 500

Typical results from this run using a 7000 psi input pulse are shown in Figures 25 and 26 for the stress and strain distributions along the I = 1 line.

As can be seen from the plots, the initial values of the variables are those input as the initial conditions. Thereafter the stress and strain time histories proceed in a rather normal manner but are displaced positively or negatively in accordance with the initial permanent set values.

SECTION VII

CONCLUSIONS AND RECOMMENDATIONS FOR FURTHER WORK

Section VI has presented the results of the computer studies which have been run to verify the validity of the theoretical analyses in comparison with known solutions and experimental test results.

The elastic steady state and elastic-plastic steady state solutions agree quite well with known closed-form solutions. In addition, the test results agree with the theoretically predicted solutions to within the expected accuracy of the experimental techniques. The case showing the multiple runs option with a prestressed specimen yields results that would be expected.

In view of the above, the following recommendations for additional work are suggested:

1) Extend the program to include other similar geometries such as spheres and cylinders with various end conditions.
2) Incorporate the capability to evaluate strain rate effects.
3) Add a subprogram to predict reverse yielding during unloading and to compute the associated stress and strain distributions.

In final summary, it is concluded that the method of analysis presented in this work and the accompanying computer programs provide a means of calculating the transient stress wave and unloading shock wave behavior in a disk or open-ended cylinder in which the plane stress assumption is not greatly in error. Of even more importance, it lends some validity to the assumption that this general approach could be applied to any problem involving propagation of one-dimensional stress waves under states of combined stress in the elastic-plastic range.

SELECTED NOMENCLATURE AND COMPUTER NAMES

Symbol	Computer Name	Description
A, B.	---	Points on r-t shock diagram (Figure 4). Coefficient matrices.
$\bar{\ }$(bar)	---	Denotes average of two adjacent values.
c	CO, CA	Elastic or plastic wave speed.
D	---	Point on r-t shock diagram (Figure 4).
$\delta(\ )$	---	Denotes jump or discontinuity in quantity in parentheses.
$\Delta\epsilon_p \approx d\epsilon_p$	DEPP	Equivalent plastic strain increment.
$d\epsilon_{ij}$		Plastic strain increment.
E	EO, EA	Modulus of elasticity or plastic tangent modulus.
ϵ_r	STNRA	Radial strain.
ϵ_θ	STNCA	Circumferential strain.
ϵ_z	STNZA	Axial or longitudinal strain.
i	I	Radial coordinate line number.
j	J	+ c Characteristic number.
$d\lambda$	---	Constant relating plastic strain increment and deviatoric stress tensor.
ν	NU	Poisson's ratio.
p	---	Pressure.
r	RA	Radial coordinate distance.
ρ	RHO	Mass density.
S_{ij}	---	Deviatoric stress tensor.
σ_r	SRADA	Radial stress.

Symbol	Computer Name	Description
σ_θ	SCIRCA	Circumferential stress.
σ_z	---	Axial or longitudinal stress.
σ_{eq}	SIGEQ	Equivalent stress.
σ_m	---	Mean stress.
σ_o	SIGMAO	Yield stress.
t	TA	Time.
u	---	Radial displacement.
v	VA	Particle velocity.
V_o	---	Initial elemental volume.
V	---	Final elemental volume.
w	---	Axial or longitudinal displacement.
1,2	---	Subscripts denoting adjacent characteristic points or variables on either side of an unloading shock.

ADDITIONAL SELECTED COMPUTER NAMES

Computer Name	Description
ALI	Aitken-Lagrangian Interpolation Routine.
ATSM	A subroutine which orders tabular data suitable for use in ALI.
CINTRP	Interpolated wave speed c.
DELEP	Increment between SIGMAE and EPSILN entries.
DELRA	Increment in radial coordinate r.
DEPRP	Radial plastic strain increment.
DEPCP	Circumferential plastic strain increment.
DEPZP	Axial or longitudinal plastic strain increment.
DERIVL	A subroutine which computes the derivatives of a tabulated function.
EINTRP	Interpolated elastic or plastic modulus.
EPSEQ	Equivalent plastic strain.
EQSEQ1	Initial estimate of equivalent plastic strain.
EPSILN	A tabular entry of strain from the stress-strain curve.
GAUSS	A subroutine which solves systems of linear equations by Gaussian Elimination.
ISTART	I-line at which unloading shock starts.
ISWST	Internal indicator controlling when strains during unloading are to be computed.
ITERM	I-line at which unloading shock terminates.
N	Integer index.
NA	Number of radial coordinate lines in characteristic grid.
NE	Number of entries of tabulated stress-strain curve.
NT	Number of entries of tabulated stress-time input.

Computer Name	Description
RA1	Inside radius of disk.
SIGE	Stress in called subroutine variable list.
SIGMAE	Tabulated stress values from stress-strain curve.
SIGMAT	Tabulated stress values from stress-time input.
SIGMAX(I)	Maximum equivalent stress attained along the ith r line.
SIGN	A subroutine which assigns the algebraic sign of one variable to another variable.
SIGT	Stress in called subroutine variable list.
TA	Time.
TANN	The trial time intercept of a - c characteristic segment on an r line from the r + 1 line.
TAPP	The trial time intercept point of a + c characteristic line segment on an r line from an r - 1 line.
TESTEP	A small test number used to determine the convergence of an iterated variable.
TIM	Time in called subroutine variable list.
TRANSL	A linear interpolation routine used to effectively translate the variables associated with the larger of the TAPP or TANN intercepts to coincide with those of the smaller.
XEPRP	Intermediate value of radial plastic strain increment during iteration.
XEPCP	Intermediate value of circumferential plastic strain increment during iteration.
XEPZP	Intermediate value of axial or longitudinal plastic strain increment during iteration.

APPENDIX A

FIGURES

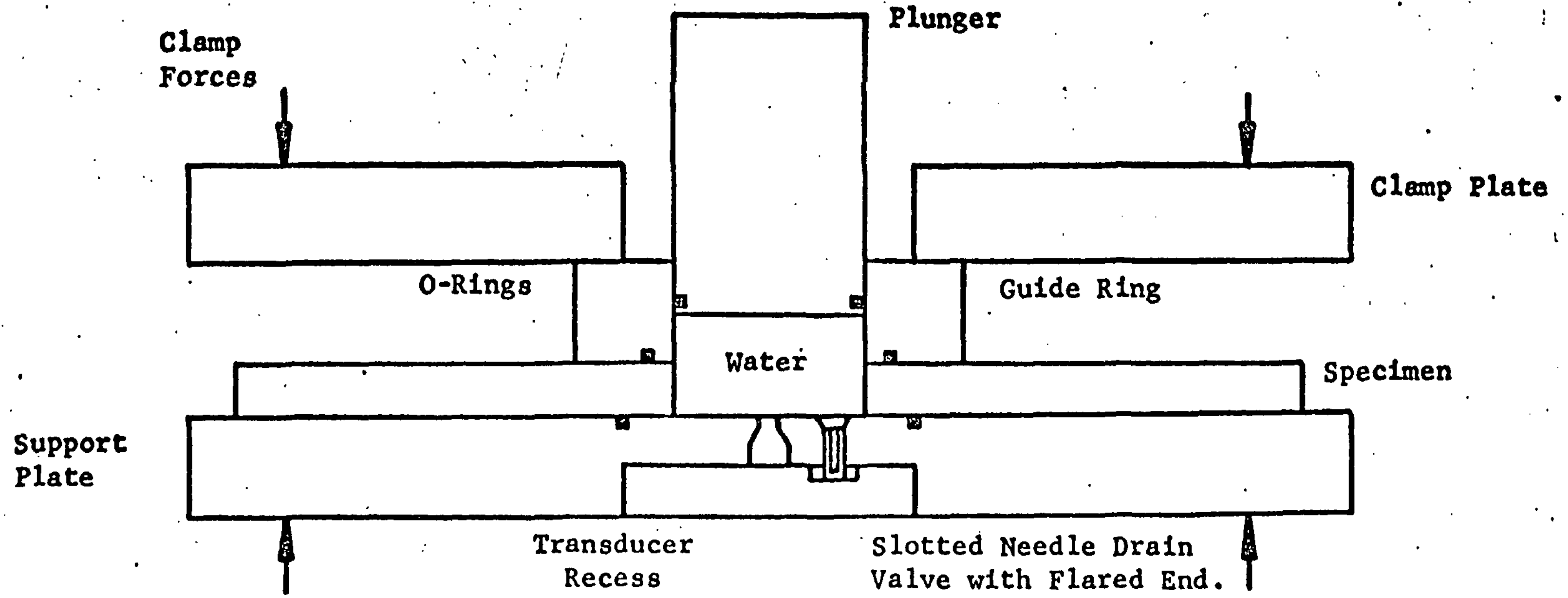

Fig. 1a.--Experimental Fixture--Sectioned Assembly Sketch

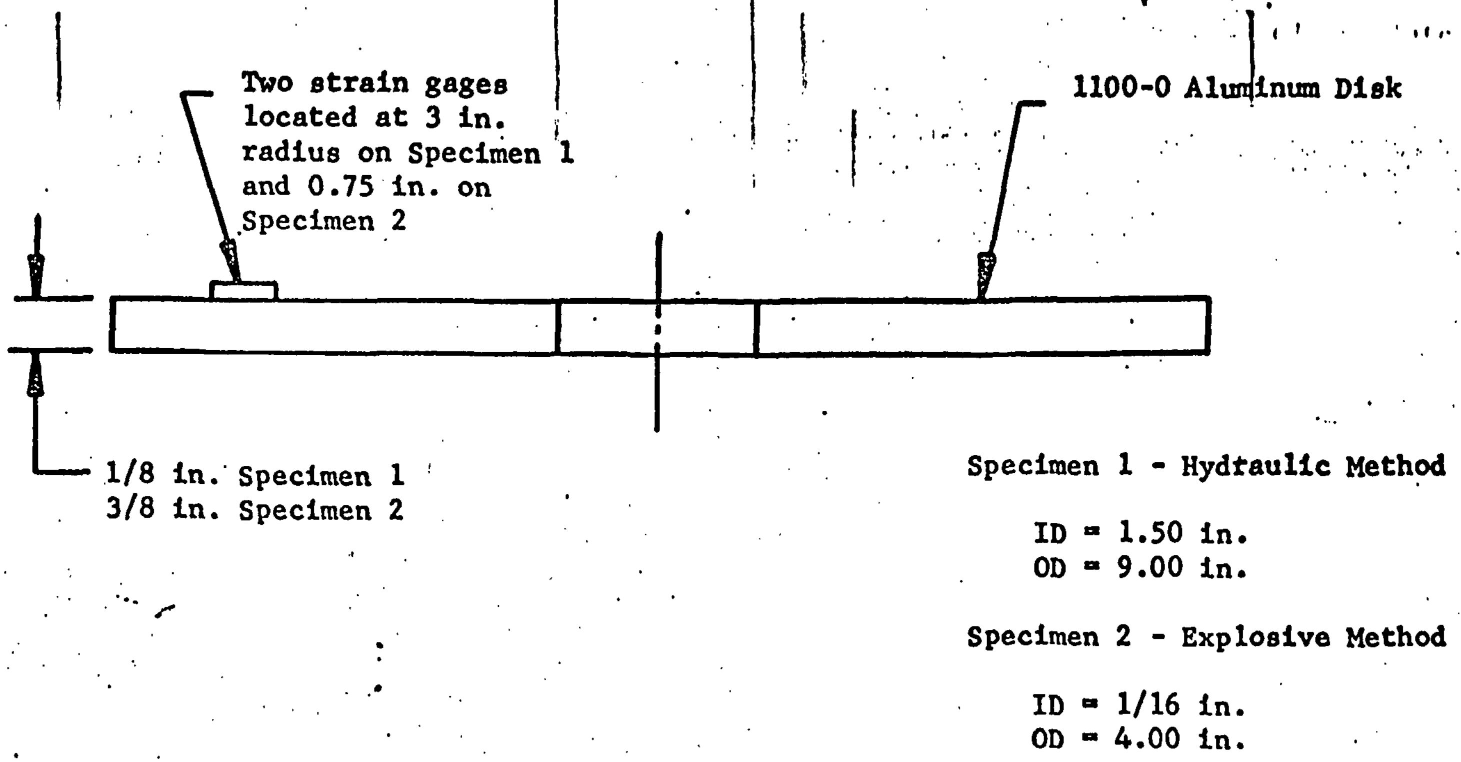

Fig. 1b.--Specimens

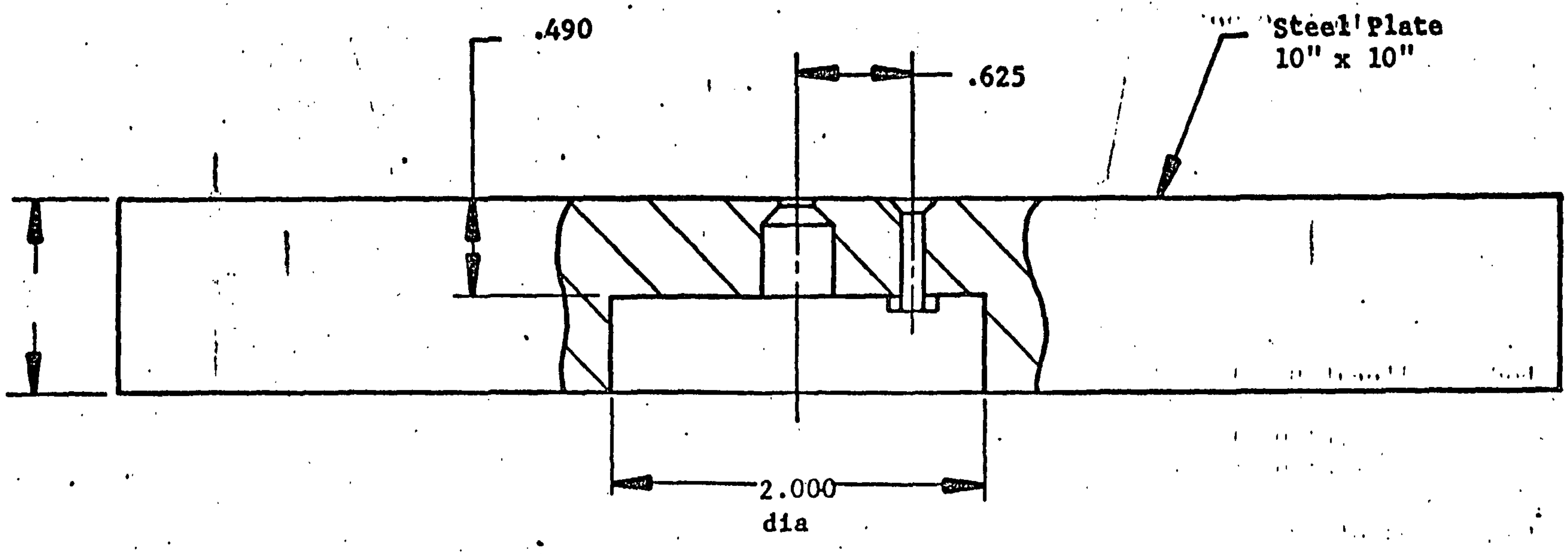

Fig. 1c.--Support Plate

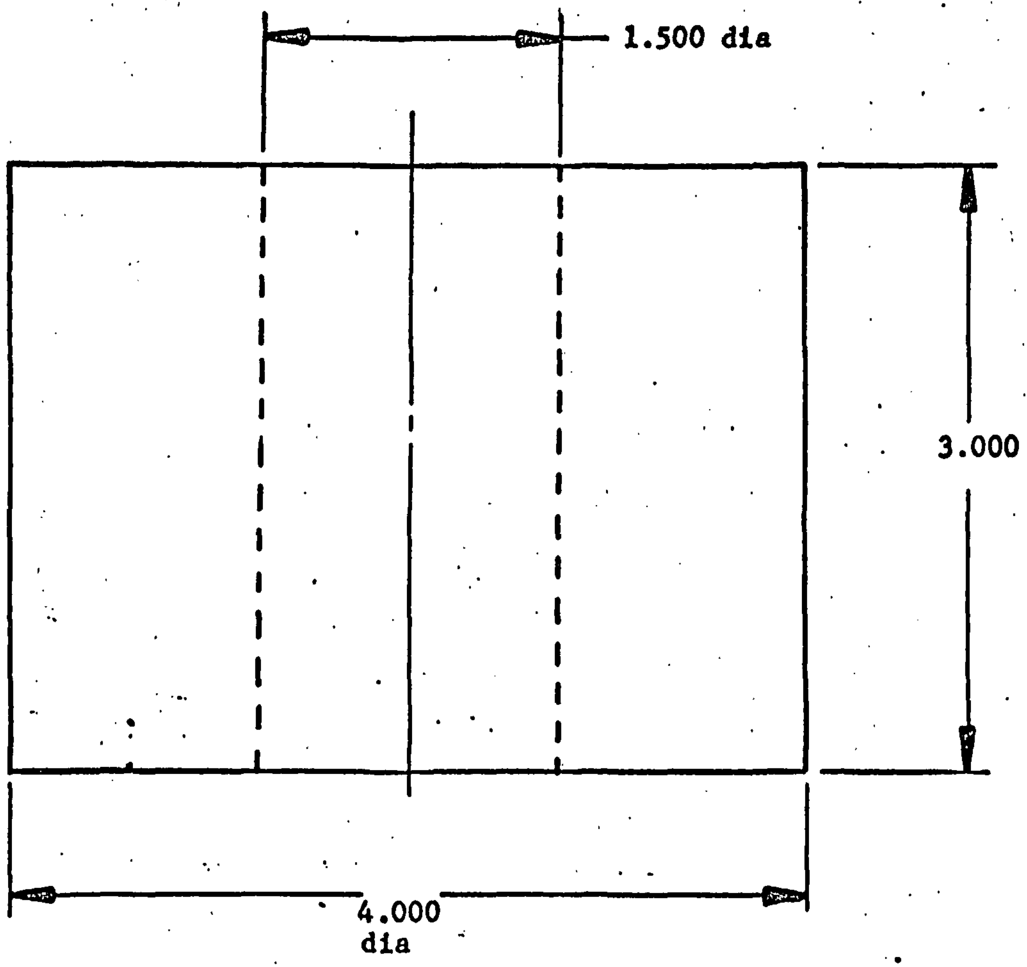

Fig. 1d.--Guide Ring

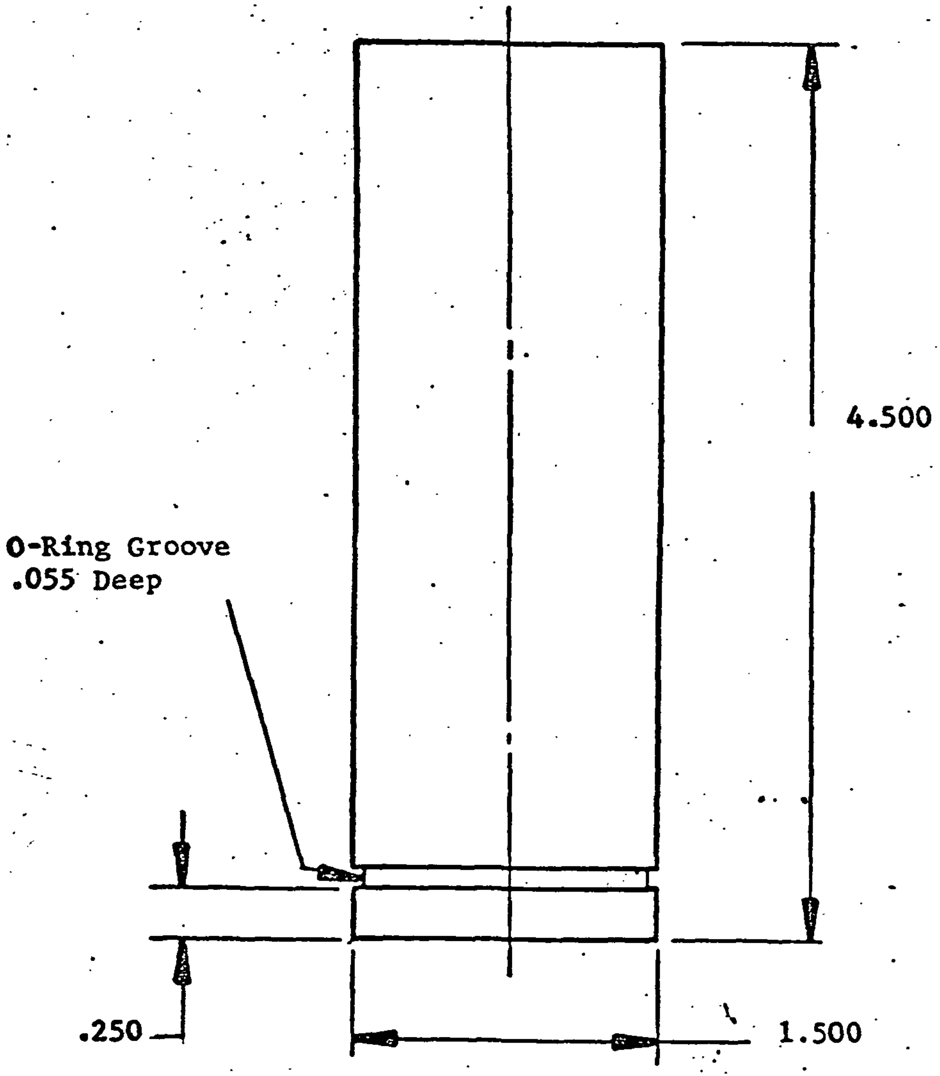

Fig. le.--Plunger

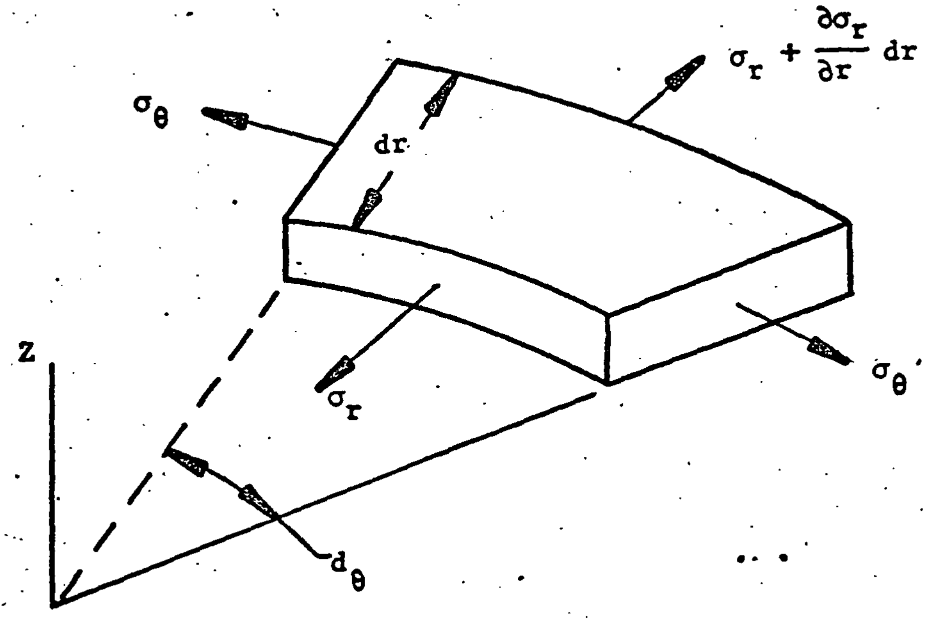

Fig. 2.--Infinitesimal Specimen Element

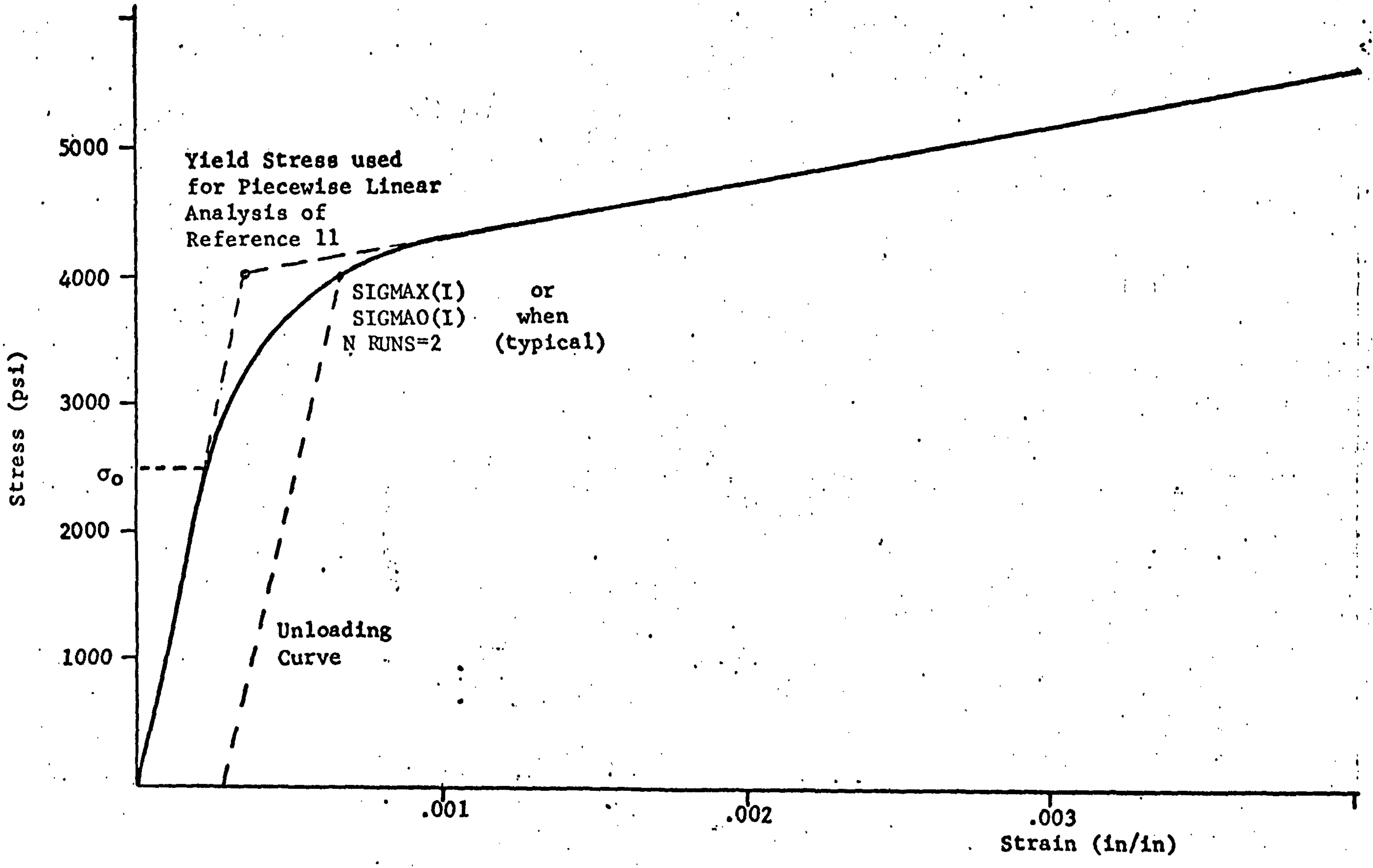

Fig. 3.--Stress-Strain Curve for Aluminum 1100-0

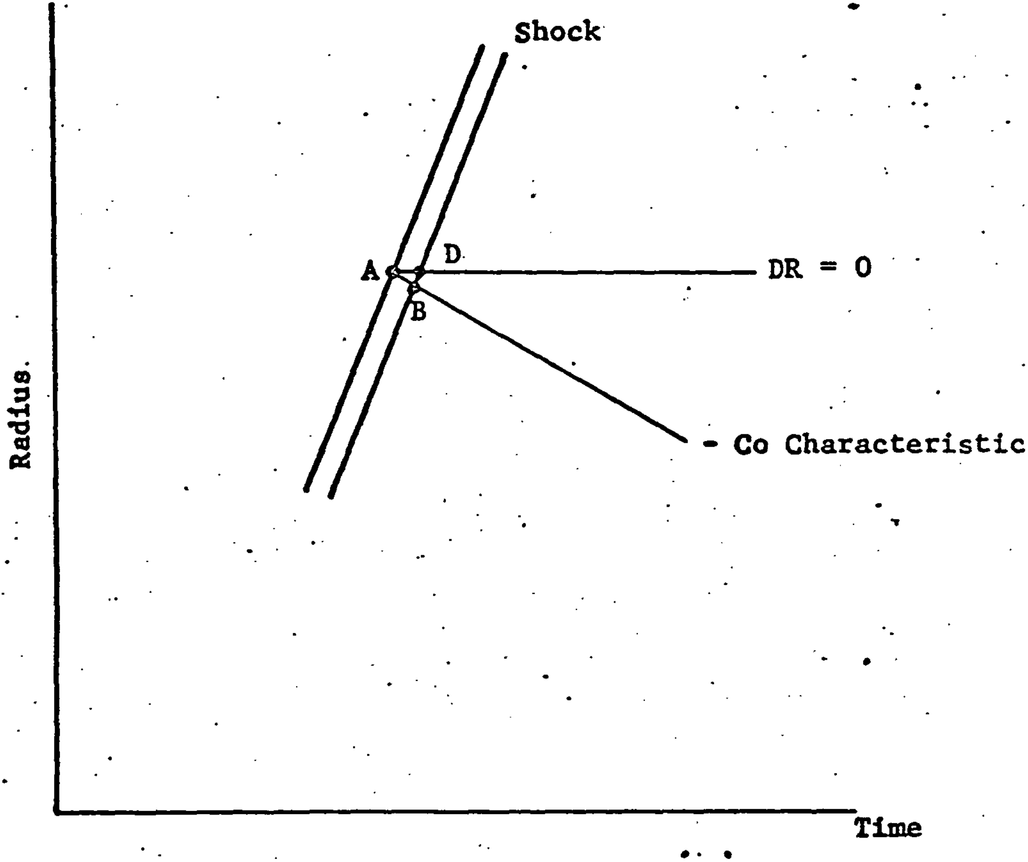

Fig. 4.--Unloading Shock Wave Schematic

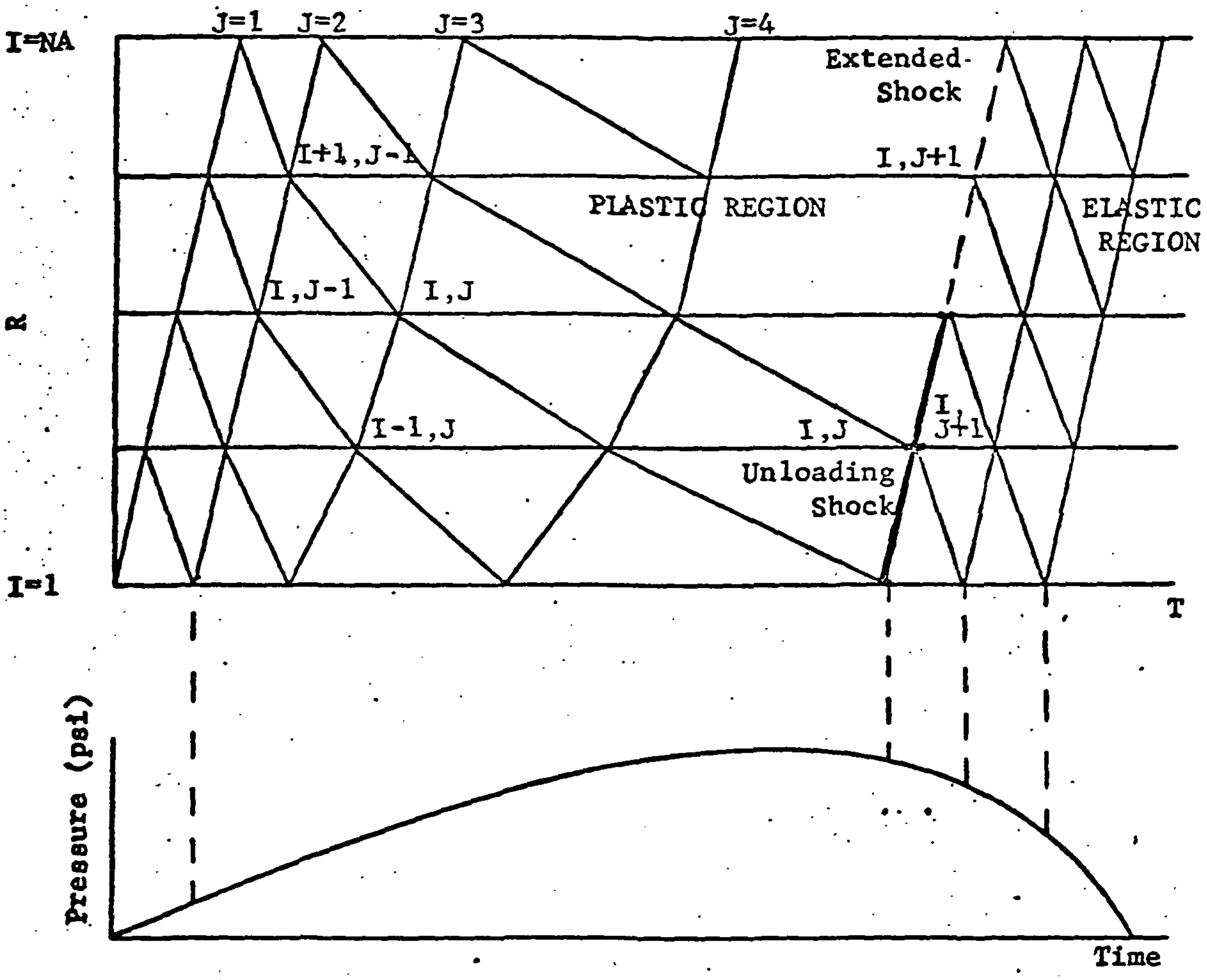

Fig. 5.--Characteristic Network with Indexing Notations and Applied Pressure Schematic.

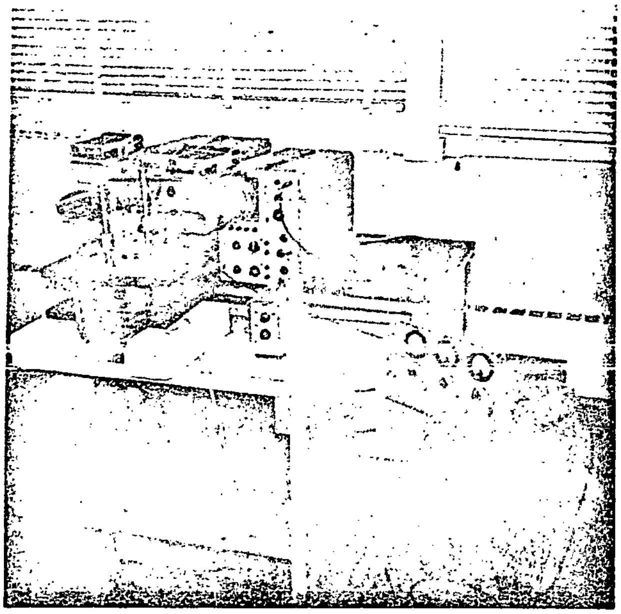

Fig. 6.--Experimental Fixture and Instrumentation
(Photograph)

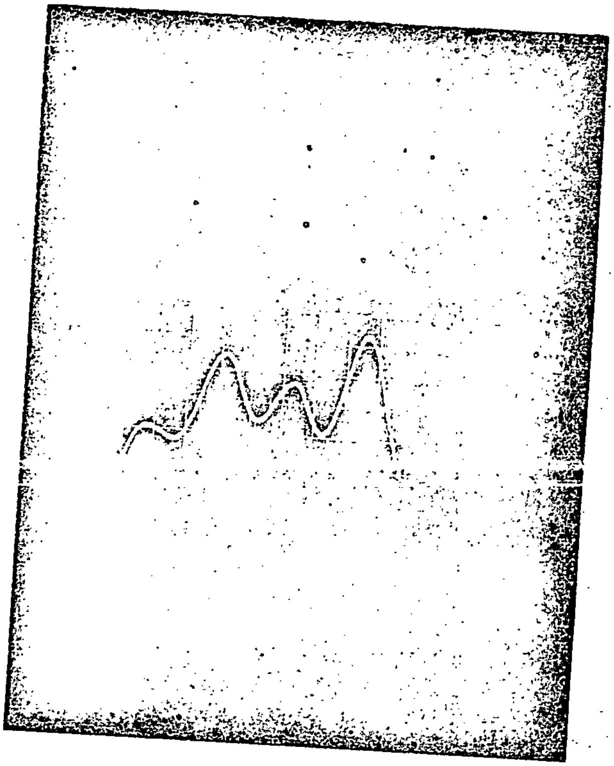

Fig. 7.--Pressure Pulse Experimental Data Using Specimen 1 of Figure 1b (Hydraulic Method).

Radial Gage - Top Trace

Circumferential Gage - Bottom Trace

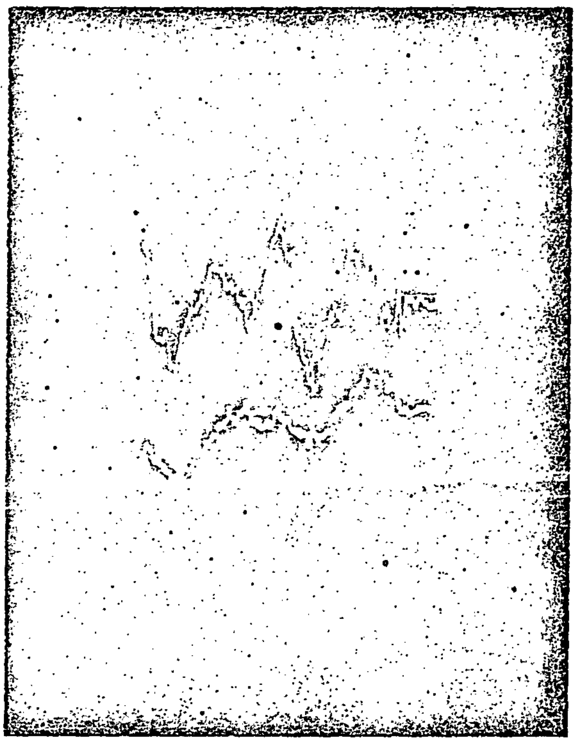

Fig. 8.--Strain History Experimental Data Using Specimen 1 of Figure 1b (Hydraulic Method).

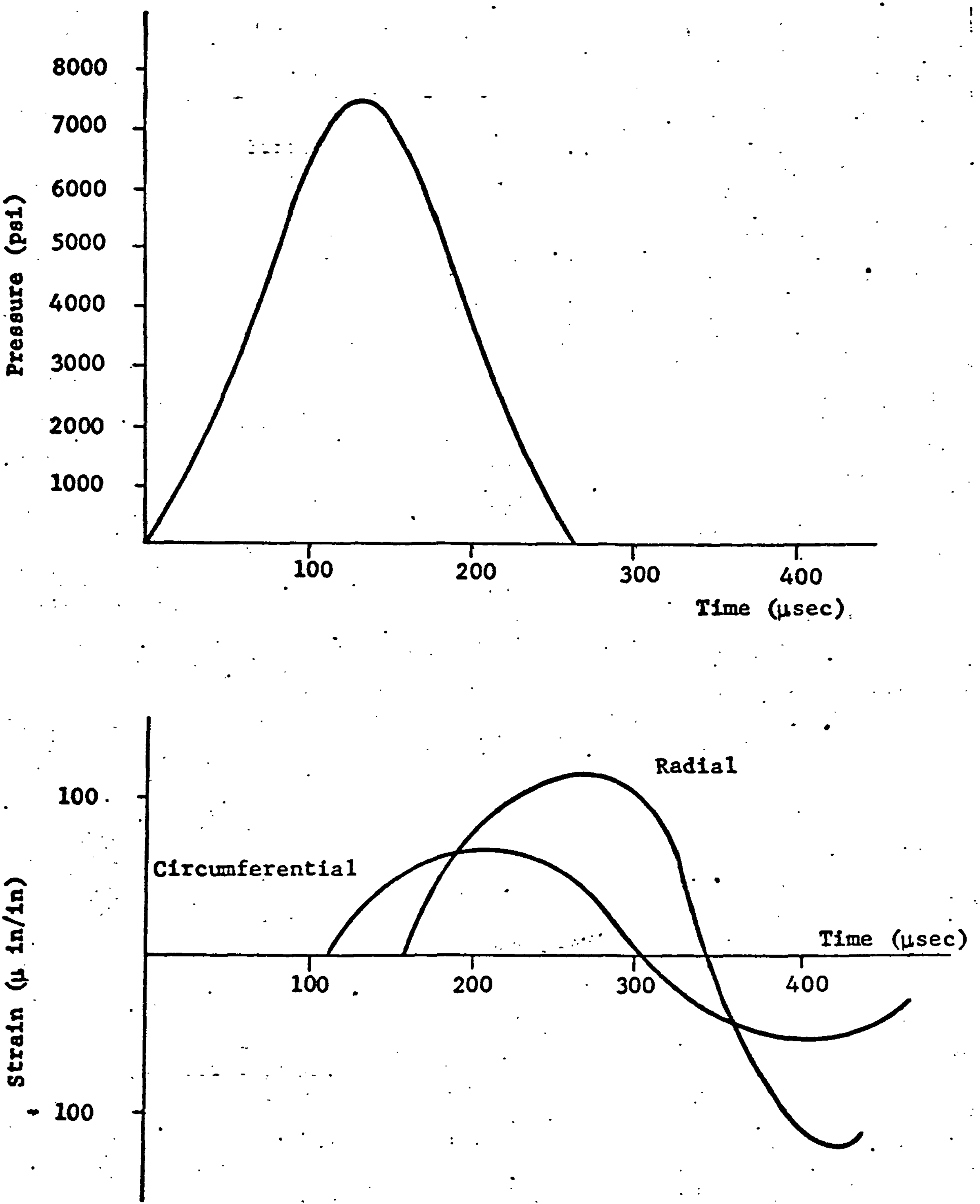

Fig. 9.--Plot of Pressure Pulse and Strain History Experimental Data (Hydraulic Method).

Fig. 10.--Pressure Pulse Experimental Data Using Specimen 2 of Figure 1b (Explosive Method).

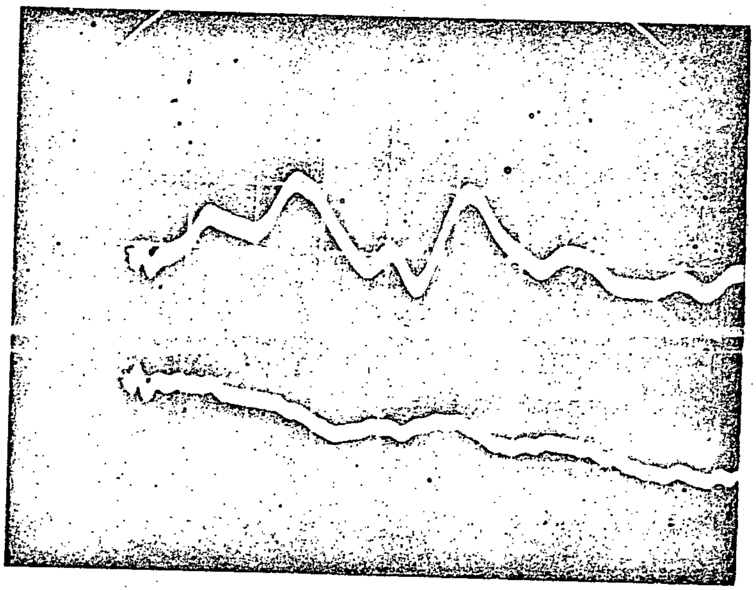

Fig. 11.--Strain History Experimental Data Using Specimen 2 of Figure 1b (Explosive Method).

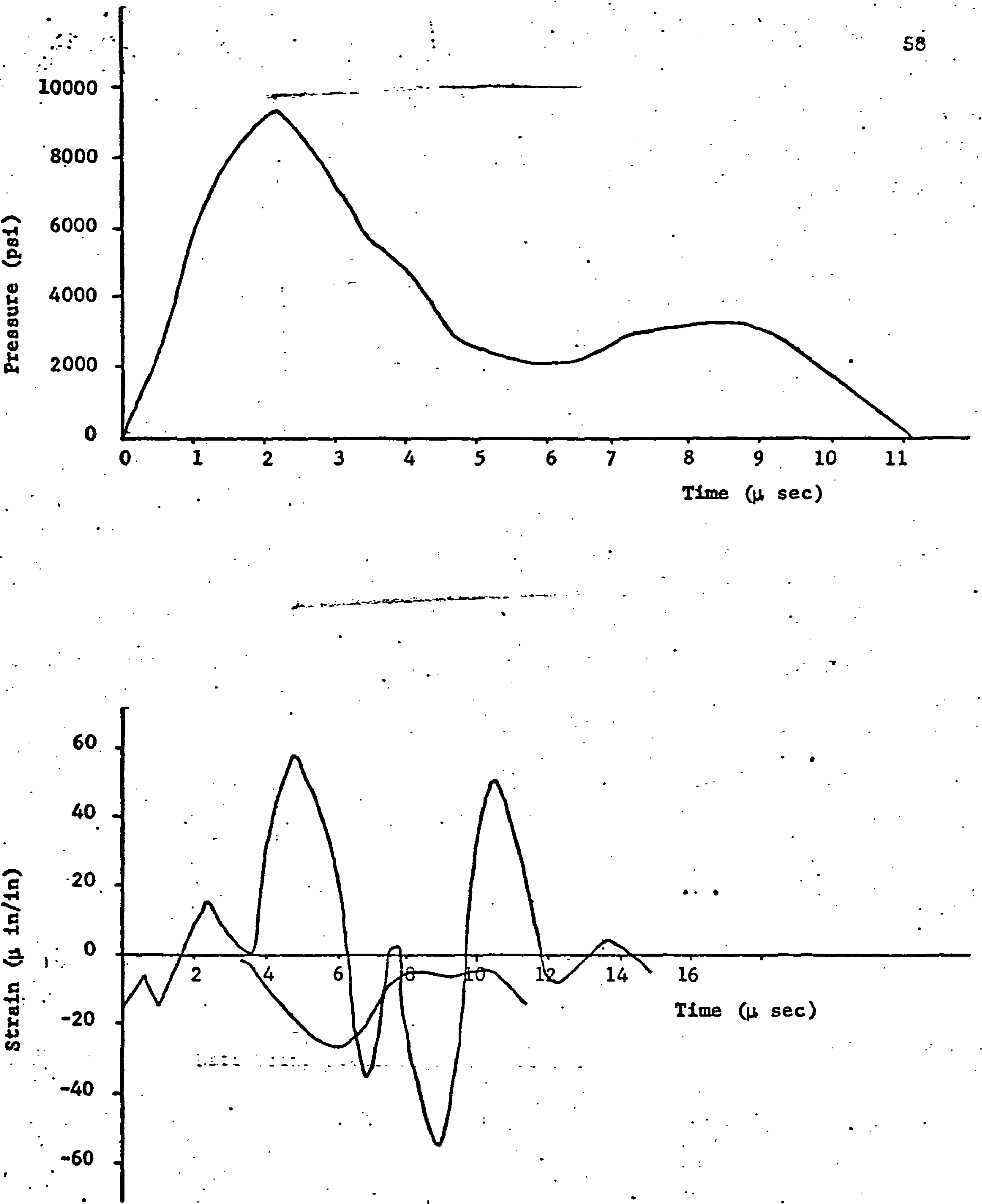

Fig. 12.--Plot of Pressure Pulse
and Strain History Experimental Data (Explosive Method).

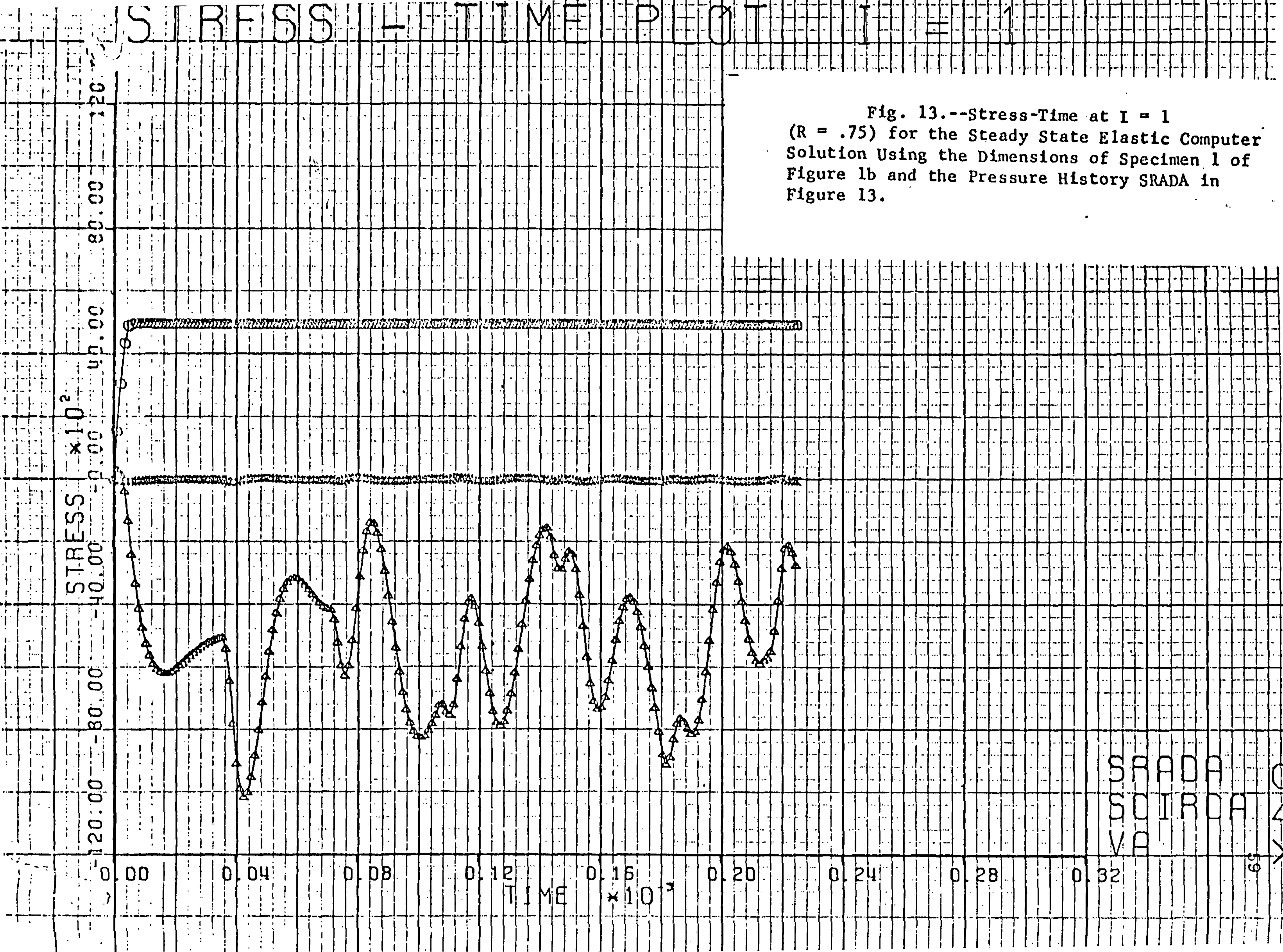

Fig. 13.--Stress-Time at I = 1 (R = .75) for the Steady State Elastic Computer Solution Using the Dimensions of Specimen 1 of Figure 1b and the Pressure History SRADA in Figure 13.

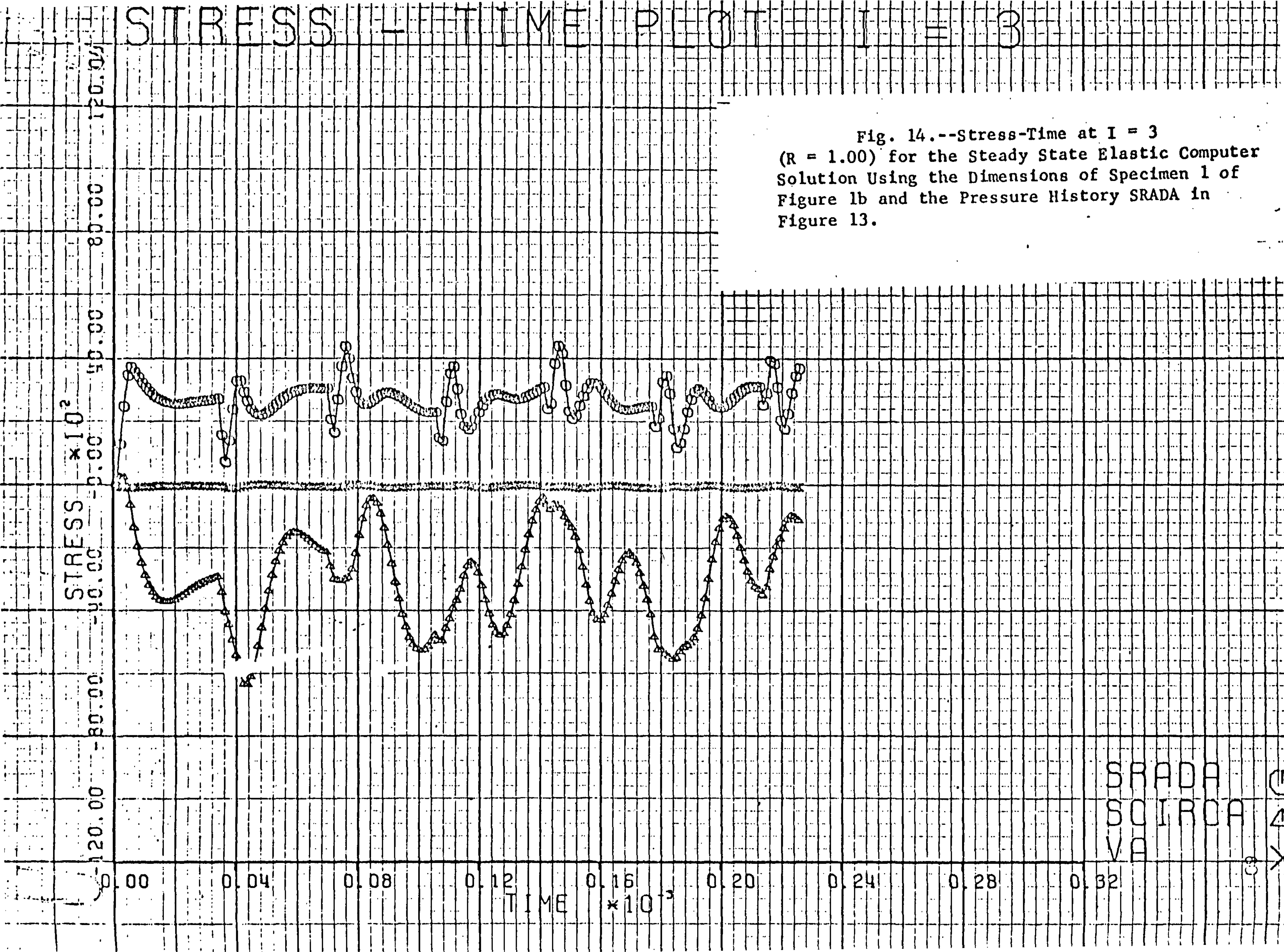

Fig. 14.--Stress-Time at I = 3 (R = 1.00) for the Steady State Elastic Computer Solution Using the Dimensions of Specimen 1 of Figure 1b and the Pressure History SRADA in Figure 13.

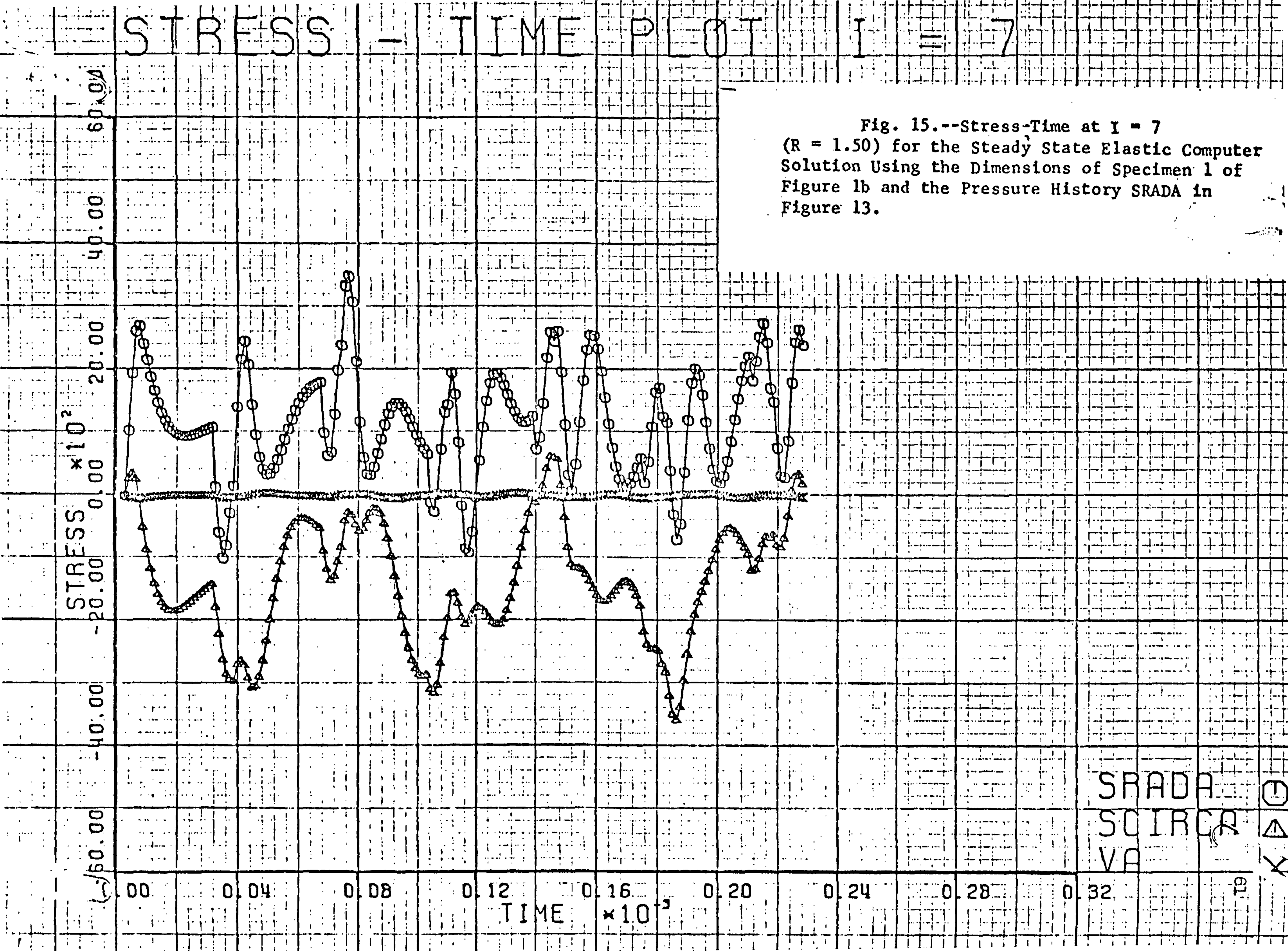

Fig. 15.--Stress-Time at I = 7 (R = 1.50) for the Steady State Elastic Computer Solution Using the Dimensions of Specimen 1 of Figure 1b and the Pressure History SRADA in Figure 13.

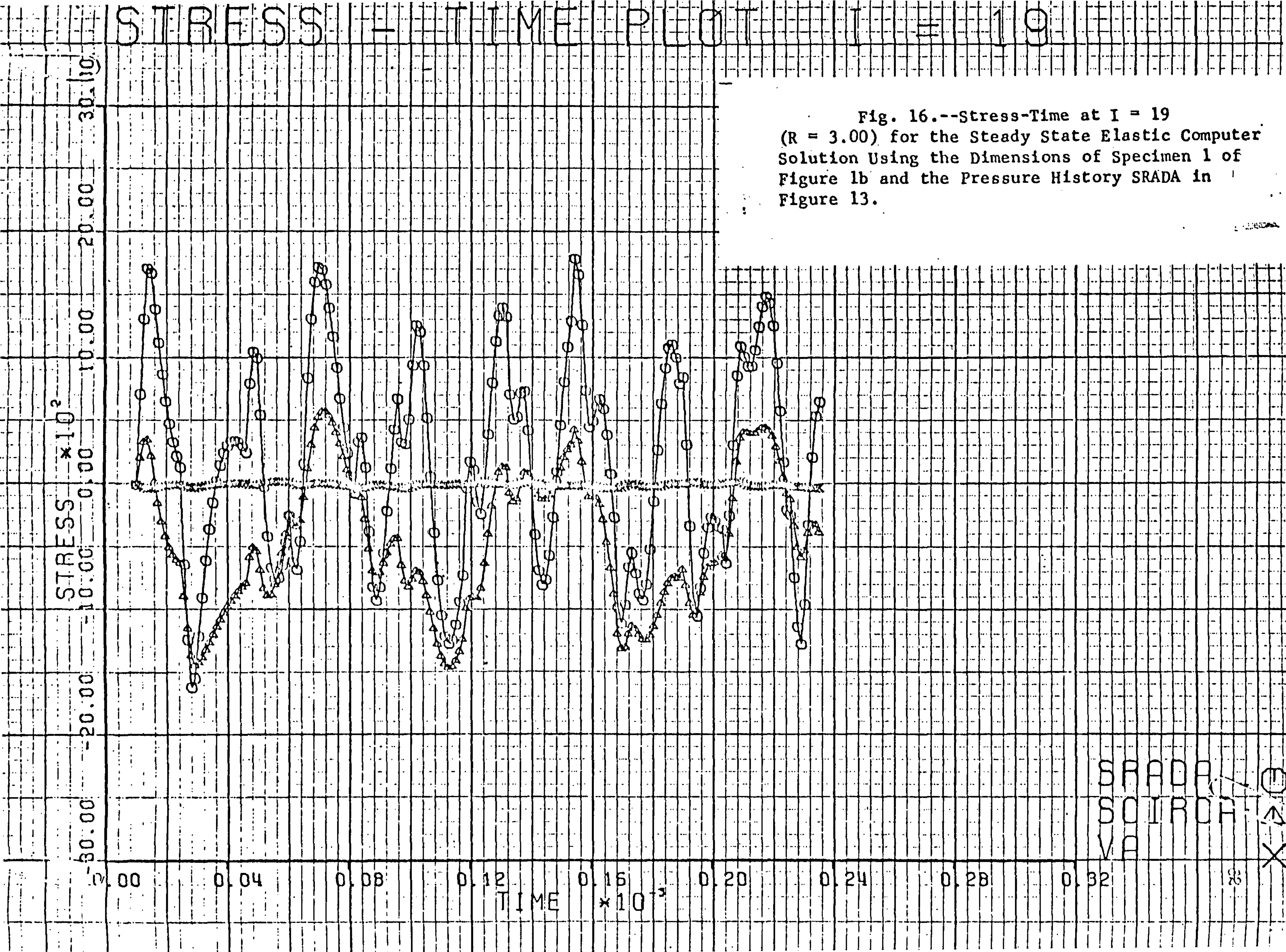

Fig. 16.--Stress-Time at I = 19 (R = 3.00) for the Steady State Elastic Computer Solution Using the Dimensions of Specimen 1 of Figure 1b and the Pressure History SRADA in Figure 13.

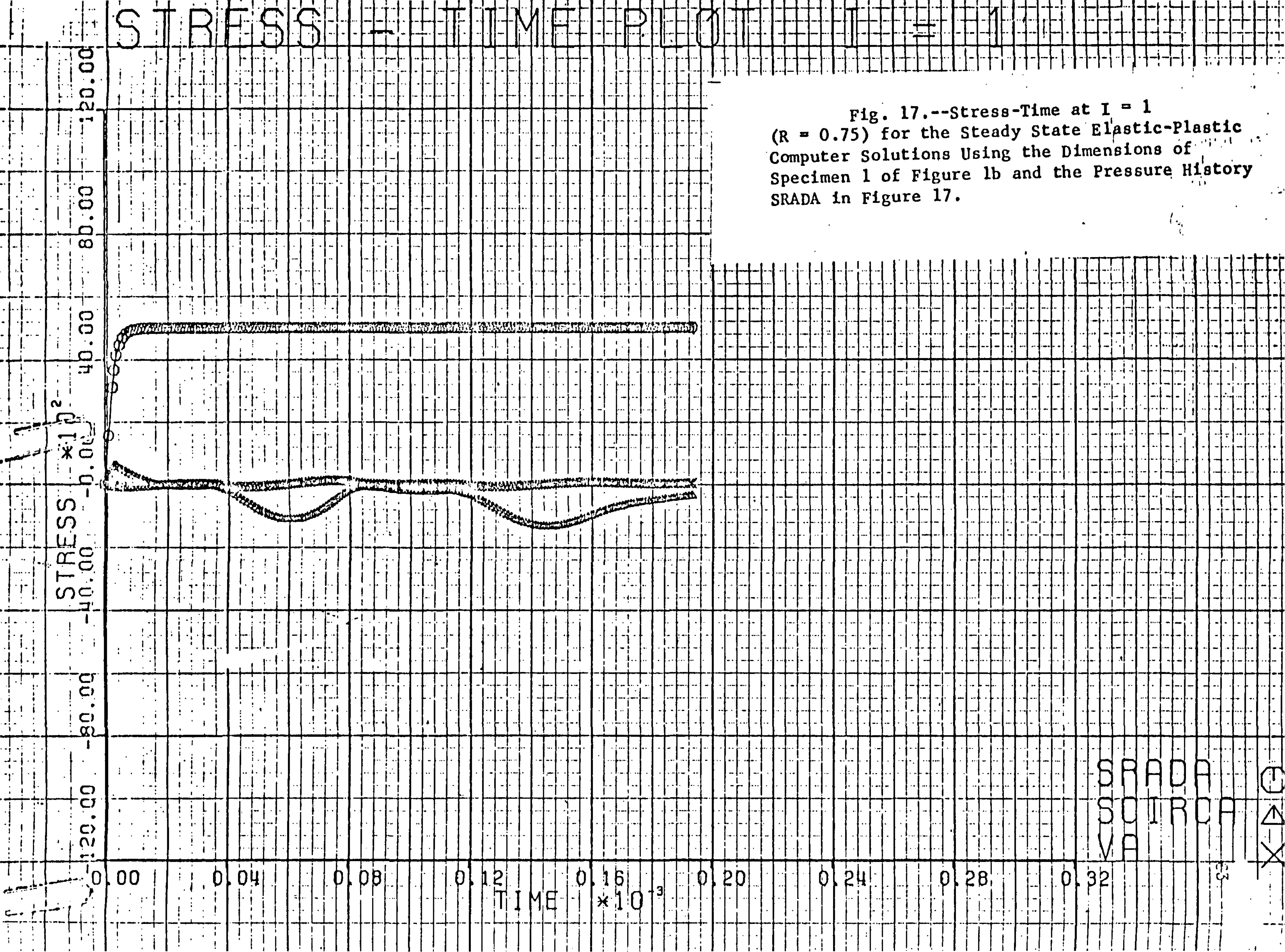

Fig. 17.--Stress-Time at I = 1 (R = 0.75) for the Steady State Elastic-Plastic Computer Solutions Using the Dimensions of Specimen 1 of Figure 1b and the Pressure History SRADA in Figure 17.

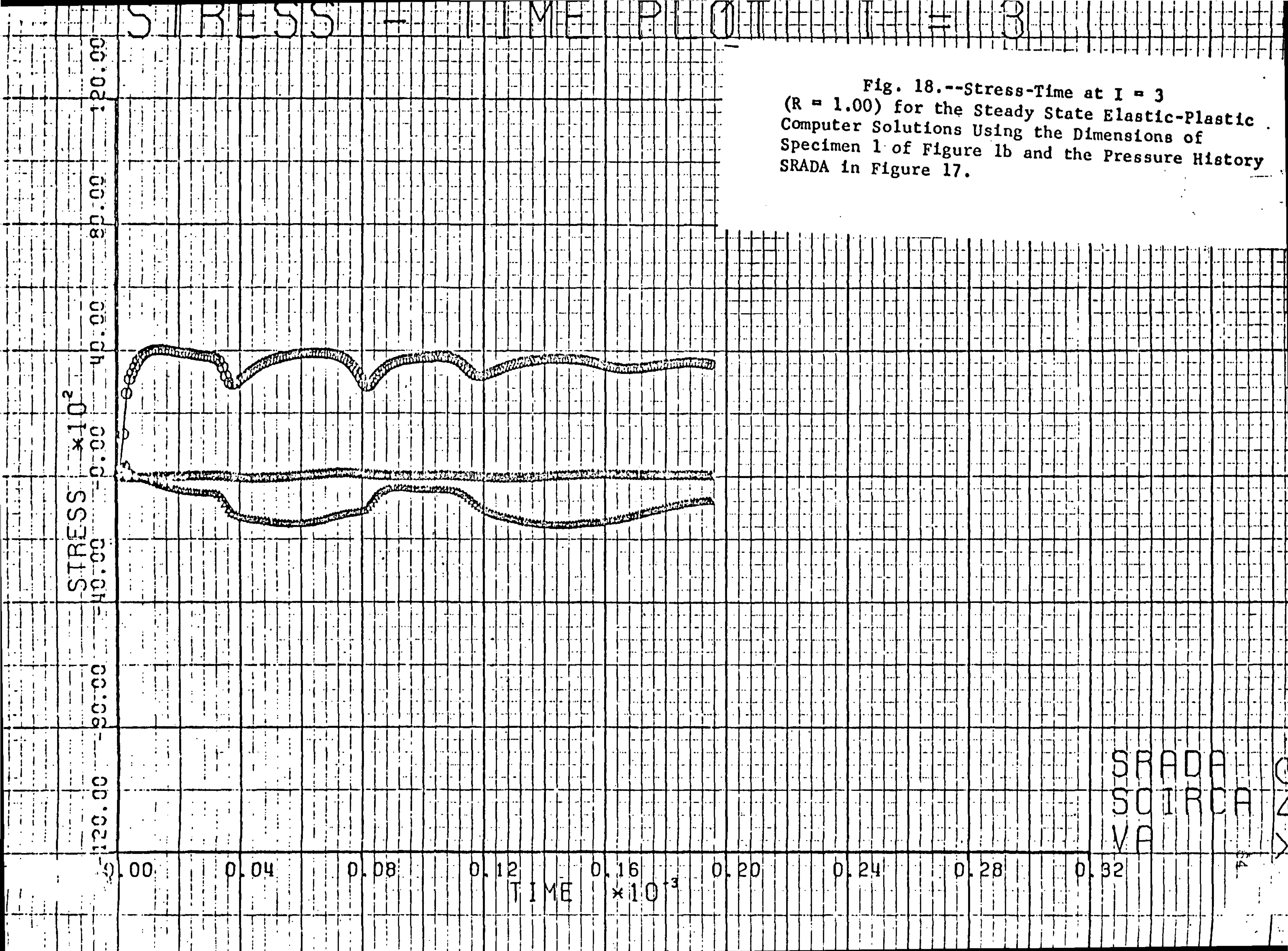

Fig. 18.--Stress-Time at I = 3 (R = 1.00) for the Steady State Elastic-Plastic Computer Solutions Using the Dimensions of Specimen 1 of Figure 1b and the Pressure History SRADA in Figure 17.

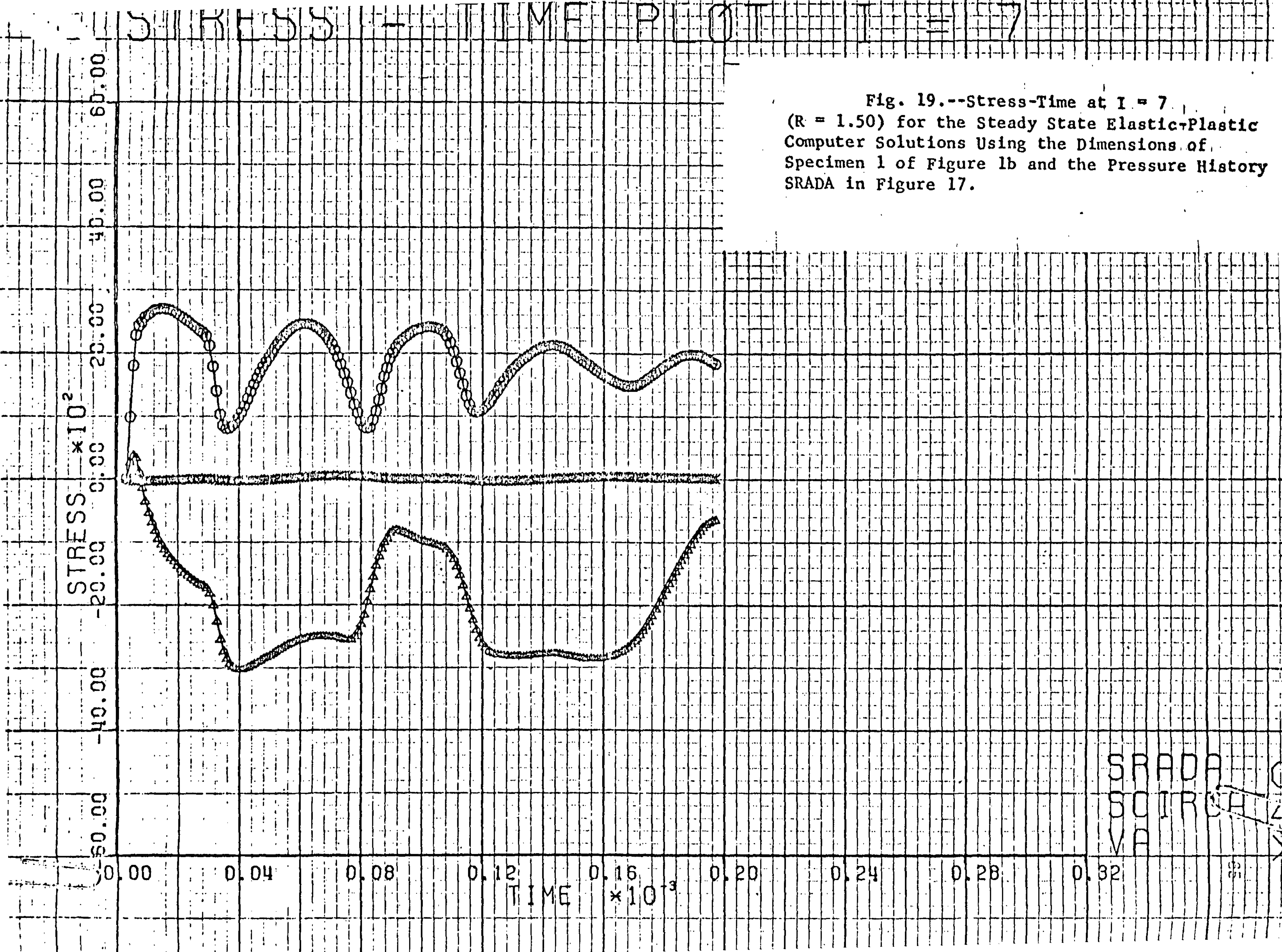

Fig. 19.--Stress-Time at I = 7 (R = 1.50) for the Steady State Elastic-Plastic Computer Solutions Using the Dimensions of Specimen 1 of Figure 1b and the Pressure History SRADA in Figure 17.

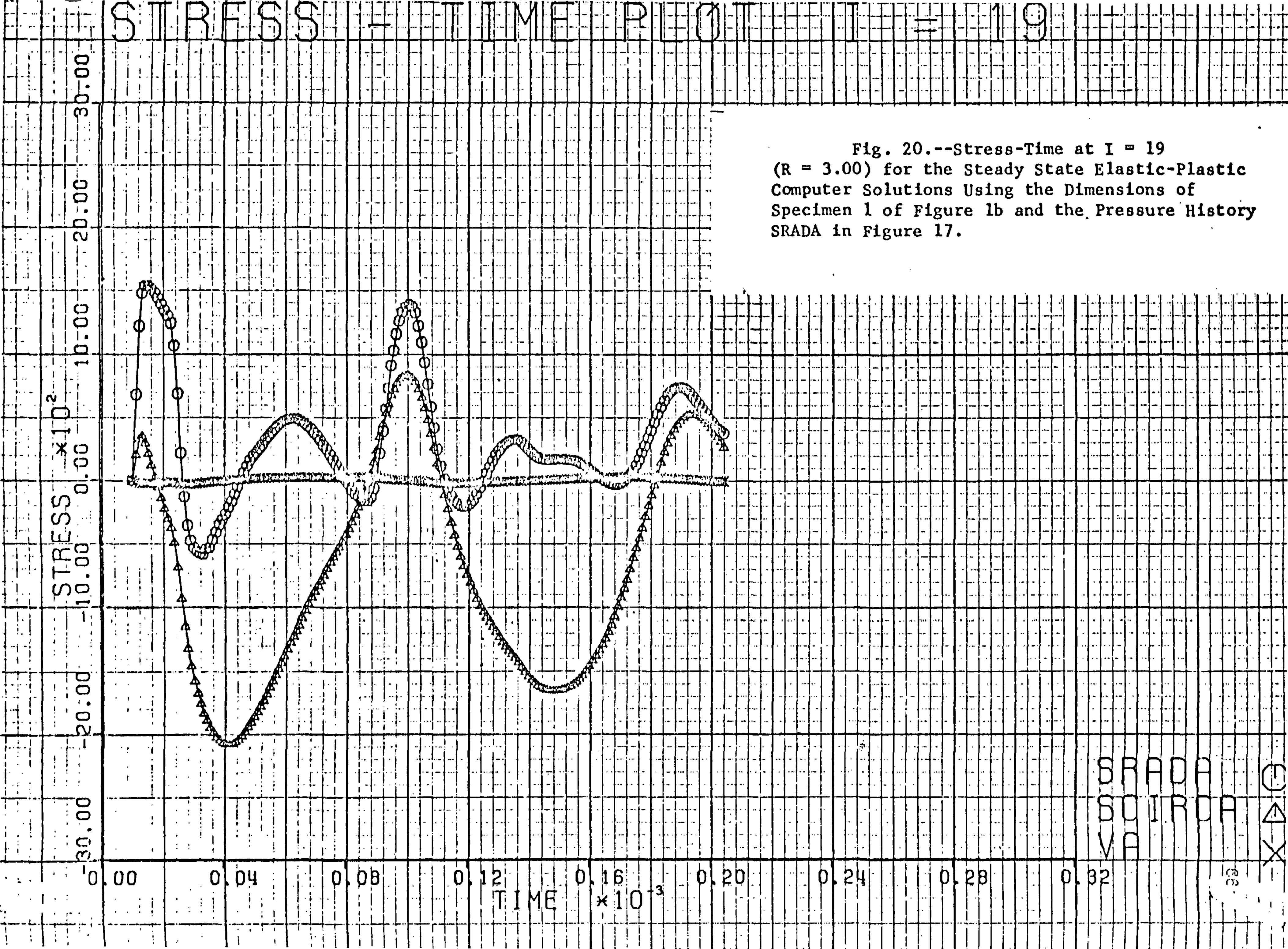

Fig. 20.--Stress-Time at I = 19 (R = 3.00) for the Steady State Elastic-Plastic Computer Solutions Using the Dimensions of Specimen 1 of Figure 1b and the Pressure History SRADA in Figure 17.

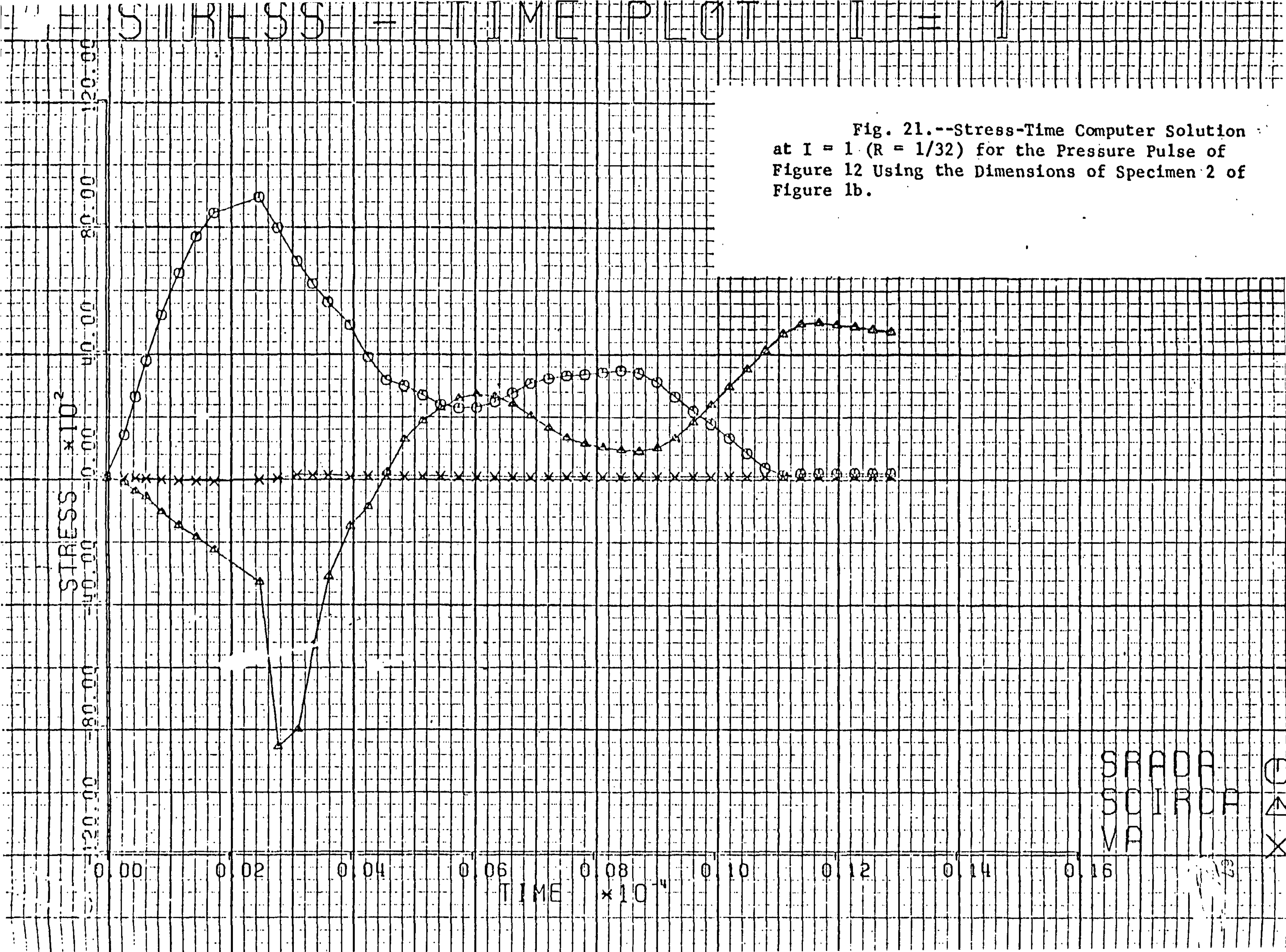

Fig. 21.--Stress-Time Computer Solution at I = 1 (R = 1/32) for the Pressure Pulse of Figure 12 Using the Dimensions of Specimen 2 of Figure 1b.

Fig. 22.--Stress-Time Computer Solution at I = 24 (R = 0.75) for the Pressure Pulse of Figure 12 Using the Dimensions of Specimen 2 of Figure 1b.

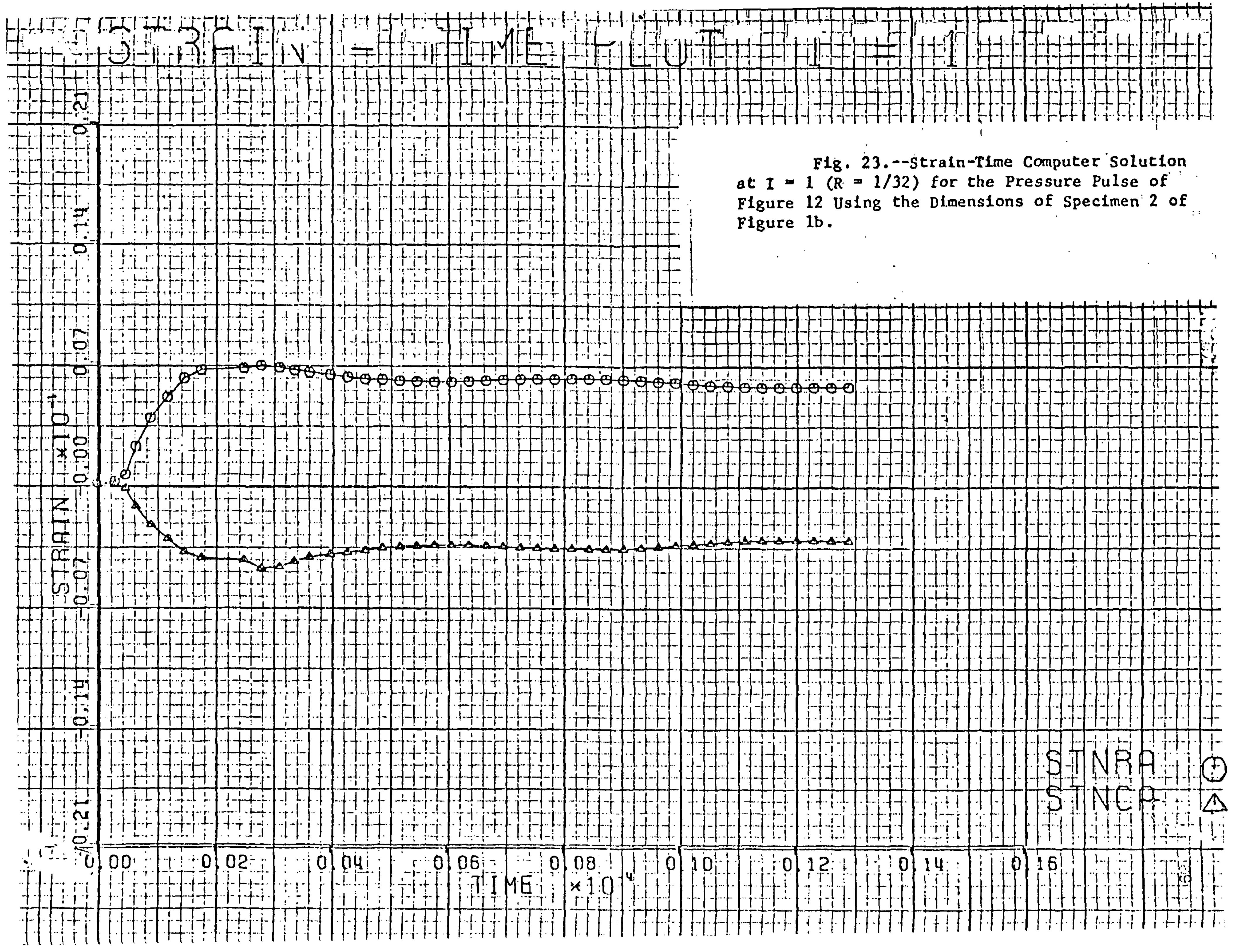

Fig. 23.--Strain-Time Computer Solution at I = 1 (R = 1/32) for the Pressure Pulse of Figure 12 Using the Dimensions of Specimen 2 of Figure 1b.

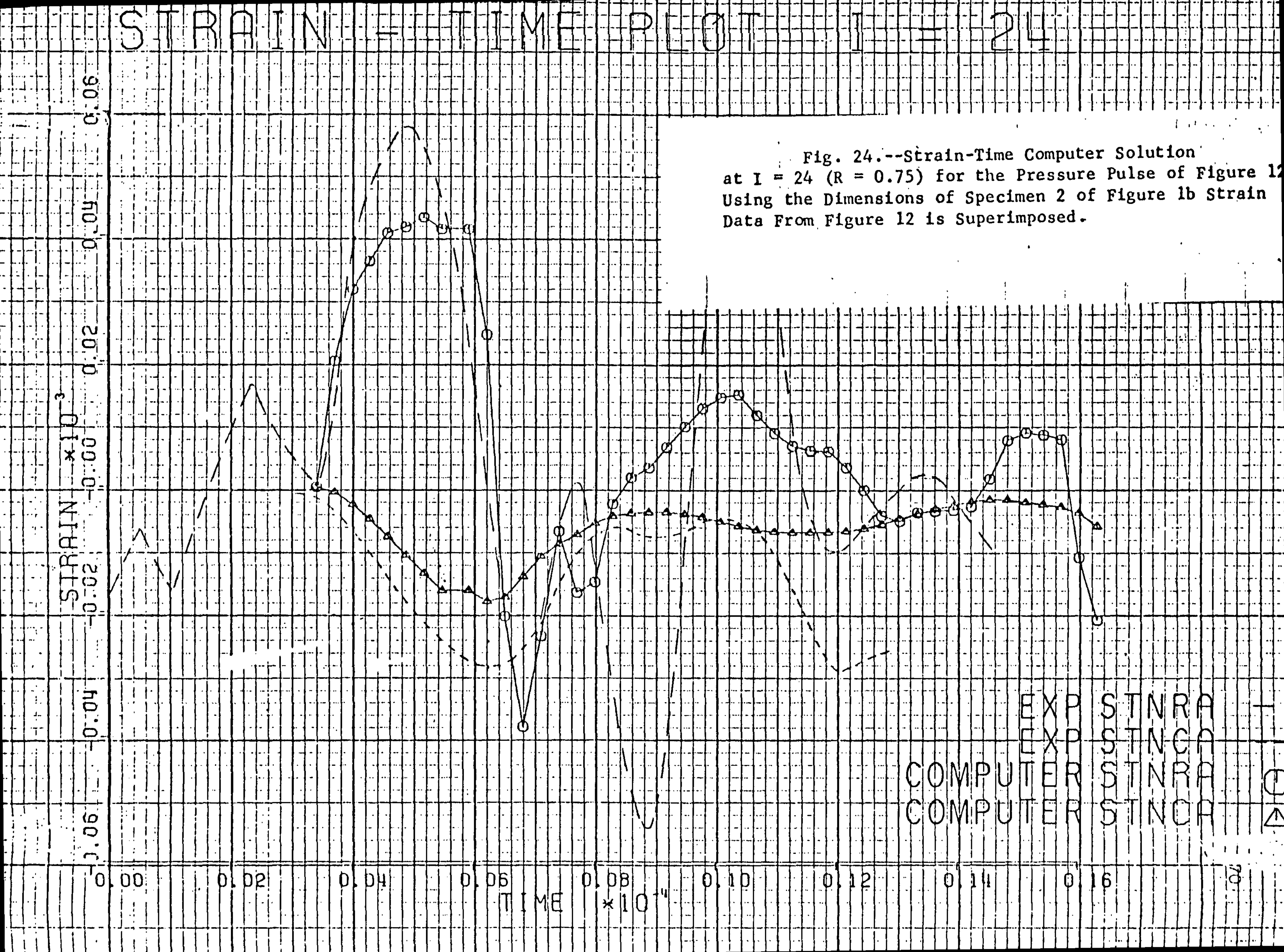

Fig. 24.--Strain-Time Computer Solution at I = 24 (R = 0.75) for the Pressure Pulse of Figure 12 Using the Dimensions of Specimen 2 of Figure 1b Strain Data From Figure 12 is Superimposed.

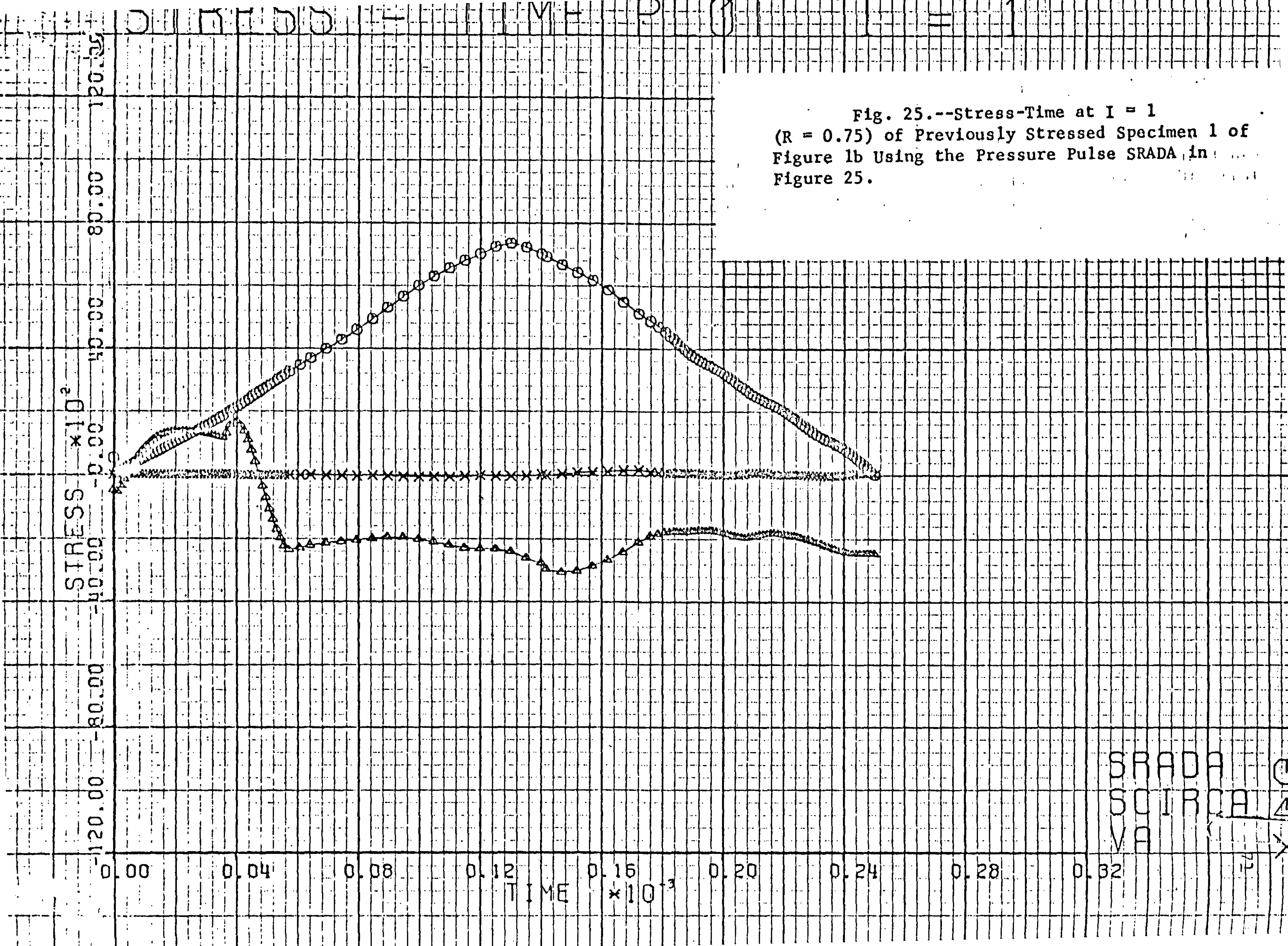

Fig. 25.--Stress-Time at I = 1 (R = 0.75) of Previously Stressed Specimen 1 of Figure 1b Using the Pressure Pulse SRADA in Figure 25.

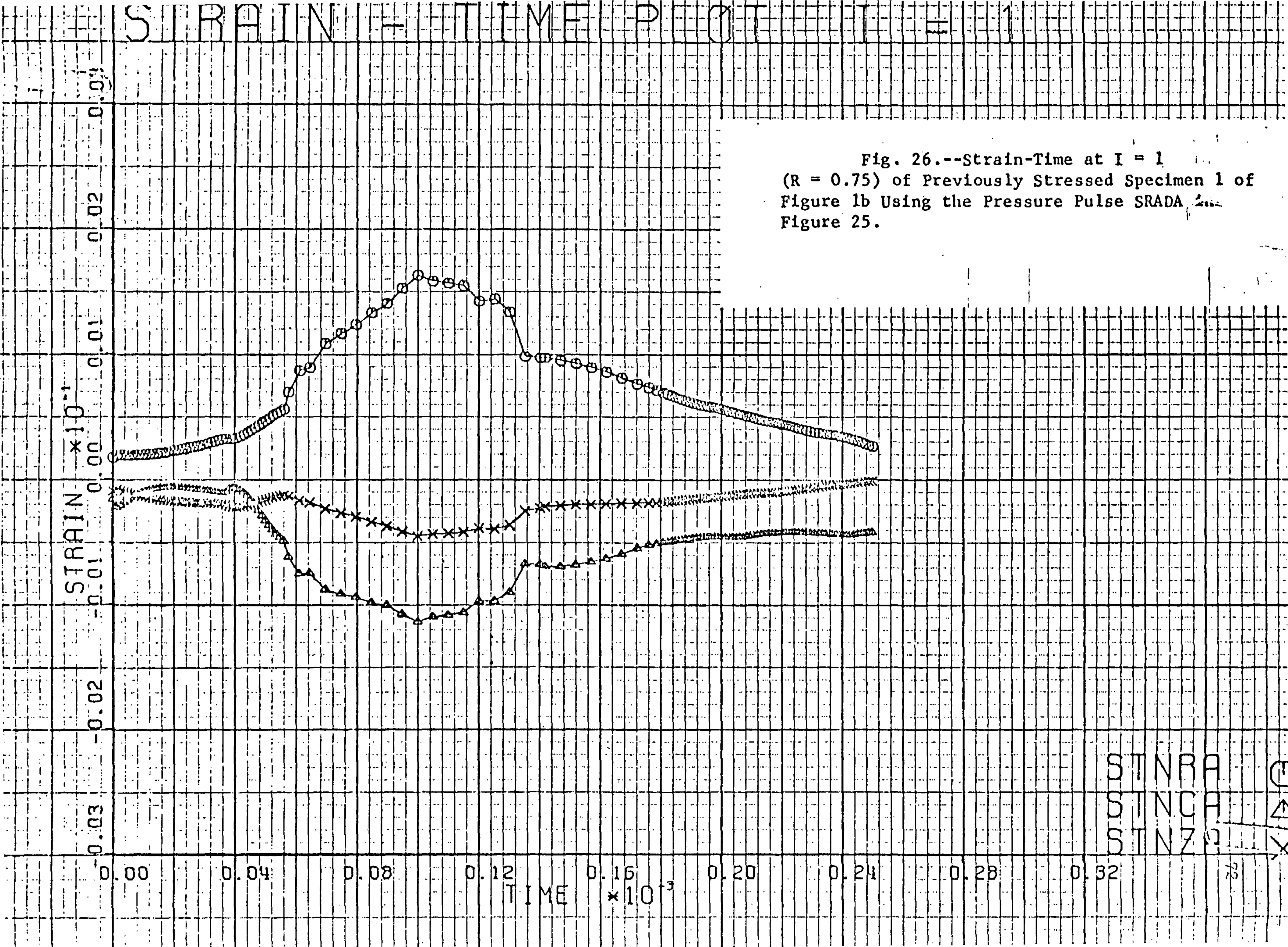

Fig. 26.--Strain-Time at I = 1 (R = 0.75) of Previously Stressed Specimen 1 of Figure 1b Using the Pressure Pulse SRADA in Figure 25.

APPENDIX B

CHARACTERISTIC DERIVATIONS

From Section III equations 3-1, 3-5, and 3-6 are

$$\frac{\partial \sigma_r}{\partial r} + \frac{\sigma_r - \sigma_\theta}{r} = \rho \frac{\partial v}{\partial t}$$

$$\frac{\partial v}{\partial r} = \frac{1}{E}\left[\frac{\partial \sigma_r}{\partial t} - \nu \frac{\partial \sigma_\theta}{\partial t}\right]$$

$$\frac{v}{r} = \frac{1}{E}\left[\frac{\partial \sigma_\theta}{\partial t} - \nu \frac{\partial \sigma}{\partial t}\right]$$

Writing this system in determinant form along with the differential changes in σ_r, σ_θ, and v gives

$$\begin{array}{lllll}
\frac{\partial \sigma_r}{\partial r} & & & - \rho \frac{\partial v}{\partial t} & = \frac{\sigma_\theta - \sigma_r}{r} \\[2ex]
& \frac{1}{E}\frac{\partial \sigma_r}{\partial t} & - \frac{\nu}{E}\frac{\partial \sigma_\theta}{\partial t} - \frac{\partial v}{\partial r} & & = 0 \\[2ex]
& - \frac{\nu}{E}\frac{\partial \sigma_r}{\partial t} & + \frac{1}{E}\frac{\partial \sigma_\theta}{\partial t} & & = \frac{v}{r} \\[2ex]
\frac{\partial \sigma_r}{\partial r} dr + \frac{\partial \sigma_r}{\partial t} dt & & & & = d\sigma_r \\[2ex]
& & \frac{\partial \sigma_\theta}{\partial r} dr + \frac{\partial \sigma_\theta}{\partial t} dt & & = d\sigma_\theta \\[2ex]
& & & \frac{\partial v}{\partial r} dr + \frac{\partial v}{\partial t} dt & = dv
\end{array}$$

Solving for $\frac{\partial \sigma_r}{\partial r}$ by Cramer's Rule yields

$$\frac{\partial \sigma_r}{\partial r} = \frac{A}{B}$$

where

$$B = \begin{vmatrix} 1 & 0 & 0 & 0 & 0 & -\rho \\ 0 & \frac{1}{E} & 0 & -\frac{\nu}{E} & -1 & 0 \\ 0 & -\frac{\nu}{E} & 0 & \frac{1}{E} & 0 & 0 \\ dr & dt & 0 & 0 & 0 & 0 \\ 0 & 0 & dr & dt & 0 & 0 \\ 0 & 0 & 0 & 0 & dr & dt \end{vmatrix}$$

and A is given on page . Expanding B on Column 3 gives

$$B = dr \begin{vmatrix} 1 & 0 & 0 & 0 & -\rho \\ 0 & \frac{1}{E} & -\frac{\nu}{E} & -1 & 0 \\ 0 & -\frac{\nu}{E} & \frac{1}{E} & 0 & 0 \\ dr & dt & 0 & 0 & 0 \\ 0 & 0 & 0 & dr & dt \end{vmatrix}$$

Continued expansion on Column 1 provides the following reduction

$$B = (dr)\left[1\begin{vmatrix} \frac{1}{E} & -\frac{\nu}{E} & -1 & 0 \\ -\frac{\nu}{E} & \frac{1}{E} & 0 & 0 \\ dt & 0 & 0 & 0 \\ 0 & 0 & dr & dt \end{vmatrix} - dr\begin{vmatrix} 0 & 0 & 0 & -\rho \\ \frac{1}{E} & -\frac{\nu}{E} & -1 & 0 \\ -\frac{\nu}{E} & \frac{1}{E} & 0 & 0 \\ 0 & 0 & dr & dt \end{vmatrix}\right]$$

By expanding the first on row 3 and the second on row 1 we arrive at

$$B = (dr)(1)(dt)\begin{vmatrix} \frac{\nu}{E} & 1 & 0 \\ \frac{1}{E} & 0 & 0 \\ 0 & dr & dt \end{vmatrix} + (dr)^2(-\rho)\begin{vmatrix} \frac{1}{E} & -\frac{\nu}{E} & -1 \\ -\frac{\nu}{E} & \frac{1}{E} & 0 \\ 0 & 0 & dr \end{vmatrix}$$

or finally,

$$B = (dr)(dt)\left[+\frac{1}{E}\,dt\right] - \rho(dr)^2\left[\left(\frac{1}{E}\right)^2 dr - \frac{\nu^2}{E^2}\,dr\right] .$$

Clearing of brackets and setting the result to zero gives

$$B = +\frac{1}{E}\,dr(dt)^2 - \rho(dr)^3\left(\frac{1}{E}\right)^2 + \rho\,\frac{\nu^2}{E^2}\,(dr)^3 = 0 .$$

If we factor the common term dr we obtain

$$dr\left[+\frac{1}{E}\,dt^2 + dr^2\left(-\frac{\rho}{E^2} + \rho\,\frac{\nu^2}{E^2}\right)\right] = 0 .$$

This equation is satisfied only when

$$dr = 0$$

or

$$dr^2\left(\rho\,\frac{\nu^2}{E^2} - \frac{\rho}{E^2}\right) = -\frac{1}{E}\,dt^2 .$$

The second relationship can be written

$$\left(\frac{dr}{dt}\right)^2 = -\frac{1}{E\left(\rho\,\frac{\nu^2}{E^2} - \frac{\rho}{E^2}\right)}$$

$$\left(\frac{dr}{dt}\right)^2 = -\frac{1}{\frac{\rho}{E}\,(\nu^2 - 1)}$$

$$= -\frac{E}{\rho(\nu^2 - 1)}$$

therefore

$$\frac{dr}{dt} = \pm\left[\frac{E}{\rho(1 - \nu^2)}\right]^{\frac{1}{2}} \quad \text{and} \quad dr = 0 \ .$$

Similarly, determinant A is

$$A = \begin{vmatrix} \frac{\sigma_\theta - \sigma_r}{r} & 0 & 0 & 0 & 0 & -\rho \\ 0 & \frac{1}{E} & 0 & -\frac{\nu}{E} & -1 & 0 \\ \frac{v}{r} & -\frac{\nu}{E} & 0 & \frac{1}{E} & 0 & 0 \\ d\sigma_r & dt & 0 & 0 & 0 & 0 \\ d\sigma_\theta & 0 & dr & dt & 0 & 0 \\ dv & 0 & 0 & 0 & dr & dt \end{vmatrix}$$

Expanding on Column 3

$$A = (dr) \begin{vmatrix} \frac{\sigma_\theta - \sigma_r}{r} & 0 & 0 & 0 & -\rho \\ 0 & \frac{1}{E} & \frac{\nu}{E} & -1 & 0 \\ \frac{v}{r} & -\frac{\nu}{E} & \frac{1}{E} & 0 & 0 \\ d\sigma_r & dt & 0 & 0 & 0 \\ dv & 0 & 0 & dr & dt \end{vmatrix}$$

Expanding on row 1

$$A = (dr)\left[\frac{\sigma_\theta - \sigma_r}{r} \begin{vmatrix} \frac{1}{E} & -\frac{\nu}{E} & -1 & 0 \\ -\frac{\nu}{E} & \frac{1}{E} & 0 & 0 \\ dt & 0 & 0 & 0 \\ 0 & 0 & dr & dt \end{vmatrix} + (-\rho) \begin{vmatrix} 0 & \frac{1}{E} & -\frac{\nu}{E} & -1 \\ \frac{v}{r} & -\frac{\nu}{E} & \frac{1}{E} & 0 \\ d\sigma_r & dt & 0 & 0 \\ dv & 0 & 0 & dr \end{vmatrix}\right]$$

Expanding the first on Column 4 and the second on row 4 yields

$$A = (dr)\left\{\left(\frac{\sigma_\theta - \sigma_r}{r}\right)(dt) \begin{vmatrix} \frac{1}{E} & \frac{\nu}{E} & 1 \\ \frac{\nu}{E} & \frac{1}{E} & 0 \\ dt & 0 & 0 \end{vmatrix} + (-\rho)\left[(-1)dv \begin{vmatrix} \frac{1}{E} & -\frac{\nu}{E} & -1 \\ -\frac{\nu}{E} & \frac{1}{E} & 0 \\ dt & 0 & 0 \end{vmatrix} + dr \begin{vmatrix} 0 & \frac{1}{E} & -\frac{\nu}{E} \\ \frac{v}{r} & -\frac{\nu}{E} & \frac{1}{E} \\ d\sigma_r & dt & 0 \end{vmatrix}\right]\right\}$$

$$A = dr\ dt\ \frac{\sigma_\theta - \sigma_r}{r}\left(\frac{1}{E}\ dt\right) + dr\ \rho\ dv\ \frac{1}{E}\ dt - dr^2\ \rho\left[\frac{1}{E^2}\ d\sigma_r - \frac{\nu}{E}\ dt\ \frac{v}{r} - \left(\frac{\nu^2}{E^2}\ d\sigma_r\right)\right]$$

Clearing parentheses and setting A = 0 gives

$$A = dr\, dt^2 \frac{\sigma_\theta - \sigma_r}{r\,E} + \rho\, dr\, dv\, dt \frac{1}{E} - \rho\, dr^2\, d\sigma_r \frac{1}{E^2}$$

$$+ \rho\, dr^2 \frac{\nu}{E}\, dt \frac{v}{r} + \rho\, dr^2 \frac{\nu^2}{E^2}\, d\sigma_r = 0$$

$$\frac{dr}{E}\left[dt^2 \frac{\sigma_\theta - \sigma_r}{r} + \rho\, dv\, dt - \rho\, dr\, d\sigma_r \frac{1}{E} + \rho\, dr\, \nu\, dt \frac{v}{r} + \rho\, dr \frac{\nu^2}{E}\, d\sigma_r\right] = 0$$

either dr = 0 or the bracket = 0. In the latter case, rewriting

$$\frac{\sigma_\theta - \sigma_r}{r}\, dt^2 + \rho\, dv\, dt = \rho\, dr \frac{d\sigma_r}{E} - \rho\, dr\, \nu \frac{v}{r}\, dt - \rho\, dr \frac{\nu^2}{E}\, d\sigma_r :$$

Multiplying by dr and divide by dt^2

$$\frac{(\sigma_\theta - \sigma_r)dr}{r} + \rho\, dv \frac{dr}{dt} = \left(\frac{dr}{dt}\right)^2 \left[\rho \frac{d\sigma_r}{E} - \rho\, \nu \frac{v}{r}\, dt - \rho \frac{\nu^2}{E}\, d\sigma_r\right]$$

since $\frac{dr}{dt} = \pm c$ or $\left(\frac{dr}{dt}\right)^2 = c^2$ and $\frac{E}{\rho} = c^2(1 - \nu^2)$

$$\frac{(\sigma_\theta - \sigma_r)}{r}\, dr \pm \rho c\, dv = c^2 \left[\frac{d\sigma_r}{c^2(1 - \nu^2)} - \rho\, \nu \frac{v}{r}\, dt - \frac{\nu^2\, d\sigma_r}{c^2(1 - \nu^2)}\right]$$

$$= c^2 \left[\frac{d\sigma_r}{c^2(1 - \nu^2)} (1 - \nu^2) - \rho\, \nu \frac{v}{r}\, dt\right]$$

$$\frac{(\sigma_\theta - \sigma_r)}{r}\, dr \pm \rho c\, dv = \left[d\sigma_r - \rho\, \nu \frac{v}{r} c^2\, dt \right]$$

Replacing dt by ± $\frac{dr}{c}$ gives

$$(\sigma_\theta - \sigma_r) \frac{dr}{r} \pm \rho c\, dv = \left[d\sigma_r \mp \rho \nu c \frac{v}{r}\, dr \right]$$

or finally, rearranging

$$d\sigma_r \mp \rho c\, dv = (\sigma_\theta - \sigma_r \pm \rho \nu c v) \frac{dr}{r} \qquad \text{3-11 and 3-12}$$

The top sign refers to propagation along the + c direction and the bottom sign to propagation along the - c direction.

Along dr = 0, there is no wave propagation therefore we can express a static relation that holds between the stresses and velocity from equation 3-6.

$$\frac{v}{r} = \frac{1}{E} \frac{d\sigma_\theta}{dt} - \frac{\nu}{E} \frac{d\sigma_r}{dt}$$

$$E \frac{v}{r}\, dt = d\sigma_\theta - \nu\, d\sigma_r$$

$$E \frac{v}{r} \frac{dt}{d\theta} = 1 - \nu \frac{d\sigma_r}{d\sigma_\theta}$$

$$\frac{d\sigma_r}{d\sigma_\theta} = \left[1 - E \frac{v}{r} \frac{dt}{d\theta} \right] \frac{1}{\nu}$$

or

$$d\sigma_r = \frac{1}{\nu} \left[d\sigma_\theta - E \frac{v}{r}\, dt \right] \qquad \text{3-13}$$

APPENDIX C

COMPUTER PROGRAM INPUT

Following is a list of the program input, the card format, and a definition of each item with clarifying discussion as required.

Format (8F10.0)

DELRA - radial increment of disk (in.). This quantity controls the characteristic mesh spacing and also strongly controls how rapidly the solution progresses. Too large a value could result in unacceptable accuracy of the finite difference equations while too small a value will cause excessively small increments of the input pressure to be interpolated thereby increasing machine running time. In the present studies values from 1/8 to 1/64 in. have been used.

RAI - inside radius of disk (in.).

RHO - specimen density $\left[\frac{\text{lbm sec}^2}{\text{in}^4}\right]$

EO - modulus of elasticity (lbf/in^2)

NU - Poisson's Ratio

DELEP - the increment between tabulated values of EPSILN(I). In the differentiation subroutine used in this work (DERIVL) this increment must be a constant.

TESTEP- a test value used to test convergence of the plastic strain increments during iteration. In the present work .00002 was used.

Format (6I5)

NA - 1 + number of radial increments into which the disk has been divided. It also equals the number of I lines.

NE - number of tabulated entries in stress-strain arrays [SIGMAE(I) - EPSILN(I)].

NT - number of tabulated entries in stress-time input [SIGMAT(I) - TIME(I)].

NRUNS - an indicator showing whether the current run is the first with unstressed material or a succeeding run with prestressed material from a previous run. For the former case set NRUNS = 1; for the latter NRUNS = 2. See also discussion of SIGMAO(I).

JLIM - an indicator which terminates the program when J ≥ JLIM. Used either as a normal termination condition or to prevent "runaway".

KK - an indicator which controls whether or not plastic wave speeds will be computed. If KK = 1 only an elastic analysis is contemplated and plastic moduli and wave speeds are <u>not</u> computed. If KK ≠ 1 plastic moduli and both elastic and plastic wave speeds are calculated.

INPUT - an indicator used to bypass the unloading shock calculations, for example, when the input consists of a "ramp" followed by a constant plateau and one wishes to ensure that inadvertent round-off or interpolating errors do not cause SIGEQ to be less than SIGMAX(I) and thereby cause unloading. If INPUT = 1 the shock calculations are bypassed. If INPUT ≠ 1 the shock calculations will be allowed to occur.

SIGMAO(I) - the stress at the proportional limit where the stress-strain curve ceases to be linear. This value is read in as an array; one for each I line. When an analysis of a previously unstressed disk is to be done each SIGMAO(I) is assigned the value of the proportional limit. However, when the disk has been previously stressed into the plastic range, some or all of the I-lines will have experienced stresses above the proportional limit. The maximum stresses for each I-line are printed out as SIGMAX(I). Those greater than the original proportional limit should be read in as the values of SIGMAO(I) prior to a succeeding run. They become, in effect, new proportional limits for their respective I-lines. When SIGMAX(I) is less than the original proportional limit, then the SIGMAO(I) for that line should be the original proportional limit.

STNRA(I), STNCA(I), STNZA(I) - these are the residual permanent set strains and are read in as 0 prior to an initial problem run. For succeeding runs the final values from the previous run which occurred after the disk was completely unloaded are to be used.

EPSEQI(I) - equivalent plastic strain initially computed by the program as the strain corresponding to the proportional limit. The final values corresponding to SIGMAX(I) are printed as output and are to be read in as initial values for succeeding runs.

Format (8F10.0)

TIME(I), SIGMAT(I) - tabular values of input time and corresponding pressure stress on the inner edge of the disk.

EPSILN(I), SIGMAE(I) - tabular values of strain (EPSILN) and corresponding stress from the stress-strain curve of the material. Only values for the plastic range are to be read, i.e., above the proportional limit.

Format (8I5)

IBRANCH - an indicator controlling the input of initial value data. If set = 1, initial values of the yield point, 3 strains, the strain corresponding to the yield point, and 2 stress components are read in for each I-line. If ≤ 0 the yield point is set to 2500 psi with all other values = 0.

The following input data is listed at the end of the program and is used when output plots of the stresses and strains as a function of time for selected I-lines are desired.

Format (6I5)

NPLOT1 - the number of I-lines for which plots are desired.

IPLOT(I1) - the specific I-line numbers for which plots are desired.

Format (8F10.0)

XMIN - the minimum value of time utilized in the plot. This would usually be 0.

DELT - the increment in time per inch of plot space available.

YMIN1 - the minimum values to be plotted of SRADA, SCIRCA, and VA on the same graph. If positive and negative values occur then YMIN1 should be chosen to at least encompass the largest negative number.

DELY1 - the increment in YMIN1 per inch of plot space available.

YMIN2 - the minimum values to be plotted of STNRA, STNCA, and STNZA on the same graph. If positive and negative values occur then YMIN2 should be chosen to at least encompass the largest negative number.

DELY2 - the increment in YMIN2 per inch of plot space available.

APPENDIX D

COMPUTER PROGRAM LISTING

The computer program listing and sample output pages are not included in this report.

REFERENCES

Papers or Reports

1. Von Karman, T. and Duwez, P. 1950. The Propagation of Plastic Deformation in Solids. Journal of Applied Physics, Vol. 21.

2. Taylor, G. I. 1942. The Plastic Wave in a Wire Extended by an Impact. British Official Report RC 329.

3. Rakhmatulin, K. A. 1945. Propagation of a Wave of Unloading. Journal of Applied Mathematics and Mechanics, Vol. 9.

4. Malvern, S. E. 1951. The Propagation of Longitudinal Waves of Plastic Deformation in a Bar of Material Exhibiting a Strain Rate Effect. Journal of Applied Mechanics, Vol. 18.

5. Bell, J. F. 1967. Theory vs. Experiment for Finite Amplitude Stress Waves. Recent Advances in Engineering Science.

6. Clifton, R. J. 1966. An Analysis of Longitudinal and Torsional Plastic Waves in a Thin Walled Tube. Proceedings of the 5th U.S. National Congress of Applied Mechanics.

7. Ziv, Moche. 1969. Two-Spatial Dimensional Elastic Wave Propagation by the Theory of Characteristics. International Journal Solids Structures.

8. Chou, P. C. and Koenig, H. A. March 1966. A Unified Approach to Cylindrical and Spherical Elastic Waves by Method of Characteristics. Journal of Applied Mechanics.

9. Fyfe, I. M. and Swift, R. P. July 1969. The Dynamic Plastic Response of Aluminum to Plane Strain Cylindrical Stress Waves. University of Washington, Department of Aeronautics and Astronautics, Report 69-3.

10. Lawrence, J. F. 1970. WONDY IIIa, A Computer Program for One Dimensional Wave Propagation. Sandia Corporation SC-DR-70-315.

Books

11. Mendelson, A. 1968. Plasticity: Theory and Application. New York: The Macmillan Company.

12. Timoshenko, S. 1956. Strength of Materials, Part II, Advanced Theory and Problems. 3rd Edition. New York: D. Van Nostrand Company.

APPENDIX D

(9 pages)

Longitudinal Vibration of Composite Bodies of Varying Area

Bulletin 42
(Part 5 of 5 Parts)

REPRINTED FROM

THE
SHOCK AND VIBRATION BULLETIN

JANUARY 1972

A Publication of
THE SHOCK AND VIBRATION
INFORMATION CENTER
Naval Research Laboratory, Washington, D.C.

DEPARTMENT OF DEFENSE
UNITED STATES OF AMERICA

Office of
The Director of Defense
Research and Engineering

LONGITUDINAL VIBRATION OF COMPOSITE BODIES OF VARYING AREA

D.J. Guzy*, J.C.S. Yang†, W.H. Walston,Jr.‡
Mechanical Engineering Department
University of Maryland
College Park, Maryland

The natural frequencies and corresponding mode shapes for composite, axisymmetric bodies of varying area undergoing longitudinal vibrations are determined both experimentally and theoretically. Composite rods, cones and conical shells of Lucite, Nylon, Polycarbonate and Polyethylene are investigated. Strain measurements are taken from strain gages mounted on the surface of the models which are excited at varying frequencies by a shaker table. Lumped parameter approximations of the continuous bodies are solved numerically on the digital computer for both fixed-free and free-free boundaries in order to determine the natural frequencies, mode shapes and relative strains. The method of characteristics is utilized in a wave propagation approach to obtain the response of a point in the model to a random input. The random input selected is white noise. The natural frequencies are obtained by performing a Fast Fourier Transform Analysis on the response.

LIST OF SYMBOLS

A	cross-sectional area
a	Lagrangian coordinate
a_{ij}	influence coefficients
c	shift rate
E	modulus of elasticity
f_1	fundamental frequency
g	gravitational constant
K	spring constant
L	length
t	time
u	particle velocity
x	distance from base
ϵ	engineering strain
ρ	density
σ	engineering stress
φ	impact function

INTRODUCTION

In recent years engineers have been required to design ballistic range models which are capable of being launched at hypersonic velocities for aerodynamic tests of ballistic missiles and space craft. At such velocities the designer is confronted with the dual problem of using materials which are structurally strong enough to withstand the severe loading conditions and materials which minimize the ablation of the missile nose due to aerodynamic heating. These models are frequently used to study boundary layer transition which could be influenced by modal vibration. The purpose of this paper is to study the vibration characteristics of the model as it is being tested in the range, and to develop an analytical means of predicting the transient response of the model under dynamic loadings.

The problem of vibration in continuous systems such as cylindrical rods has been investigated extensively in various research papers and textbooks [1-4]. However, vehicles are generally made up of conical shells, sections with abrupt changes in area, and laminated sections of different materials. There is a definite lack of experimental and analytical developments concerning vibration

* Graduate Assistant
† Associate Professor
‡ Associate Professor

and wave propagation in structures of varying area and/or multi-layered with changing impedances.

Experimental tests were performed using a shaker table to excite the models. Models were made from Plexi-glass (Lucite), Nylon, Polycarbonate (Lexan), Polyethylene, and the combination thereof. Strain gages and accelerometers were mounted on various positions on the model to determine the natural frequency, mode shape, and transient responses in the model. Two theoretical approaches, classical and wave propagation, were utilized. Natural modes of vibration and mode shapes were determined by first the classical approach, which constitutes the solution to the boundary value problem and in turn the eigenvalue problem. Numerical solutions were obtained by using a system of spring-masses. In the wave propagation approach the method of characteristics was utilized. A numerical integration of the characteristic equations for the range model,in conjunction with appropriate procedures to ensure that the conditions on the external boundaries as well as the continuity conditions at the sections with the step changes in area and varying impedances are satisfied, will yield the stress, displacement, and the particle velocity anywhere in the model [5]. Since this method is applicable for any type of loading, the natural frequencies can be obtained by applying a random input to the model and then performing a Fourier analysis on the response of some point in the model.

EXPERIMENTAL INVESTIGATIONS

A variety of models including rods, composite rods, composite cones and composite conical shells were fabricated and tested. Sketches of these models are shown in Fig. 1. Plastic materials were utilized rather than metals in order to maintain lower natural frequencies. An upper limit on the frequency of the forcing function was imposed by the shaker which was used - MB Electronics Model PM-50.

All models were constructed from solid plastic rods which were turned on a lathe to their final dimensions. In the case of a composite model, the sections were glued together using an epoxy adhesive. Strain gages were then mounted on the surface and the model was glued to a base plate which was bolted to the shaker table. As the input frequency to the shaker was varied, the output from the strain gages was noted. In this manner the natural frequency of each model was determined.

Since the elastic modulus of many plastic materials varies due to manufacturing inconsistencies, age and environment in addition to the effects of turning on the later, experiments were performed in order to determine the proper value of the modulus for the materials being used. Solid rods were used as the test specimen since the fundamental frequency equation for longitudinal vibration of free-fixed rods is well established.

$$f_1 = \frac{1}{4L}\sqrt{\frac{Eg}{\rho}} \tag{1}$$

The fundamental natural frequency of each rod was determined experimentally as was the density. Using this information and Eq. (1) the value of the modulus for each material was calculated. These experimentally determined values are given in Table 1, and are used in all subsequent calculations.

TABLE 1

Experimentally Determined Values of the Modulus of Elasticity and Density

Material	E (lb/in^2)	ρ(lb/in^3)
Polyethylene	2.8×10^5	0.0348
Lucite	3.3×10^5	0.0420
Nylon	6.0×10^5	0.0430
Lexan	3.9×10^5	0.0447

A series of tests involving composite rods made up of two rods glued end to end were performed. These experimental results, given in Table 2 and Fig. 2, are restricted to the first two natural frequencies due to the upper frequency limit of the shaker. The results of the lumped parameter computer analysis which is explained in the next section is also given there.

The next series of tests involved composite cones made up of a base and a tip glued together. Experiments were performed with the base and tip of the same materials as well as different materials. Table 3 and Fig. 3 illustrate the results of these experiments and also the lumped parameter computer results. This also gave a check on the influence of the epoxy bond between the sections. Based on the results, it was concluded that the influence of the epoxy was negligible.

The final experiments were performed using a concial shell as the base and a conical solid of a different material as the tip. These results are shown in Table 4 and Fig. 4.

LUMPED PARAMETER COMPUTER ANALYSIS

The physical models are approximated by a lumped parameter system consisting of concentrated mass elements and concentrated spring elements. Each model is divided into equal length segments with the mass treated as concentrated at the mid-point of the segment. The rods are divided into 16 segments and the cones into 24 segments. The mass of each segment varies as its volume in the case of the cones. The mass elements are connected by spring elements with spring constants determined from the properties of the material according to the equation:

$$\frac{1}{K^{i}_{i-1}} = \frac{1}{E}\int_{x(i-1)}^{x(i)} \frac{dx}{A(x)} \qquad (2)$$

where x is measured from the base and:

K^{i}_{i-1} = spring constant between i th and (i-1) th positions

$x(i)$ = distance at i th position

$x(i-1)$ = distance at (i-1) th position

The computer program utilizes the influence coefficients, a_{ij}, which are determined by

$$a_{ij} = a_{ji} = \sum_{L=1}^{i} \frac{1}{K(L)} \qquad i \le j \le n \qquad (3)$$

The computer program which is used to analyze the lumped parameter models first determines the eigenvalues by (1) pre-multiplying the mass matrix by the influence coefficients to obtain the dynamic matrix, (2) transforming the dynamic matrix to a Hessenberg matrix. The natural frequencies are then determined from the eigenvalues. The eigenvectors and mode shapes are then calculated

Natural frequencies obtained by this method are compared to the experimental results in Tables 2,3, and 4 and in Figures 2,3, and 4. The first and second mode shapes and corresponding material frequencies, for additional composite cones, both solids and shells, are computed by this lumped parameter appraoch. These results are given in Table 5 and in Figures 5 and 6. The relative values of strain for the first and second modes are also computed and are shown in Figures 7 and 8.

Table 2

Composite Rods, Experimental vs. Lumped Parameter Frequencies (See Fig. 2 for dimensions)

Material		Frequency (KHz)			
Base	Tip	Experimental 1st	Experimental 2nd	Lumped Parameter 1st	Lumped Parameter 2nd
Polyethylene	Lucite	1.6	5.35	1.64	5.27
Nylon	Lexan	2.0	6.0	2.16	5.98
Nylon	Polyethylene	2.25	5.6	2.28	5.68

Table 3

Composite Cones, Experimental vs. Lumped Parameter Frequencies (See Fig. 3 for dimensions)

Material		Frequency (KHz)			
Base	Tip	Experimental 1st	Experimental 2nd	Lumped Parameter 1st	Lumped Parameter 2nd
Polyethylene	Nylon	4.45	10.2	4.52	10.17
Polyethylene	Lucite	4.5	----	4.53	9.21
Polyethylene	Polyethylene	4.5	9.2	4.64	9.26

Table 4

Composite Cone, Shell Base with Solid Tip, Experimental vs Lumped Parameter Frequencies.

(See Fig. 4 for dimensions)

Material		Frequency. (KHz)			
Base	Tip	Experimental		Lumped Parameter	
		1st	2nd	1st	2nd
Polyethylene	Lucite	3.15	8.1	3.18	8.14

Table 5

Composite Cones, Lumped Parameter Frequencies
(Base 1 in. dia. × 3 in. long, Tip 3 in. long)

Material		Frequency (KHz)		Graph Symbol
Base	Tip	1st	2nd	
Poly. solid	Poly. solid	4.64	9.25	Δ
Poly. solid	Lucite solid	4.45	9.21	*
0.1 in. Poly shell	Lucite solid	3.60	10.06	•
0.1 in. Poly shell	Poly. solid	3.80	10.22	o
0.2 in. Poly shell	Poly. solid	4.38	11.01	□

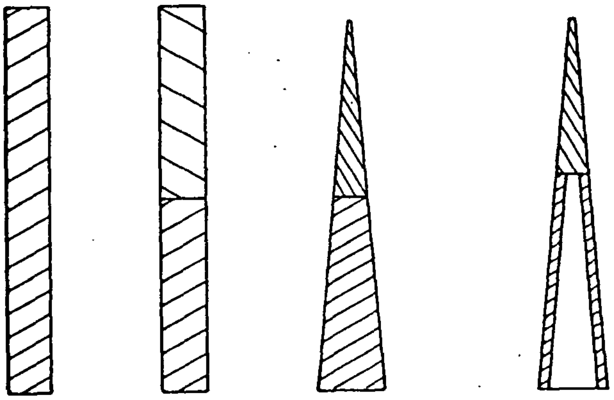
(a) (b) (c) (d)

Fig. 1 - Experimental models

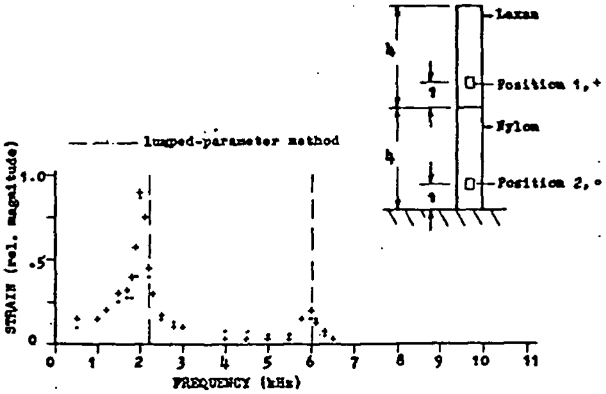

Fig. 2 - Composite rods, experimental vs. lumped parameter frequencies

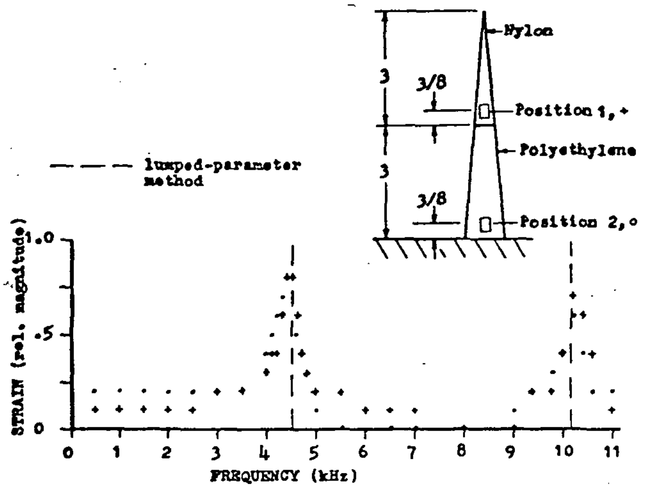

Fig. 3 - Composite cones, experimental vs. lumped parameter frequencies

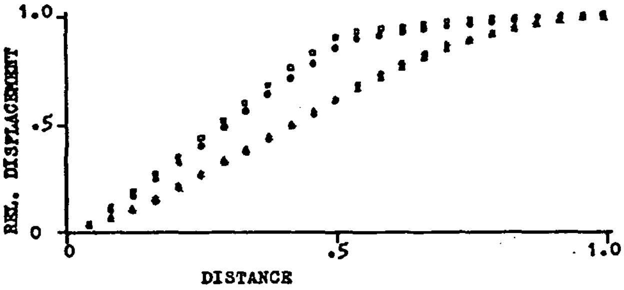

Fig. 5 - Composite cones, first mode shapes (see Table 5 for symbols)

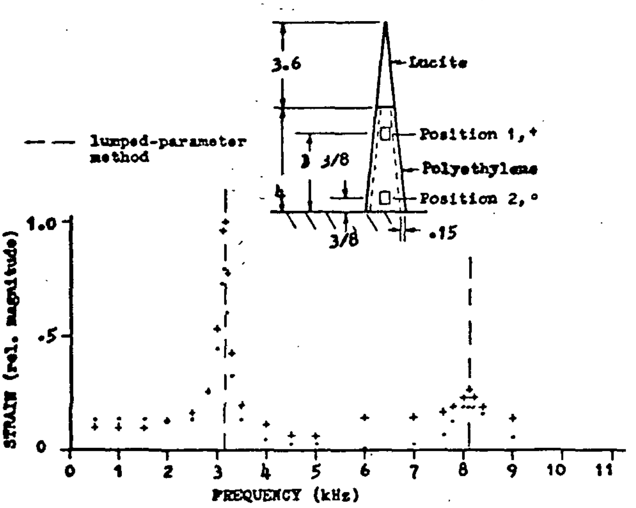

Fig. 4 - Composite cones, shell base with solid tip, experimental vs. lumped parameter frequencies

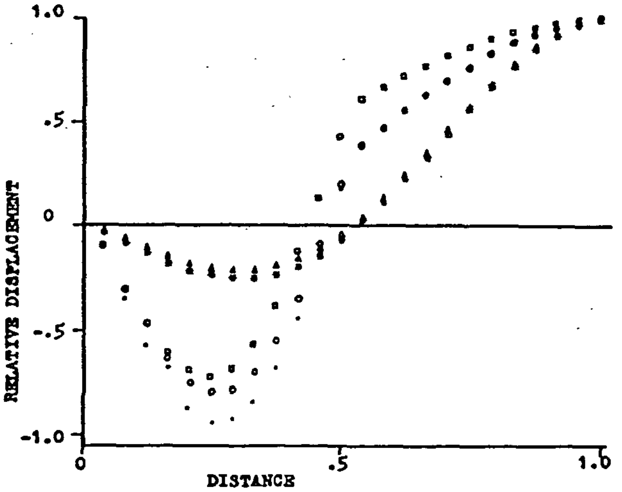

Fig. 6 - Composite cones, second mode shapes (see Table 5 for symbols)

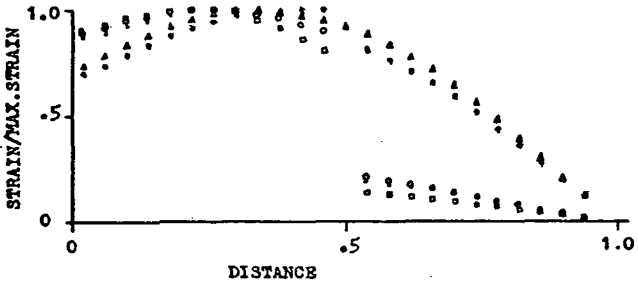

Fig. 7 - Composite cones - first mode strain (see Table 5 for symbols)

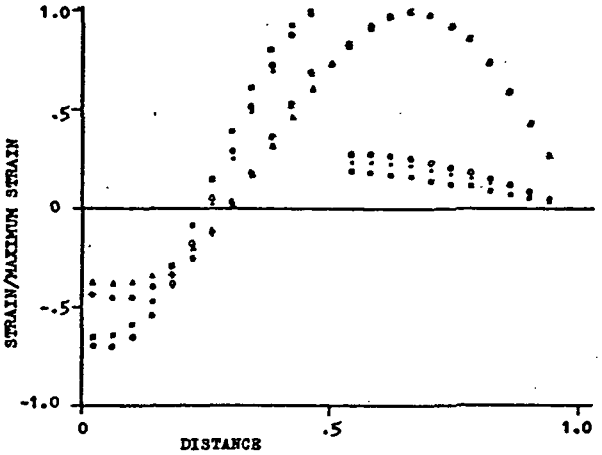

Fig. 8 - Composite cones - second mode strain
(see Table 5 for symbols)

WAVE PROPAGATION ANALYSIS

The stress wave propagation theory used in this analysis was developed independently by T. Von Karman [6] and G. I. Taylor [7] in 1942 and used by many investigators in various forms since that time. It is a one dimensional elastic-plastic theory used to determine the transient properties of solid materials under dynamic loading.

The response of materials is governed by the equations of continuity and momentum which are given in the Lagrangian coordinate system as follows:

$$\frac{\partial u}{\partial a} = \frac{\partial \varepsilon}{\partial t} \tag{4}$$

$$\frac{\partial u}{\partial t} = \frac{1}{\rho A} \frac{\partial(\sigma A)}{\partial a} \tag{5}$$

From the above equations the characteristic equations may be obtained:

$$\frac{\partial(u \pm \varphi)}{\partial t} \mp c \frac{\partial(u \pm \varphi)}{\partial a} = \frac{\sigma}{\rho A} \frac{\partial A}{\partial a} \tag{6}$$

where

$$c^2 = \frac{1}{\rho} \frac{\partial \sigma}{\partial \varepsilon} \tag{7}$$

and

$$d\varphi = c\,d\varepsilon \tag{8}$$

A numerical integration of the characteristic equations in the range model, in conjunction with appropriate procedures to ensure that the conditions on the external boundaries as well as the continuity conditions at the sections with the step changes in area and varying impedances are satisfied, will yield the stress, displacement, and the particle velocity anywhere in the model [5]. Since this method is applicable for any type of loading a random input was applied to the model. The random input signal selected is white noise which has a delta function as its autocorrelation function. The transient response at a point on the model was obtained numerically on the IBM 7094 computer. A Fast Fourier Transform method was performed on the response to obtain the natural frequencies of the structure. The advantages of the Fast Fourier Transform are two-fold. The number of actual arithmetic operations is reduced drastically, causing increases in speed of several orders of magnitude for reasonable record lengths. Also, because of the fewer operations performed, truncation and roundoff errors are reduced, producing a more accurate result. The results of the wave propagation analysis are compared to the lumped parameter analysis for free-free boundaries in Figures 9, 10 and 11 for various models.

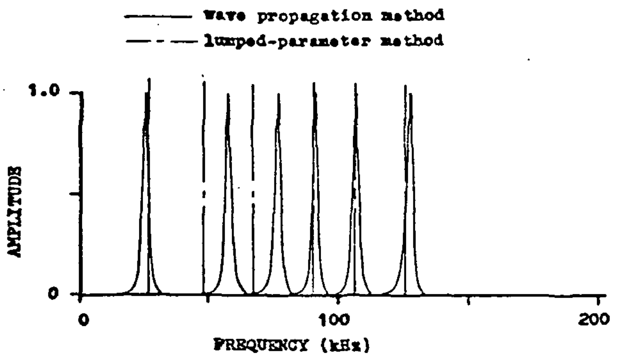

Fig. 9 - Composite cone, natural frequencies, polyethylene base, lucite tip

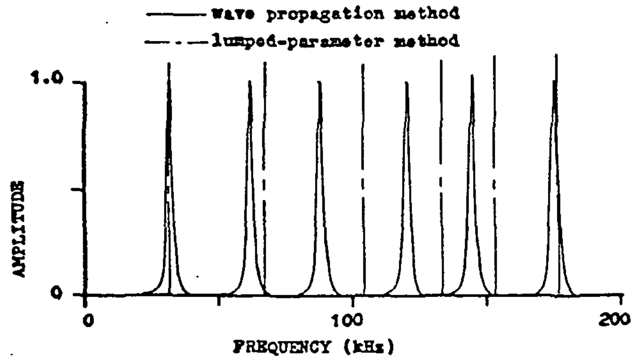

Fig. 10 - Composite cone, natural frequen--cies, lucite shell base, polyethylene tip

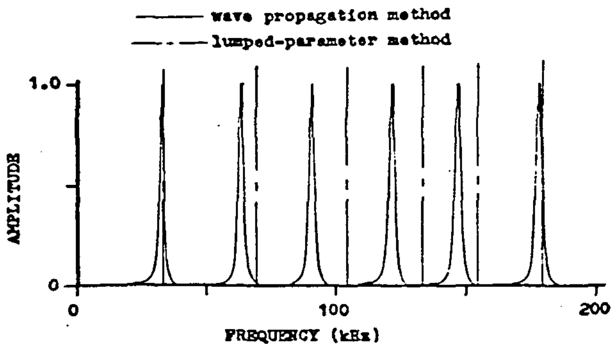

Fig. 11 - Composite cone, natural frequencies, polyethylene shell base, polyethylene tip

DISCUSSION OF RESULTS

The natural frequencies for various composite rods, cones and conical shells obtained experimentally and by the lumped parameter approach compare favorably. The maximum deviation is less than 3% for the composite cones and conical shells. The second natural frequency for the polyethylene-lucite cone was not obtained experimentally because of difficulties in the experimental set-up(Table 3). Subsequent modifications eliminated the difficulties, however the dzta was not retaken.

Unfortunately the material properties of the different plastic materials do not vary greatly. The use of materials having a wider range of properties should give more significant results for composite bodies. Metals offer certain advantages over plastics such as a wider range of properties, more stable properties,and easier machining-particularly for conical shells. The use of metals is recommended if a higher frequency input is available.

The mode shapes and relative strains are presented from the lumped parameter approach only. Since strain gages were employed at only two locations on each model, comparison was possible only at those points. Therefore these results were not considered significant and are not presented.

Comparison of the two theoretical predictions, lumped parameter and wave propagation for the free-free boundary was very erratic and poor. The fundamental natural frequencies for the various composite cones and conical shells compared reasonably well but not the higher modes. This confirmed the fact that while elastic wave propagation analysis might give good results for problems with a short duration input loading, it does not give very good results for long time input loading. In addition, the wave propagation analysis is a one-dimensional analysis. For conical modes where the area varies, it is dependent on the cone angle and the number of grid points used in representing the model. For one dimensional problems such as longitudinal vibration of composite rods, axially symmetric longitudinal vibration of circular cylinders and spherical shells, good agreements can be expected. (Natural frequencies were obtained for two-layer composite rods, cylindrical and spherical shells using the wave propagation approach. Results compared well with the theoretically computed results. The results for these calculations and comparison are not presented in this paper.)

CONCLUSIONS

The lumped parameter method using a series of mass elements and linear springs can be used to analyze the longitudinal vibration problem of composite axisymmetric bodies of varying area as verified by experimental vibration tests on simple composite rods, cones and conical shells.

The one dimensional elastic wave propagation approach utilized in computing the natural frequencies of the composite models did not give good results. In order to obtain better results using the one dimensional wave propagation analysis for the changing area problem with a long time input loading, much finer gird points must be utilized which require increased running time and storage space on the computer.

More research is needed to determine the effect of cone angle, impedance change, material properties,etc. on the vibration characteristic.

ACKNOWLEDGMENTS

Portions of this paper are part of a thesis presented by D. J. Guzy as a partial requirement for the Master of Science degree at the University of Maryland. Certain segments of this investigation were sponsored by N.A.S.A. Ames Research Center, Moffett Field, California under NASA Grant No. NGR 21-002-292 and under a grant from the Minta Martin Foundation.

REFERENCES

1. J. R. Hutichinson, "Axisymmetric Vibrations of a Solid Elastic Cylinder Encased in a Rigid Container", J. Acoust. Soc. Am., Vol. 42, No. 398, 1967.

2. C. T. Sun and K. C. Valanis, "Axially Symmetric Wave Propagation of a Finite Solid Cylinder", Engineering Res. Inst., Iowa State Univ., 1967.

3. H. D. McNiven and D. C. Perry, "Axially Symmetric Waves in Finite, Elastic Rods", J. Acoust. Soc. Am., Vol. 34, No. 433, 1962.

4. M. Rumerman and S. Raynor, "Natural Frequencies of Finite Circular Cylinders in Axially Symmetric Longitudinal Vibration", J. Sound Vib., Vol. 15, p.529, 1971.

5. J. C. S. Yang and A. Seigel, "Stress Waves in Multi-Layered Cylinders and Conical Frustrums", The Shock and Vibration Bul., No. 40, Part 4, 1969.

6. T. vonKarmon,"On the Propagation of Plastic Deformation in Solids", NORC Report A-29 (OSRD No. 365), Jan., 1942.

7. G. I. Taylor, "The Plastic Wave in a Wire Extended by an Impact Load", R. C. Report No. 329, June 1942.